Optical and Infrared Observations of the Nature and Evolution of Active Galaxies

Mark Guy Yates

Presented for the Degree of Doctor of Philosophy
at the University of Edinburgh

1988

This thesis has been composed
by me and the work described
in it is my own work except
where specifically acknowledged
in the text.

To Mum and Dad.

ABSTRACT

The work of this thesis divides into two main areas, the evolution of the environments of powerful, high–redshift radio galaxies, and the astrophysics of low–redshift active galaxies as inferred from optical, near– and far–infrared observations.

A study of the relationship between the radio and infrared luminosities of a sample of 60 high–redshift 3C radio galaxies reveals that the two quantities are correlated for the most powerful (and thus most distant) examples. It is suggested that the most powerful radio galaxies are subject to galaxy cannibalism, and will tend to lie in rich environments. Imaging of a sample of 26 powerful radio galaxies ($0.15 < z < 0.82$) is presented in order to test this hypothesis. It is found that radio galaxies at $z > 0.3$ lie in environments as rich as Abell class 0–1 clusters. The environments of these galaxies are four to five times richer than those at low redshift ($z < 0.3$). However, it is not possible to establish unequivocally whether radio luminosity or epoch is the fundamental parameter determining the richness of environment. About half of the classical–double (FR II) type sources lie in rich environments.

Deep *IRAS* observations of 18 3C radio galaxies ($0.01 < z < 0.2$) are discussed, and the spectral energy distributions of the six detected objects constructed. The two broad–line radio galaxies show a peak at $25\,\mu$m, possibly associated with a warm ($T \simeq 180$ K) dust component. Most of their luminosity is radiated in this component. The narrow–line radio galaxies have large far–infrared luminosities, and this component has a much greater luminosity than either the X–ray or radio components. However, there is no evidence for a $25\,\mu$ peak.

Near–simultaneous optical and infrared spectrophotometry of a sample of eight optically bright quasars and one broad–line radio galaxy are presented. Study of their Paα/Hα and Hα/Hβ ratios reveals that they can not be well modelled by either reddened or unreddened photoionization models. The observed line–ratios of 3C273 are used as reference points, and reddenings are derived for rest of the sample with respect to this quasar. Three of the quasars have 1–2 mag. of dust with respect to 3C273, and data at other wavelengths supports this conclusion. Two further quasars have infrared line–ratios which suggest that they too are subject to reddening.

CONTENTS

Chapter 1

Introduction to the thesis.

This thesis takes a slightly different form from many British scientific dissertations and essentially consists of the contents of four separate papers, exactly as they have been (or will) be published in a refereed journal (*Mon. Not. R. astr. Soc.*), with as little extraneous material as possible. As such it is very similar in style to those presented on the Continent. The main reason for my taking this approach is that I have tried to aim for as high a fraction of material that is both original and publishable as possible. With this aim, I have omitted the customary introductory ramble through the foothills of the subject (in this case active galaxies and cosmology). It would be tempting to discuss at great length the background to these subjects, such as the choice of cosmology (and the associated parameters H_o and Ω_o), but I have little that is original to say on these matters and the ground has already been capably covered by Weinberg and Gunn amongst many others. Similarly, I have omitted the final summary chapter wherein the author attempts to tie the whole thing together (often by very tenuous means) in the hope that the whole will be greater than the sum of the parts.

Rather, I have decided to introduce each of the four papers that follow with a short and informal prologue. This attempts to put the work of the chapter into a broad context, and explain why it was worth attempting in the first place. Then follows the paper in its entirety, beginning with the summary, and ending with the references for that paper. The style exactly follows that of *Monthly Notices*, and where the paper has already been published (chapters 2 and 3) I have not made any subsequent changes to the text. Finally, I have added a short postscript to each chapter. This aims to indicate to the reader whether, in February 1988, he should still believe any of the foregoing discussion (some of which was completed three years ago), and proposes directions for future work. Astronomy is progressing at such a rapid rate, that I feel that a critical evaluation of the science presented here in the light of work currently in progress is in order.

Most scientific research is nowadays done in collaboration with others, and the work presented here is no exception. The prologue to each paper indicates to what extent my collaborators are absolved from any inaccuracies or half–truths in the work that follows.

Chapter 2

The relationship between the radio and infrared luminosities of 3CR radio galaxies.

Published in *Mon. Not. R. astr. Soc.*, (1986), **221**, 311.

Prologue to *"The relationship between the radio and infrared luminosities of 3CR radio galaxies"*.

One of the first topics that I studied during my first few months at Edinburgh was galaxy cannibalism and its possible effect on the interpretation of the Hubble diagram, in particular the infrared Hubble diagram that had been constructed by Lilly and Longair using 3CR radio galaxies. Although it has long been appreciated that galaxy interactions may affect the form of the redshift–magnitude relation, quantifying the effect of this cannibalism, or even establishing its presence has met with little success. In the former case, this was, and still is due to limitations in the theory, and in the latter, due to the sheer difficulty of observing the companions of faint and distant radio galaxies. A further worry with a Hubble diagram constructed using powerful radio galaxies (and a worry at first apparently unconnected with cannibalism) was that, because the 3CR sample is radio–flux limited, those galaxies at the highest redshift are also the most radio luminous. It was possible that a correlation between radio and infrared luminosity was producing the observed evolution on the infrared Hubble diagram. The following paper sets out to test this hypothesis, and as it turned out, brought us back to thinking about cannibalism.

This and the following paper were done in collaboration with John Peacock and Lance Miller (Royal Observatory, Edinburgh). Their role was an advisory one, and I take full responsibility for the data and interpretation presented in chapters 2 and 3.

Summary

High–redshift ($z > 1$) 3CR radio galaxies are known to be brighter in the infrared than their low–redshift counterparts; this has been interpreted as being entirely due to the evolution of their constituent stellar populations. There is however a great difference between the radio luminosities of the high and low–redshift galaxies; we therefore examine statistically the possibility of a correlation between the infrared and radio luminosities of these objects. We show that there is in fact a positive correlation between these two parameters for the most radio luminous galaxies: the 3CR radio galaxies are not simply evolving standard candles. We argue that the observed infrared luminosities of the most powerful radio galaxies are attributable to a combination of this correlation and the evolution of their stellar populations. We further suggest that the correlation is caused by the most powerful radio galaxies occurring in dense cluster environments, where their stellar luminosities are increased by cannibalism.

1 Introduction

It is well known that the stellar luminosities of radio galaxies correlate with their radio powers. The work of Fanti & Perola (1977) and Auriemma *et al.* (1977) demonstrated that mean optical luminosity rises with radio power up to the point where the radio power is high enough for 'classical double' sources to be encountered. Beyond this point, the optical luminosity drops by about one magnitude. This is because galaxies associated with radio sources just below the classical–double power threshold are in general cD galaxies in rich clusters, whereas classical doubles at redshifts $z < 0.2$ are usually giant ellipticals in less dense environments (Longair & Seldner 1979, Prestage & Peacock 1988, Lilly, McLean & Longair 1984). For classical double sources, no dependence of optical power on radio luminosity has been suggested. The above studies, however, considered few galaxies with redshifts greater than 0.1 and thus only sampled classical–double sources of a relatively low radio luminosity. The recent infrared photometric study of a sample of 90 3CR radio galaxies by Lilly & Longair (1984, hereafter LL), complete both in K magnitude and in redshift, now provides an excellent data set with which to re–examine this relationship over a wide range of radio luminosities. K magnitudes, especially at high redshifts, effectively measure the stellar content of galaxies (Lilly, Longair & Miller 1985) in all but the broad–lined radio galaxies (BLRGs). LL therefore interpreted the brighter magnitudes of the high redshift galaxies, when compared with a non–evolving model on the the infrared Hubble diagram as showing evidence of luminosity evolution in the stellar populations of these giant elliptical radio galaxies. However, in a flux–limited sample it is obviously very important to understand the relationship, if any, between the stellar and radio luminosities of the galaxies at the highest powers. To test the implicit assumption that after applying aperture, redshift–K, and stellar evolution corrections, the 3CR galaxies are indeed standard candles, we have investigated statistically the relationship between these galaxies' magnitudes, radio luminosities and redshifts.

2 The analysis

The complete 3CR sample of LL includes all galaxies in the compilation of Laing, Riley & Longair (1983, hereafter LRL) with declinations less than 55° and redshifts > 0.03, and excludes all quasars or suspected quasars. We have defined a subset of this sample of 90 galaxies by including in our analysis only classical double radio sources (type II of Fanaroff & Riley 1974) and excluding the known BLRGs. Although the sample of LL includes nine FR I type galaxies we have excluded these from our analysis since it is already known that they are associated with more luminous galaxies in denser environments when compared with FR II types at similar redshift. Four FR II galaxies in this sample are near stars and are therefore without measured K magnitudes, four do not yet have spectroscopic redshifts and two have no optical identification. It is not expected that the omission of these galaxies from the analysis will introduce any significant bias. A total of 60 galaxies met the above criteria.

Infrared K magnitudes (already corrected for galactic extinction) and redshifts were taken from LL with the addition of the redshift for 3C 239 ($z = 1.78$) recently obtained by Spinrad *et al.* (1985). Flux densities and spectral indices at 178 MHz were taken from LRL. We have corrected the infrared magnitudes to a standard 43 kpc diameter aperture using the curve of growth given by Sandage (1972); the resulting aperture corrections to the original data are small for the higher redshift galaxies, which comprise the majority of the sample. Lilly & Longair (1982) showed that the $K - z$ Hubble diagram was well described by the 'C' model of Bruzual (1983). This takes into account passive evolution: the change in galaxy K luminosity due only to stellar evolution with no additional star formation after an initial burst. This is the most natural null hypothesis to consider although the exact amount of passive evolution expected is model dependent. There are three free parameters: the redshift of formation, the deceleration parameter q_o, and the slope of the initial mass function (IMF). The

observations of LL indicate (see their fig. 9) that one set of reasonable choices for these parameters is $q_o = 0.5$, an IMF slope $x = 1.35$ (the Salpeter value), and a formation redshift of 3.5. We have used the C models tabulated by Bruzual (1983) to determine the passive stellar evolution appropriate for these parameters. This allows us to calculate absolute magnitudes using the K–correction provided by this model and in addition, apply an evolutionary correction to reduce our magnitudes to a standard epoch ($z = 0$). If the 3CR galaxies were a homogeneous set at all redshifts, subject to no other evolutionary changes, these corrected magnitudes would be constant for all redshifts.

For the sample of 60 galaxies, the corrected absolute K magnitudes are plotted against radio power in Fig. 1 and against redshift in Fig. 2. In the latter plot the sample has been divided into four radio luminosity bins, each containing 15 members and plotted with a different symbol. These radio luminosity bins are defined in order of decreasing radio luminosity (units W Hz^{-1} ster^{-1}) as follows: (i) $\log P_{178} > 27.6$, (ii) $27.1 < \log P_{178} < 27.6$, (iii) $26.4 < \log P_{178} < 27.1$, and (iv) $\log P_{178} < 26.4$. Since the relationships between absolute magnitude and radio power ($M - P$) and absolute magnitude and redshift ($M - z$) are related by the implicit relation between radio power and redshift in a flux–limited sample, a statistical analysis is necessary to disentangle the underlying relationships. We can, however, note immediately from Fig. 2 a clear stratification in that at any given redshift, the galaxies in the bins of higher radio luminosity tend to have brighter absolute magnitudes. The best example of this is given by 3C 295, which is exceptionally radio luminous for its redshift (i.e. well above the 3CR flux limit of 10 Jy). This is one of the two brightest galaxies in the infrared, even though it lies at only $z = 0.459$.

In order to determine objectively whether any significant correlations are present, we have used the Spearman partial rank correlation analysis described by Macklin (1982); this allows us to test the correlation between absolute mag-

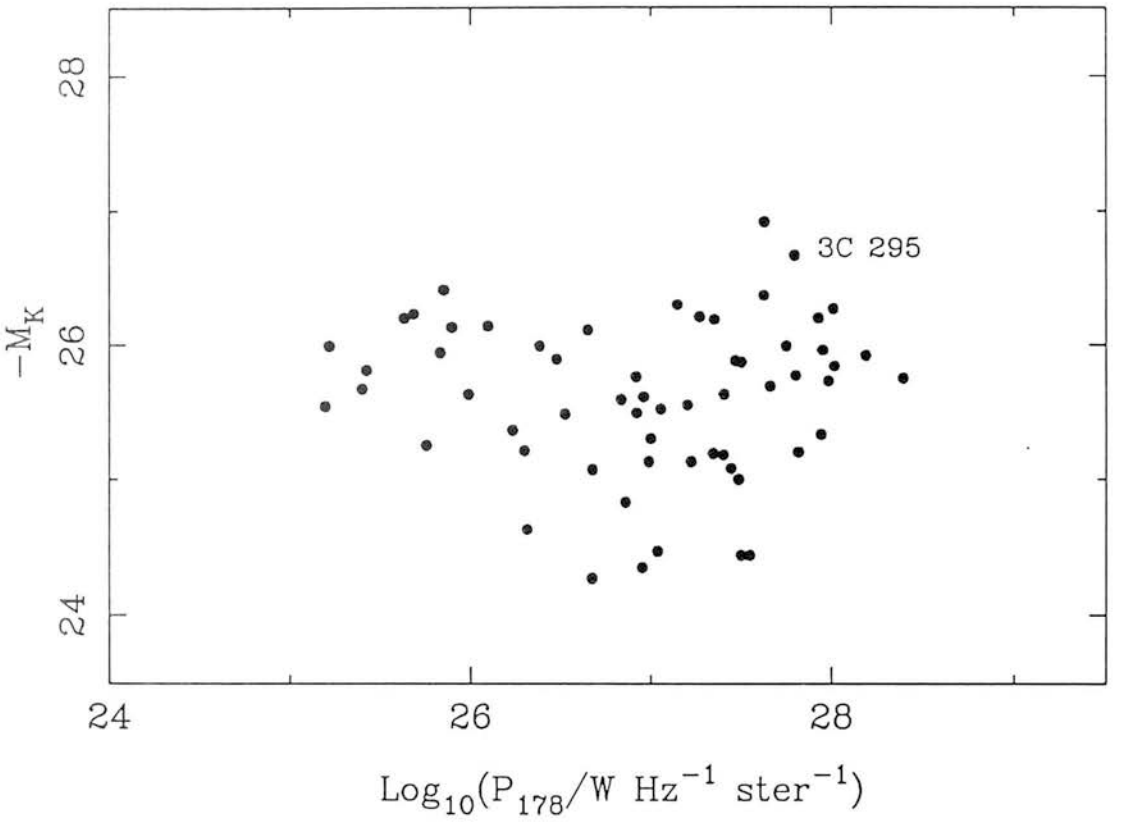

Figure 1. Absolute K magnitude plotted against radio power at 178 MHz.

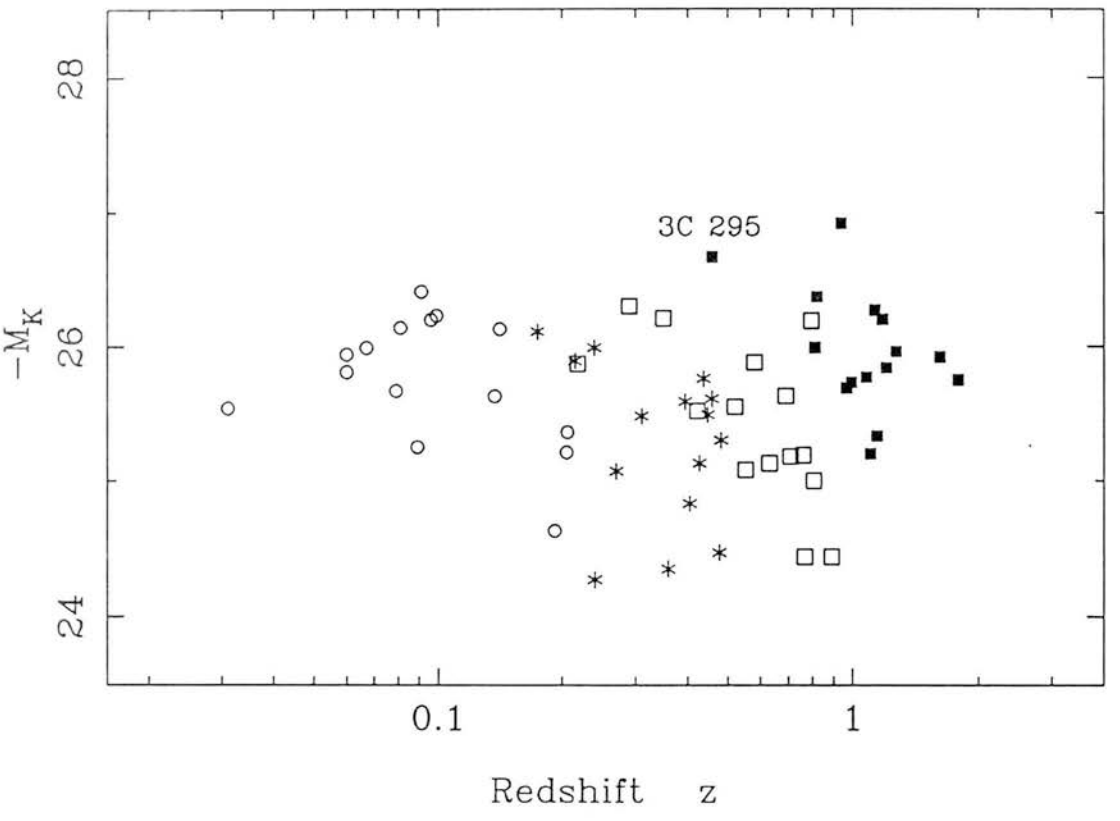

Figure 2. Absolute K magnitude plotted against redshift. The sample is divided into four radio power groups, represented in order of decreasing radio power by filled squares, open squares, asterisks and open circles.

nitude (M) and radio power (P) in the presence of the correlation of either with redshift (z). The correlation of radio luminosity with redshift is due to the selection of the sample by radio flux density. The null hypothesis is that any $M-P$ correlation is entirely due to a combination of separate $P-z$ and $M-z$ correlations. If this null hypothesis cannot be accepted, there must be some additional real correlation between radio luminosity and absolute magnitude, independent of redshift.

To carry out the analysis, we need the first order Spearman correlation coefficients r_{MP} and r_{Mz} (from Figs. 1 and 2) and the coefficient r_{Pz} for the connecting relation. The value of r_{Pz} comes from the $P-z$ plot for the sample, which is shown in Fig. 3. Note that, although the relation between P and z is very tight, there is a spread of P values at a given z. The partial rank test for the true correlations of M and P at constant z exploits this information via the statistic

$$r_{MP,z} = \frac{r_{MP} - r_{Mz}r_{Pz}}{[(1-r_{Mz}^2)(1-r_{Pz}^2)]^{1/2}} \qquad (1)$$

where $r_{MP,z}$ is the partial correlation coefficient for M and P at constant redshift z, and r_{MP}, r_{Mz} and r_{Pz} are the Spearman rank correlation coefficients between M and P, M and z, and P and z respectively. One feature of this statistic that is worthy of particular attention is the factor $(1-r_{Pz}^2)$ in the denominator. In the problem under discussion here, r_{Pz} is very close to 1 so that any difference between r_{MP} and the 'expectation value' in the null hypothesis $r_{Mz}r_{Pz}$ is increased by a large factor. This amplification illustrates the power of the test: with P and z being very nearly perfectly correlated, the $M-P$ and $M-z$ plots should appear almost identical. Even a small difference between them therefore provides evidence for a strong effect, not accounted for in the null hypothesis. Similarly, it is possible to find $r_{Mz,P}$ – i.e. the $M-z$ correlation at constant P.

Table 1 presents the first– and second–order (i.e. partial) coefficients; the

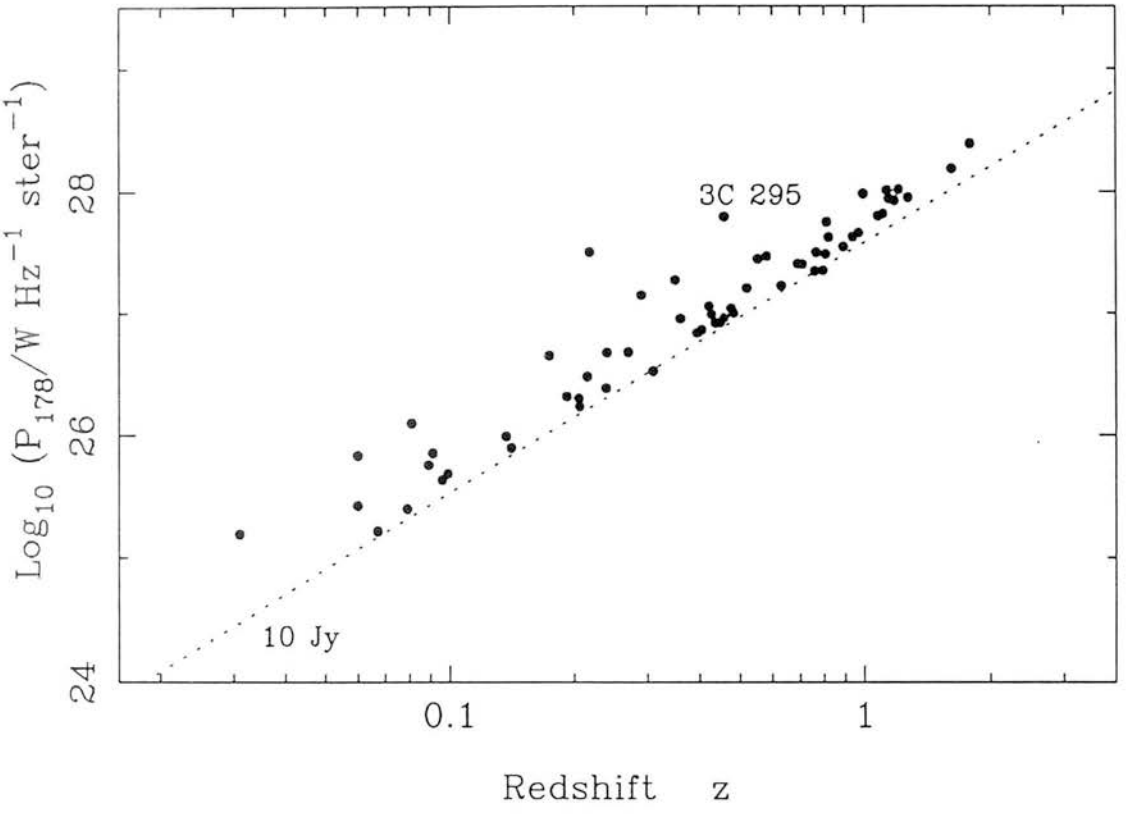

Figure 3. Radio luminosity correlated with redshift. The 10–Jy flux limit which defines inclusion in the compilation by Laing, Riley & Longair (1983) is shown.

Table 1. Rank correlation coefficients.

Correlation	r	t	
MP	0.050	0.379	
Mz	−0.050	0.379	
Pz	0.950	23.096	
MP, z	0.309	2.456	($\sim 1.5\%$)
Mz, P	−0.309	2.456	($\sim 1.5\%$)

significance is calculated in terms of the Student's t statistic:

$$t = r \left(\frac{N - \alpha}{1 - r^2} \right)^{1/2}, \tag{2}$$

where r is the correlation coefficient under consideration (first or second order), N is the number of data pairs and $\alpha = 2$ in the case of the first order coefficients and 3 for the second order ones. This is not the statistic advocated by Macklin (1982), who used a normal approximation to the t distribution. Our procedure is the analogue of that for the parametric partial rank test (Kendall & Stuart 1977, 1979) but gives results very close to Macklin's. The corresponding significance levels indicate the probability that the observed correlations could arise by chance. It is seen from the partial coefficients that M correlates with P, at the 1.5% level of significance and *anti*–correlates with z at the 1.5% level. In order to test the usefulness of the t statistic as a measure of the significance of our results, we have conducted a Monte Carlo simulation to establish independently the probability that our observed partial coefficients could occur by chance. It was found that our quoted significance levels, derived using the t statistic, are conservative by about a factor of two. Our correlations are therefore significant at the 0.75% level rather than the 1.5% level estimated from the t statistic. The sizes of the correlation of M with P and the anti–correlation of M with z are equal but of opposite sign; there is no first–order correlation of M and z for the sample, as we should expect since M has been corrected using the C model for a formation redshift of 3.5 which Lilly & Longair (1982, 1984) found to be a good fit to the data. Although the observed correlations are dominated by the very infrared luminous galaxies such as 3C 295 and 123 ($z = 0.218$), this need not be a cause for concern since this is just telling us that these two galaxies are the most spectacular examples of the trend linking radio and infrared luminosities.

3 Discussion

3.1 *K-z* RELATIONS AND STELLAR EVOLUTION

The results in Section 2 indicate that radio and infrared luminosities correlate. The continuing infrared photometric survey of a sample of radio galaxies selected at lower radio flux densities (1 Jy at 408 MHz; Lilly, Longair & Allington-Smith 1985), when complete, will allow us to test this result further by providing a sample of galaxies at redshifts around one, but with lower radio luminosities than the 3CR galaxies whose limiting flux density is 10 Jy at 178 MHz. In the meantime it is worth noting that the mean absolute magnitude of the 23 3CR galaxies in the sample of LL with $z > 0.6$ is -25.7 (standard error ± 0.1), whilst the corresponding mean for the five 1-Jy galaxies which do at present have published redshifts and infrared photometry in this redshift range is -25.1 (standard error ± 0.2). Application of the Mann–Whitney U–test indicates that the probability that the two samples are drawn from the same parent distribution is smaller than 4% (for the one–tailed test). This provides additional independent evidence for the above result, and suggests that in general, the 1–Jy galaxies will have fainter absolute magnitudes than the 3CR galaxies. On the infrared Hubble diagram of LL they will therefore tend to lie above the passively evolving (C model) fit to the data at high redshifts. The close correspondence of the respective Hubble diagrams for the 3CR radio galaxies and the less powerful 1–Jy galaxies at lower redshifts ($z < 0.5$; Lilly, Longair & Allington-Smith 1985) indicates that the correlation discussed here can only be important for radio galaxies of the highest radio luminosities.

As a further test, we have divided our 60 galaxy sample about the median radio luminosity ($\log P_{178} = 26.96\,\mathrm{W\,Hz^{-1}\,ster^{-1}}$) into a high–power subsample and a low–power subsample. On performing the partial rank analysis separately on these two samples, no correlation was found between radio–power and absolute magnitude at constant redshift for the low power sample. For the high power

sample, a correlation was found at the 0.8% significance level (calculated using the t statistic), slightly stronger than that observed for the 60–galaxy sample as a whole. This provides further evidence that the correlation is only important for galaxies of the highest radio luminosities ($\log P_{178} > 27\,\mathrm{W\,Hz^{-1}\,ster^{-1}}$). The analysis was repeated a further time for the high power sample but with the omission of 3C 295, the most spectacular example of a galaxy with a very luminous radio and infrared luminosities. The resultant correlation was significant at the 4% level (calculated using the t statistic) and at the 2% level when calculated via the Monte Carlo method.

This correlation has important implications for our understanding of the evolution of stellar populations in radio galaxies. It has previously been assumed that these galaxies are a homogeneous set of standard candles. Under this assumption, it is sufficient that any model magnitude–redshift law satisfy the constraint $r_{Mz} = 0$, which the C model (with $q_o = 0.5$) does (see Table 1). In the presence of a correlation with radio power, we can still treat the galaxies as a homogeneous set, providing we account for the radio bias that is introduced in a sample selected by radio flux density. If the radio–infrared correlation is independent of epoch, we require that after having applied the correction for stellar evolution, the galaxies behave like standard candles i.e. $r_{Mz,P} = 0$. This requirement is in fact satisfied by Bruzual's non-evolving (NE) model (for $q_o = 0.5$), rather than the passively evolving model we have applied in this analysis. This model is unphysical, since we know that the stellar populations of the galaxies must be evolving to some extent. Possible solutions would be to adopt a low value of q_o (i.e. $q_o = 0.0$), a steeper initial mass function, or a combination of these two. Such choices would reduce the amount of stellar evolution from about one magnitude at $z = 1$ (as obtained by LL) to a value of about 0.5 mag. The additional apparent evolution on the Hubble diagram would then be accounted for by the radio–infrared luminosity correlation. We shall not pursue this point in detail because it seems likely that the radio-infrared

correlation may *not* be independent of epoch. This conclusion depends on a possible mechanism for the correlation, which we discuss next.

3.2 CANNIBALISM AND THE RADIO–INFRARED CORRELATION

A likely mechanism for the above correlation is hinted at by the bright absolute magnitude of 3C 295, a cD galaxy in a rich cluster and thus a galaxy which has probably undergone cannibalism (Hausman & Ostriker 1978). As noted earlier, at low redshifts ($z < 0.2$), classical-double radio galaxies of the sort considered here do not appear to lie in rich clusters (Longair & Seldner 1979). However, that work did not extend to high enough redshifts to encompass the top decade of radio power which we have been able to include in our analysis here. We suggest therefore that the most powerful radio galaxies known are those rare sources which are associated with rich clusters of galaxies, and which are subject to processes such as cannibalism: the most radio luminous galaxies occur at high redshift and therefore have stellar luminosities enhanced by dynamical evolution. Cygnus A (excluded from LRL on account of its low galactic latitude) is another galaxy comparable with 3C 295; it is especially luminous for its redshift in both the radio and optical wavebands, and is a cD galaxy in a cluster (Spinrad & Stauffer 1982). Cygnus A provides further support for a link between radio power and cluster environment. In consequence, we suggest that other 3CR galaxies with high radio power and high redshift ($z > 0.5$) may also be the brightest members of clusters and subject to the same dynamical evolution as 3C 295 ($z = 0.459$) and Cyg A. In general, however, galaxies of such high radio power ($P_{178} > 10^{27}\mathrm{W\,Hz^{-1}\,ster^{-1}}$) lie at such high redshifts ($z > 0.6$) that at present we do not have sufficiently deep imaging to determine the nature of their environment.

Nevertheless, we believe that the idea of the most powerful radio galaxies lying in rich clusters provides a convincing explanation for our results. Apart from accounting for the abnormally bright absolute K magnitudes of galaxies such as

3C 295, it can also explain why the NE model has an absolute magnitude-redshift dependence at constant radio power ($r_{Mz,P}$) close to zero. This is because the luminosity evolution of FRII radio galaxies is a combination of two distinct kinds of behaviour: at low radio powers, classical double sources do not lie in dense environments and thus undergo mainly stellar evolution. Conversely, at high radio powers, dynamical evolution may dominate. In this case, seeking a single 'best–fitting' evolutionary magnitude redshift model with $r_{Mz,P} = 0$ is meaningless; we must first correct for dynamical effects. Although this may be very difficult in practice, an encouraging inference of this present study is that these effects may well be small, *provided* we restrict ourselves to galaxies of moderate radio power.

4 Conclusions

We have examined the assumption that the 3CR radio galaxies are evolving standard candles and find that the most powerful radio galaxies ($\log P_{178} > 27\,\mathrm{W\,Hz^{-1}\,ster^{-1}}$) display a correlation between absolute infrared magnitude (equivalent to stellar luminosity) and radio luminosity, which we interpret as being due to their unusual cluster environments. 3C 295 and Cygnus A, cD galaxies in clusters, are both powerful radio galaxies and have bright absolute magnitudes: we suggest that other high radio power galaxies will also be subject to dynamical evolution. In consequence, the infrared Hubble diagram of Lilly & Longair (1984) does not simply reflect the effects of passive evolution of the stellar populations. The most exciting result of this analysis is the discovery of a possible link between radio galaxy environment and radio power.

Acknowledgments

We appreciate useful discussions with M.S. Longair. MGY is grateful for support from an SERC Research Studentship.

References

Auriemma, C., Perola, G.C., Ekers, R., Fanti, R., Lari, C., Jaffe, W.J. & Ulrich, M.H., 1977. *Astr. Astrophys.*, **57**, 41.

Bruzual, G., A., 1983. *Rev. Mex. Astron. Astrofis.*, **8**, 63.

Fanaroff, B.L. & Riley, J.M., 1974. *Mon. Not. R. astr. Soc.*, **167**, 31P.

Fanti, R. & Perola, G.C., 1977. *Radio Astronomy and Cosmology, I.A.U. Symp. No. 74*, p.171, ed. Jauncey, J.L., Reidel, Dordrecht, Holland.

Hausman, M.A. & Ostriker, J.P., 1978. *Astrophys.J.*, **224**, 320.

Kendall, M.G. & Stuart, A., 1977. *Advanced Theory of Statistics*, 4th edn., Vol 1, Griffin.

Kendall, M.G. & Stuart, A., 1979. *Advanced Theory of Statistics*, 4th edn., Vol. 2, Griffin.

Laing, R.A., Riley, J.M. & Longair, M.S., 1983. *Mon. Not. R. astr. Soc.*, **204**, 151.

Lilly, S.J. & Longair, M.S., 1982. *Mon. Not. R. astr. Soc.*, **199**, 1053.

Lilly, S.J. & Longair, M.S., 1984. *Mon. Not. R. astr. Soc.*, **211**, 833.

Lilly, S.J., Longair, M.S. & Allington-Smith, J.R., 1985. *Mon. Not. R. astr. Soc.*, **215**, 37.

Lilly, S.J., Longair, M.S. & Miller, L., 1985. *Mon. Not. R. astr. Soc.*, **214**, 109.

Lilly, S.J., McLean, I.S. & Longair, M.S., 1984. *Mon. Not. R. astr. Soc.*, **209**, 401.

Longair, M.S. & Seldner, M., 1979. *Mon. Not. R. astr. Soc.*, **189**, 433.

Macklin, J.T., 1982. *Mon. Not. R. astr. Soc.*, **199**, 1119.

Prestage, R.M. & Peacock, J.A., 1988. *Mon. Not. R. astr. Soc.*, in press.

Sandage, A., 1972. *Astrophys. J.*, **173**, 485.

Spinrad, H., Djorgovski, S., Marr, J. & Aguilar, L., 1985. *Publ. astr. Soc. Pacific*, **97**, 943.

Spinrad, H. & Stauffer, J.R., 1982. *Mon. Not. R. astr. Soc.*, **200**, 153.

Postscript at February 1988.

Things have become rather more complicated at $z > 1$ than was apparent in late 1985 when this paper was written. Two important discoveries made since then are the Lyman α cloud associated with 3C326.1 at $z = 1.82$ by Spinrad and collaborators, and the demonstration by Le Fèvre and collaborators that at least one of the $z > 1$ radio galaxies (and possibly others) are being gravitationally amplified by foreground galaxies, thus increasing their apparent luminosities. Whilst our statistical analysis of the the data remains sound, the French group at least would argue that gravitational amplification rather than cannibalism may produce the correlation between infrared and radio luminosity. However, they need to demonstrate that gravitational amplification is important for the majority of the 3CR sample at high–redshift in order for this process to have a noticeable effect on the form of the Hubble diagram. Le Fèvre and coworkers are currently pursuing an extensive optical imaging and spectroscopy programme with this aim in mind, using the Canada–France–Hawaii telescope under conditions of excellent seeing at Mauna Kea. Spinrad and collaborators interpret the the Lyα cloud at $z = 1.82$ as a 3CR galaxy in the process of formation which will possibly lead to the formation of a giant elliptical or cD galaxy. That such dynamic activity is taking place at comparatively late epochs is in keeping with a cannibalism interpretation for the high luminosities of the 3CR galaxies at $z > 1$. The obvious observational test of the importance of cannibalism in the evolution of high–redshift radio galaxies, namely an estimate of the richness of their environments, is the subject of the

paper which follows in the next chapter.

Chapter 3

The cluster environments of powerful, high redshift radio galaxies.

To be published in *Mon. Not. R. astr. Soc.*

Prologue to *"The cluster environments of powerful, high redshift radio galaxies"*.

This work follows on directly from the findings of the previous paper: we had asserted that cannibalism may be important in the evolution of the most distant radio galaxies – now the task was to confirm or reject that hypothesis observationally and so I embarked on the extensive imaging programme discussed in the following paper. This project has occupied the greater part of my time at Edinburgh and the paper will be submitted shortly.

Summary

We present deep imaging of a sample of 26 powerful radio galaxies in the redshift range $0.15 < z < 0.82$, and derive amplitudes of the galaxy cross–correlation function (B_{gr}) about each source, a measure of the richness of environment. The powerful radio galaxies in this sample at $z > 0.3$ generally occupy environments as rich as Abell class 0–1 clusters of galaxies, four to five times richer than the environments of the lower redshift, $z < 0.3$, radio galaxies. This trend in cluster environment is similar to that seen in radio–loud quasars over the same redshift range. Our previous work on the 3CR sample (Yates, Miller & Peacock 1986) suggested that the fundamental parameter determining the richness of environment is the radio luminosity of the galaxy, rather than its redshift. Our direct imaging confirms that the most powerful radio galaxies do inhabit rich environments. However, we are unable to distinguish whether radio luminosity or epoch is the dominant factor determining the richness of the environment. This is because our most powerful galaxies are also the most distant. About half of our FR II type galaxies occupy environments as rich as Abell class 1 clusters, in contrast with the well known tendency for low–redshift ($z < 0.1$) FR II types to lie in poor environments. We suggest that these high–redshift cluster FR IIs are the analogues of Cygnus A and 3C 295, galaxies powerful enough to support double–lobe structure despite the presence of a dense intracluster medium.

Nearly three quarters of our sources can be adequately classed as giant–ellipticals – high surface brightness morphological peculiarities only occur in a minority of cases. One quarter of our sample have multiple nuclei, a phenomenon that is rare for those radio galaxies in poor environments.

1 Introduction

This paper aims to study the cluster environments of powerful radio galaxies in the redshift range $0.15 < z < 0.82$, using the amplitude of the cross-correlation function as a measure of the cluster richness. It thus extends to higher redshift the work on the environments of powerful radio galaxies by Longair & Seldner (1979, hereafter LS) and Prestage & Peacock (1988, hereafter PP) which was generally confined to $z \lesssim 0.15$. In so doing, we can sample galaxies that are intrinsically more radio luminous than was possible in these two studies, and also study the evolution of cluster environments to greater look–back times. Consequently, there are several important questions that a systematic CCD imaging survey of distant, powerful radio galaxies and a study of their cluster environments can address.

The most powerful radio galaxies, such as those in the 3CR sample, have frequently been used as cosmological probes on the Hubble diagram, their redshifts extending to $z \simeq 1.8$. The optical counterparts of these radio sources have traditionally been described as normal giant elliptical galaxies, although good imaging has only been available for the low–redshift objects, and very deep high quality CCD imaging is only just beginning to to elucidate the morphologies of the higher redshift examples (e.g. Spinrad & Djorgovski (1987), Djorgovski, Spinrad & Dickinson (1988), Le Fèvre *et al.* (1988)). Recent comprehensive photometric studies have been undertaken in the infrared by Lilly & Longair (1984) and the optical by Spinrad & Djorgovski (1987). In these studies it was inferred that the high–redshift ($z \geq 1$) 3CR galaxies are brighter in absolute terms than their low–redshift counterparts, an effect Lilly & Longair attributed to the evolution of the galaxies' stellar populations. An important property of the 3CR sample is that it is radio–flux limited, thus the most distant objects are also the most intrinsically radio–luminous. Yates, Miller & Peacock (1986) studied the relationship between the infrared and radio luminosities of the 3CR

galaxies employed by Lilly & Longair (1984) and found that there was a correlation for the most powerful objects. We suggested that this effect may be due to these galaxies undergoing dynamical evolution (cannibalism), and implying that they will lie in rich environments. Accurate estimates of the richness of environment for the 3CR galaxies at $z > 0.2$ have never been obtained, information that is vital to understanding the stellar and dynamical evolution of these high–redshift objects. Most studies that have used powerful radio galaxies as cosmological probes have tacitly assumed that the environments of the high–redshift objects are analogous to those of the better studied, low-redshift ($z < 0.1$) examples, an assumption that this paper intends to test.

Seldner & Peebles (1978) and LS pioneered the use of the amplitude of the cross-correlation function as an estimate of the richness of the environment, the latter work studying 3CR radio galaxies at $z < 0.1$ and a number of 4C galaxies, and correlating with galaxies in the Zwicky and Lick catalogues. They found that the classical double (Fanaroff–Riley (FR) type II) sources (the type used exclusively on the Hubble diagram) do not lie in rich regions of space, their cross–correlation functions having amplitudes similar to those of galaxies selected at random in the Universe. The more relaxed (FR I) sources, however, were found to lie in regions of space where the amplitude of the cross-correlation function is four to five times that of galaxies selected at random.

Prestage & Peacock (1988) extended this work to $z \simeq 0.15$, correlating about 200 powerful radio galaxies in three samples with the Lick galaxy counts, and galaxy counts derived from COSMOS scans of UK Schmidt plates, confirming the distinction in environments of the FR I and FR II types noted by LS. Studies of cluster environments are indirect probes of the intergalactic medium surrounding radio sources and may provide important clues as to the cause of the different radio structures seen in FRIs and FRIIs. For example, a natural explanation for the tendency of FR II, classical–double sources to lie in regions

of low galaxy density, rather than clusters, is that the centres of clusters of galaxies have an intergalactic medium that is of too great a pressure to allow the formation of lobe structures. These two studies did not sample galaxies of comparable radio power to those seen at $z \gtrsim 1$ and thus in order to be able study the role that the environment plays in the evolution seen on the Hubble diagram, it is necessary to study galaxies at higher redshifts. As such, this present study is in many ways a logical extension of LS and PP.

Yee, Green & Stockman (1986, hereafter YGS) and Yee & Green (1987, hereafter YG) have applied an analysis of the amplitude of the cross–correlation function to a sample of optically bright radio–loud quasars at redshifts up to $z \simeq 0.65$, using *r(Gunn)* CCD imaging, and this present work is the radio galaxy analogy of that experiment. YGS found that between between $z = 0.4$ and 0.6 the average quasar–galaxy cross–correlation amplitude increases by about a factor of three for their sample. Some of their radio–loud quasars at $z \simeq 0.6$ were found in environments as rich as Abell class 1 clusters. They interpret this result as indicating that the environments of some rich clusters may have undergone substantial evolution since $z \simeq 0.6$, allowing them to support quasar activity at that epoch, and it is of great interest to see whether the environments of powerful radio galaxies show a similar behaviour.

Finally, the morphologies of the radio galaxies themselves are of great interest, since multiple nuclei and prominent peculiarities are often indicative of merging and other dynamical activity. Heckman *et al.* (1986) have obtained optical imaging of 43 low–redshift radio galaxies and claim that between one quarter and one third of their most powerful examples (generally FR II types) are strongly peculiar at high levels of surface brightness, a claim that may have important implications for our understanding of the evolution of the most powerful objects. This present survey extends the study of the morphologies of powerful radio galaxies to higher redshifts, and consequently to greater radio lu-

minosities; what good optical imaging that already exists for the high–redshift objects is of very variable quality and is at present largely unpublished.

This present work is very much in the way of a reconnaissance, our prime aim being to first establish whether clustering is prevalent at $z > 0.2$, and so we have chosen to image in one band only, identifying interesting objects suitable for further multi-waveband study of their cluster populations. In Sections 2 and 3 we discuss the sample and observations, and in Sections 4 and 5 the data reduction and calculation of the cross–correlation function amplitudes. In Section 6 we discuss the more interesting objects individually, and in Section 7 the trends in the data as a whole, including a comparison of the environments of radio galaxies and quasars at high redshift. Section 8 presents our conclusions.

2 The sample

Our sample consists of 26 powerful radio galaxies in the redshift range 0.15 to 0.82. All have $|b| > 20°$, and spectroscopic redshifts. Ideally one would aim to study a complete sample of radio galaxies, but the constraint of having to obtain imaging primarily from the southern hemisphere (the Isaac Newton Telescope on La Palma having not completed its commissioning at the start of the project) precluded the use of the much studied Laing, Riley & Longair (1983) 3CR sample as the sole basis for our survey. Instead, we have constructed a sample comprising 17 equatorial 3CR sources (taken from both this catalogue and that of Spinrad *et al.* 1985), 8 Parkes radio sources, and an additional source from the University of Texas Radio Observatory survey: these last 9 sources were initially selected from the compilation of Véron–Cetty & Véron (1983). In selecting the sources, our primary aim was to choose the most powerful objects available at each redshift, without reference to their properties in any other waveband. The paucity of powerful objects visible from the southern hemisphere in our adopted redshift range, with good identifications and spectroscopic redshifts means that our sample contains virtually all the known galaxies with $S_{178\mathrm{MHz}} > 1$Jy and

$\delta < 0°$ meeting such criteria. High resolution mapping of southern radio sources is still very incomplete, even for the most powerful objects, and it was only possible to establish radio structures for 17 of the galaxies. Our sample thus consists of 14 FR II types, 2 FR Is, 1 compact source and 9 sources of unknown structure. Rather than restrict our sample size still further, we decided to image all the above mentioned galaxies regardless of their radio structure. Whilst there may be some optical bias in that only objects with a spectroscopic redshift could be included in our study, we believe that the sample is otherwise unbiassed with respect to optical properties. Originally the upper redshift boundary for the sample was $z = 0.6$, however, a new identification was established for 3C 263.1 during the course of the project superceding that at $z = 0.366$ (Spinrad, private comm.) and having a redshift $z = 0.824$.

Table 1 gives details of the sample, including flux densities at 178 MHz and spectral indices (generally from the compilation of Spinrad *et al.* 1985), and radio structures where known. We define the spectral index in the sense $S_\nu \propto \nu^{-\alpha}$. Radio luminosities are calculated at 178 MHz, and we will assume $H_o = 50$ $km\,s^{-1}$ Mpc^{-1}, and $\Omega_o = 0$ throughout. Photometry of the radio galaxies is presented and discussed in Section 4.3.

3 Observations

CCD observations were obtained for the sample galaxies at the Anglo-Australian, European Southern, and Cerro Tololo Inter-American Observatories. Table 2 gives the details of the telescopes and CCDs used at each observatory. Each radio galaxy was observed in the R band using a *KPNO/Mould* interference filter (central wavelength 6400Å). Table 1 indicates at which observatory each galaxy was observed. Total integration times were typically 30–40 minutes, and consisted of three or four 10 minute exposures. After each 10 minute exposure the telescope was moved 1–2 arcsecs in a random direction so as to improve sampling. Each on–source observation was accompanied by an offset frame,

Table 1. The sample.

IAU	Other	z	b°	Tel.[(a)]	S_{178} Jy	α[(b)]	$\mathrm{Log_{10}\,P_{178}}$ $\mathrm{WHz^{-1}ster^{-1}}$	Type[(c)]
0035+130	3C 16	0.405	−49.4	E	11.2	0.94	26.95	II
0035−023	3C 17	0.220	−64.8	E	20.0	0.52	26.57	I
0051−038	3C 26	0.211	−66.4	E	8.3	0.60	26.16	?
0116+082	PKS	0.594	−53.8	E	7.9	0.59	27.12	?
0211−479	PKS	0.22	−63.9	E	6.8	0.84	26.13	II
0442−184	PKS	0.281	−35.9	E	3.2	0.83	26.03	?
0511−48A	PKS	0.306	−36.0	C	16.8	0.78	26.83	II
0938−014	PKS	0.382	+36.0	C	3.3	0.67	26.32	?
0939+139	3C 225.0B	0.58	+44.0	C	21.3	0.94	27.60	II
0947+145	3C 228	0.55	+46.0	C	21.8	1.00	27.57	II
1137+169		0.204	+70.5	C	1.6	0.70	25.42	?
1140+223	3C 263.1	0.824	+73.8	C	18.2	0.87	27.89	II
1159−104	PKS	0.266	+50.4	C	6.2	0.60	26.25	?
1232+216	3C 274.1	0.422	+83.2	A	16.5	0.87	27.15	II
1239−044	3C 275	0.480	+58.0	A	14.5	0.68	27.19	II
1425−011	3C 300.1	0.308	+53.1	C	14.1	0.68	26.75	II
1452−041	3C 306.1	0.442	+46.6	A	13.5	0.90	27.11	?
1602+014	3C 327.1	0.463	+37.0	A	23.6	0.81	27.39	II
1641+173	3C 346	0.162	+35.8	E	10.9	0.52	26.03	I
1648+050	3C 348	0.154	+28.9	E	351.0	1.00	27.52	II
1934−638	PKS	0.183	−29.4	E	14.9	1.20	26.32	C
2037−029	PKS	0.192	−25.4	E	2.8	0.83	25.62	?
2120+155	3C 434	0.322	−23.7	A	4.8	0.61	26.32	II
2126+073	3C 435	0.471	−30.0	E	11.6	0.87	27.11	II
2309+090	3C 456	0.234	−46.4	E	10.6	0.69	26.37	?
2310+050	3C 458	0.289	−49.8	A	14.5	0.76	26.71	II

Notes:

(a): Telescope used. A=AAT 3.9m, C=CTIO 1.5m, E=ESO 2.2m.

(b): Spectral index defined $S_\nu \propto \nu^{-\alpha}$

(c): I=FR I, II=FRII, C=Compact.

Table 2. Observing Log.

Telescope	CCD	Pix. scale $\hat{''}$/pix.	F.O.V. arcmins	Nights
CTIO 1.5m	RCA 320×512 pix.	0.30	1.6×2.6	1986 Feb. 11–14
AAT 3.9m	RCA 320×512 pix.	0.49	2.6×4.2	1986 June 7–9
ESO 2.2m	RCA 320×512 pix.	0.36	1.9×3.1	1986 Aug. 6–10

generally about 5–10 arcmins from the source, and in a direction so as to optimize the exclusion of interfering bright foreground stars. Integration times for these offset frames were matched exactly to those of the on–source frames. This is a smaller offset than that employed by YGS (generally 1°) – our aim in these offset frames was to avoid the cluster itself, but to try to reduce the possibly large variations in the background surface density due to the presence of large–scale structure. At $z = 0.5$ for example, 1° corresponds to a metric distance of 291 Mpc in our assumed cosmology, an unnecessarily large offset. Although it is possible to use any size of offset (provided that it is greater than the angular correlation function at that magnitude), any large–scale clustering will increase the variance in the background determination (Peebles 1980). First results from faint redshift surveys such as that by Koo & Kron (1987) in *SA57* (with $\langle z \rangle = 0.24$ and a limiting magnitude $B \simeq 22$) indicate clustering on scales of 100 h^{-1} Mpc ($h \equiv H_o/100\,km\,s^{-1}\,Mpc^{-1}$), with very strong overdensities and underdensities.

In two cases (3C 327.1 and 3C 434), it did not prove possible to obtain an offset frame; Section 4.4 discusses these two cases. For all sources where the weather was not photometric (a problem largely confined to the AAT data) shorter calibration frames were taken in photometric weather at a later date so as to enable the deeper non-photometric data to be properly calibrated.

A problem worth considering in the context of this present survey is the likelihood of intercepting a low–redshift cluster of galaxies in the line of sight to a $z = 0.5$ radio galaxy, for example. The Gunn, Hoessel & Oke (1986) survey of distant clusters includes a region which they believe to be complete to $z \simeq 0.5$ and the cluster surface density is 11 per square degree to this redshift. The clusters will obviously subtend a wide range of angular diameters on the sky, depending on their redshifts, but for illustrative purposes, if we assume that the average area subtended is 0.01 deg^2 per cluster, equivalent to a circle of radius

1Mpc at $z = 0.25$, then about 10% of the sky would be covered by clusters to $z = 0.5$ (assuming no clusters overlap). If each cluster subtends the equivalent of a 1 Mpc radius at $z = 0.15$ the corresponding area covered is just over 20%.

4 Data Reduction

4.1 PRELIMINARY CCD REDUCTION

No significant secular trends in the bias levels were detected in any of the CCDs and so mean bias frames were derived for each night and used to subtract the bias offset from each exposure. The dark frames indicated that the dark–current was negligible for the three chips used. All our data frames were sky limited (with exposure time ~10 mins.) and so a master flat-field frame was created for each night by stacking 10–15 different data frames taken during that night, median filtering the resulting stacked frame, and finally normalising. Frames with particularly bright objects, or high surface densities of objects (thus reducing the sky area available for sampling) were not used in this flat–field derivation. Using this master–flat, it was possible to routinely achieve a flat–field in the data frames $\leq 1\%$ – in addition, this sky–based technique is very effective at removing fringing in the frames, a problem that was particularly evident in the data from the AAT. At this stage, the frames were given a first gentle cleaning using *FIGARO* software in batch mode, so as to remove the worst of the cosmic-ray events and fix the few bad columns; all three CCD chips used in this experiment were cosmetically very good. Finally, the individual 10 minute frames were registered and stacked.

4.2 OBJECT SELECTION

The first stage in the construction of an object catalogue for each frame is the preliminary selection of a list of candidate objects. This was done using a variant of the Image Analysis Mode (IAM) software used on the COSMOS measuring machine at Edinburgh (MacGillivray & Stobie 1984). This software produces

a catalogue of all "objects" comprising $\geq n$ pixels above a given sky threshold. x and y coordinates and a measure of the ellipticity of such objects are also calculated. Although the software also sums the pixel values for each object, resulting in a magnitude estimate, the IAM software was used solely as means of locating candidate objects, the photometry being obtained later, as described in Section 4.3. The minimum number of pixels n, and the sky threshold must be chosen so as to ensure completeness, but not so as to generate an unacceptably large number of spurious objects.

In practice, it was found that $n = 5$ pixels ($\simeq$1 arcsec at the largest pixel scale encountered here) offered the best compromise between completeness and generation of excessive spurious objects, although the aim at this stage of the analysis was always to attain over–completeness. The optimal sky level for each frame was obtained by trial: the median sky level on the frame being taken as the initial choice. A high-contrast image of the frame was displayed and about 10 objects selected at the limit of visibility to act as a check for the completeness of the computer–derived candidate object list. For frames where there were variations in the sky level across the field care was taken to choose a sample of objects well distributed across the field. After running the IAM software the resultant catalogue was examined to check that the 10 test objects had been included. If any had been excluded the sky threshold was lowered and a new candidate list obtained. In some cases all the test objects and large numbers of spurious objects were included in the trial runs and so the threshold level was correspondingly raised. In retrospect, after deriving an estimate of the completeness, used in the galaxy counting (see Section 4.4), the majority of these test objects ($\simeq 2\sigma$) were found to be $\simeq 1.5$ magnitudes fainter than this finally adopted completeness; thus we are confident that our base catalogue is deep enough to enable us to compile a complete catalogue of good signal–to–noise objects ($\geq 5\sigma$) for use in the clustering experiment.

Our photometry was zero–pointed on to the *R(Cousins)* system (hereafter R_C) using the standard stars obtained throughout the night (Graham 1982). All our data were obtained at airmasses less than 1.7, and 75% at less than 1.5; mean extinction terms were derived for each telescope. Colour terms in the R_C band are generally < 0.01 mags. and were ignored. The resultant catalogue of (x,y) positions for each object was then used in conjunction with the *FIGARO* aperture photometry software. Before any photometry was attempted, the frames were given a second cleaning, this time interactively so as to remove any remaining cosmic ray events, and flag regions affected by bad columns or pixels. Aperture photometry was obtained for every object in the catalogue (using the (x,y) positions as centroid) in a series of concentric apertures, initially ranging from 5 to 24 pixels diameter; sky measures for each object were taken from annuli of inner and outer diameters of 30 and 35 pixels. An estimate of the internal error on the magnitude is derived on the basis of the dispersion in the sky–estimate. The resulting growth curves were then examined and all objects where the flux reached a constant level were written to a file. The magnitudes thus derived are total magnitudes. All those objects where the error on the measured flux was never less than 40% in any aperture were rejected. Those objects which did not terminate at a diameter of 24 pixels were retained for further analysis.

Two factors were responsible for the flux not terminating at a diameter of 24 pixels: i) the object was larger than this, and ii) there was more than one object in the aperture i.e. two or more objects are merged. In the former case, a suitable series of larger apertures was chosen interactively and the termination diameter and total magnitude found. In the latter case, (x,y) coordinates of the merged candidates were obtained interactively, and best–bet diameters chosen as a compromise. As a final check, all photometered objects were plotted and compared by eye with the data frame to check for obvious omissions, badly

represented objects, and spurious objects. Any remaining difficulties found at this stage were fixed interactively. Whilst this visual check was extremely time-consuming it was deemed an essential one since no set of algorithms can yet produce a 100% clean catalogue, or can surpass the eye's discriminatory ability. The magnitudes derived for each field were corrected for galactic extinction, using the HI maps of Burstein & Heiles (1982) to estimate $E(B-V)$, and adopting $A_R/A_V = 0.748$ (Rieke & Lebofsky (1985)).

Whilst an accurate star–galaxy classification would obviously be desirable, there is as yet no evidence that this can be achieved in a manner free from systematic errors at the magnitudes we are primarily interested in i.e. $R_C = 21 - 23.5$. YGS attempted a star–galaxy separation as deep as $r(Gunn) = 22.5$, but their stellar number–magnitude plot (their Fig. 7) shows an alarming rise in the stellar component at $r>21.5$. The key point is that because this experiment employs offset frames to sample the background (stars and galaxies) for each source, we do not need to introduce any possibly systematic errors by attempting a star–galaxy separation, assuming that there are no gross gradients in the stellar surface density. There is a particular necessity to avoid magnitude dependent systematic errors in that our limiting magnitudes, being a function of the telescope used and the conditions, are not uniform from source to source and span some 2 magnitudes.

Furthermore, models of star–counts in our Galaxy at $R > 20$ tend to suggest that the stellar contribution to the object counts should be very small. For example, two representative fields studied in the R band by Bahcall & Soneira (1981) in the direction of the galactic centre (l = 0°, b = 50°) and the anti–centre (l = 180°, b = 50°) predict integrated surface number densities for $R \leq 23$ of 20864 and 4925 stars per deg^2 respectively. This corresponds to 33 and 8 stars per *ESO* 2.2m CCD frame, for example.

In Table 3 we present total R_C magnitudes for each of the radio galaxies,

Table 3. Optical properties of the sample.

IAU	Other	z	R_C [a]	m_{lim} [b]	Type[c]	LSB[d] features	n[e]
0035+130	3C 16	0.405	19.27	22.89	dB		1
0035−023	3C 17	0.220	19.40	22.51	gE		0
0051−038	3C 26	0.211	17.48	21.81	gE		0
0116+082	PKS	0.594	19.84	22.69	gE		0
0211−479	PKS	0.22	16.43	21.85	pec	√	1
0442−184	PKS	0.281	19.06	22.89	gE		0
0511−48A	PKS	0.306	17.92	22.47	gE	√	1
0938−014	PKS	0.382	19.33	22.35	gE		1
0939+139	3C 225.0B	0.58	19.44	22.31	dB		1
0947+145	3C 228	0.55	20.39	22.21	pec		0
1137+169		0.204	16.99	22.17	gE	√	0
1140+223	3C 263.1	0.824	20.56	22.17	gE		0
1159−104	PKS	0.266	17.56	22.16	gE	√	0
1232+216	3C 274.1	0.422	19.28	23.51	gE		0
1239−044	3C 275	0.480	20.04	22.88	gE		0
1425−011	3C 300.1	0.308	18.84	22.29	gE		0
1452−041	3C 306.1	0.442	18.51	23.68	dB	√	1
1602+014	3C 327.1	0.463	20.39	22.89	gE		0
1641+173	3C 346	0.162	17.21	22.87	gE		0
1648+050	3C 348	0.154	16.27	22.56	gE		0
1934−638	PKS	0.183	17.65	22.06	dB		1
2037−029	PKS	0.192	17.41	23.12	pec	√	0
2120+155	3C 434	0.322	19.08	23.08	gE		0
2126+073	3C 435	0.471	18.83	23.13	pec		0
2309+090	3C 456	0.234	17.90	23.16	gE		0
2310+050	3C 458	0.289	20.65	22.91	gE		0

Notes:

(a): Total *R(Cousins)* magnitude, corrected for galactic extinction.

(b): Adopted completeness magnitude.

(c): Optical morphology. gE=giant elliptical, dB=dumbbell, pec=peculiar.

(d): Low surface brightness features e.g. tails and wisps.

(e): Number of secondary nuclei within a projected radius of 19.2 kpc.

corrected for galactic extinction as described above.

4.4 COMPLETENESS

In determining the completeness of our samples we adopt a similar approach to that of YGS, estimating Δm, the difference between the completeness magnitude (m_{lim}) and the detection limit (m_{det}), the latter defined by a suitable signal–to–noise ratio. For each frame (source and offset) we calculated the magnitude of a stellar object of S/N = 5 in a 2 arcsec diameter aperture: this is the detection limit for each frame. The actual signal–noise–ratio used in deriving an estimate for the detection limit is not crucial, the only requirement being that the equivalent magnitude should be less than that of the completeness magnitude finally adopted for each field, i.e. $m_{det} > m_{lim}$. Then we derived differential number–magnitude distributions for each frame and noted the difference (Δm) between the peak of the distribution and the detection limit. In order to improve statistics, we have derived mean values of Δm for the data at each of the three telescopes, resulting in values of -0.46 mags (standard error on the mean ± 0.43) at ESO, -0.87 mags (± 0.32) at the AAT, and -0.77 mags (± 0.39) at CTIO. YGS derived a value of $\Delta m = -0.8$ mags for their data, with a detection limit defined in the same way as ours i.e. a signal–to–noise ratio of 5. In view of the errors on our values at each of the telescopes we will adopt the mean of the three values, -0.64 mag., a value not dissimilar to that estimated by YGS for their data.

The estimated completeness magnitudes, m_{lim}, for each source are given in Table 3, and in each case is the brighter of the completeness magnitudes derived individually for the source and offset frames. For sources 3C 327.1 and 3C 458 which did not have their own offset frames we had to be content with using offset frames from other sources at similar galactic latitudes. The offset frames for PKS 0442–194 and 3C 16 were used for 3C 327.1 and 3C 458 respectively, and the relevant completeness magnitudes are shown.

5 Derivation of cluster strengths

5.1 THE SPATIAL CROSS–CORRELATION AMPLITUDE (B_{gr})

LS and PP give a detailed discussion of the derivation of the amplitude of the spatial cross–correlation function B_{gr}. We here provide only a brief summary of the approach used in the analysis.

The distribution of galaxies about the radio source can be represented in terms of the spatial cross–correlation function

$$n(r)dV = \rho[1 + \xi(r)]dV \tag{1}$$

where $n(r)$ is the number of galaxies in volume element dV, distance r from the radio source, and ρ is the mean number density of galaxies. We will take the spatial cross–correlation function in the usual form

$$\xi(r) = B_{gr}\left(\frac{r}{Mpc}\right)^{-\gamma} \tag{2}$$

where B_{gr} is the amplitude of the cross–correlation function about the radio–galaxy. We will take $\gamma = 1.77$ (Groth & Peebles, 1977), noting that PP demonstrate that the results are in fact insensitive to an incorrect choice of γ, providing $\gamma \sim 2$ for all the sources. In this present experiment we will assume that there is no evolution in γ with redshift. YG studied the slope of the cross–correlation function for their quasar sub–samples with mean redshifts $\langle z \rangle = 0.42$ and 0.65, and obtained values of γ comparable to that seen at zero–redshift, indicating that this assumption of no evolution is reasonable.

LS showed that if the spatial correlation–function is of the above form, and assuming spherical symmetry about the radio–source, then at redshift z this will result in an observed angular correlation

$$w_z(\theta) = A_{gr}(z)\left(\frac{\theta}{deg.}\right)^{-(\gamma-1)} \tag{3}$$

where

$$A_{gr}(z) = H(z)B_{gr}. \tag{4}$$

$H(z)$, the conversion function, is calculated for a given galaxy luminosity function at the required redshift z and A_{gr} is calculated from the observed data (as shown in Section 5.2). The key points in this analysis are that i) the use of the correlation function allows us to statistically account for unrelated field galaxies, and ii) that the conversion function $H(z)$ takes into account the effect the different magnitude limits have on the observability of clustering as a function of redshift.

5.2 CALCULATION OF A_{gr}

Equation (3) indicates that A_{gr} can be related to observables via the two–dimensional correlation function

$$N(\theta)d\Omega = N_g[1 + w(\theta)]d\Omega \tag{5}$$

where $N(\theta)d\Omega$ is the number of galaxies in solid angle $d\Omega$ at angular distance θ from the radio galaxy and N_g is the average surface density of galaxies. From equations (3) and (5) we have

$$\int N(\theta)d\Omega = \int N_g d\Omega + N_g A_{gr} \int \theta^{-(\gamma-1)} d\Omega \tag{6}$$

which we will write as

$$N_{obs} = N_{bc} + N_g A_{gr} J. \tag{7}$$

N_{obs} is the total number of objects observed in the source frame and N_{bc} the number of objects in the offset frame. N_g is derived from the offset frame and J is the integral of the correlation function over the area of the source frame. We estimate $N_t = N_{obs} - N_{bc}$ objects to be associated with the radio galaxy and so

$$A_{gr} = \frac{N_t}{N_g J} \tag{8}$$

Note that this calculation results in an A_{gr} that is dimensionless. In cases where unequal areas were counted on the source and offset frames (e.g. due to the exclusion of areas contaminated by very bright stars) the values of N_{obs} and N_{bc} must be normalised.

Ideally, one would aim to study the environments of the radio galaxies out to a standard metric radius, 1 Mpc for example. This is not really practical over the large redshift range studied here ($0.15 < z < 0.82$) without a large investment of telescope time for the lower redshift objects so as to match the proper areas sampled at the higher redshifts. The range of areas sampled varies from 0.28 Mpc^2 for 3C 348 to 2.45 Mpc^2 for 3C 275. In order to make the best use of the data we have calculated N_{obs} over the largest area available in each case *i.e.* the whole CCD frame. PP compare values of A_{gr} for their Lick composite sample, calculated using counting radii of 1° and 1 Mpc respectively. The sample covers the redshift range 0.01–0.15 and there are no strong systematic differences between the two sets of A_{gr} values. Their 1° sampling radius encompasses about 10 times the proper area at $z = 0.15$ as at $z = 0.01$, similar to the range of proper areas encountered in this present work.

5.3 THE CONVERSION FUNCTION $H(z)$

The conversion function $H(z)$ is given by LS

$$H(z) = \frac{I_\gamma}{N_g} \left(\frac{D}{1+z} \right)^{3-\gamma} \Phi(m_{lim}, z) \tag{9}$$

I_γ is a definite integral, with the value 3.78 for $\gamma = 1.77$, and D is the comoving distance to the source. Equation (3) shows that the dimensionless value of A_{gr} derived from equation (8) must be multiplied by the appropriate factor $\theta^{-(\gamma-1)}$ before the value of B_{gr} is calculated using $H(z)$ in equation (4). These are the

A_{gr} values that will be tabulated in Table 6. B_{gr} will have units Mpc$^{\gamma}$. N_g is the average surface number density of galaxies to the limiting magnitude m_{lim}: we have used the galaxy counts of YGS to estimate this number. These galaxy counts are presented in the *r(Gunn)* band and so we have transformed them to the R_C band using the transformation between the Thuan & Gunn and Cousins systems derived by Bessell (1986)

$$(V-R)_C = 0.290 + 0.586(g-r) + 0.060(g-r)^2 \qquad (10)$$

and galaxy colours from Sebok (1986). Finally, $\Phi(m_{lim}, z)$ is the integral number of galaxies per unit volume which at redshift z are observed to be brighter than m_{lim}. This quantity is the most uncertain component of the conversion function, since it is dependent on our choice of cosmology (H_o, Ω_o), the normalization (ϕ^*), slope (α) and characteristic magnitude (M^*) of the luminosity function, the morphological mix, and the K– and evolution corrections associated with each morphological type.

We adopt a different approach to that employed by YG, who attempted to derive self–consistent estimates of the shape of the luminosity function by using the galaxies associated with their quasars. Since our primary aim is to to detect clustering, rather than to attempt to address the more difficult question of the evolution of the luminosity function, we prefer to assume comparatively secure zero–redshift parameters for the luminosity function and couple this with the best current estimates of how the galaxies are likely to evolve with redshift (via the use of suitable K– and evolution corrections). YG had a significantly larger number of quasars than we have radio galaxies but nevertheless, they could not tightly constrain the derived values of M^* – they suggest $\simeq$0.5 mag. evolution in M^* from $z = 0$ to $z = 0.6$, but the error bars are very large and the precise values are strongly dependent on the assumed cosmology and zero–redshift luminosity functions. Using M^* as a probe of luminosity evolution, a

standard candle in effect, must be a very inefficient method given i) the difficulty of obtaining a standard value (if such a thing is meaningful) at zero–redshift, and ii) the statistical nature of this experiment where no redshifts or colours are available for the presumed cluster members.

We have therefore chosen two local luminosity functions from the literature, those presented by Sebok(1986) and King & Ellis (1985), the latter derived from the Durham/AAT redshift survey. We will refer to these as Models 1 and 2 respectively. Table 4 lists the parameters for each luminosity function. These two luminosity functions are discussed by YG who present values for the characteristic magnitudes M^* for the *r(Gunn)* band – we have derived the equivalent R_C values using the transformation given above.

We have taken K– and evolution corrections for each morphological type from the recent spectral synthesis models of Guiderdoni & Rocca–Volmerange (1987, hereafter GRV). These models offer several important improvements over the widely used models of Bruzual (1983), and are calculated for a range of eight star–formation histories corresponding to morphological types E (two models), S0, Sa, Sb, Sc, Sd and Im. They are ideal for this present work where we would like to be able to account for the different rates of evolution relevant for each component of the luminosity function. The reader is referred to GRV for a full description of the models, and we confine ourselves here to a brief discussion of the key features.

The models employ stellar tracks from the four main stages of stellar evolution: the main–sequence, the giant branch, the horizontal branch (HB) and the asymptotic giant branch, the latter stage being omitted from Bruzual's models. Thirty stellar spectra are used, covering the wavelength range 220Å to 10680Å at a resolution of 10Å, and thus offer a higher resolution than those used by Bruzual (typically 20–50Å). It has been widely appreciated that his models do not satisfactorily accommodate the far–UV region of the spectrum

Table 4. Luminosity functions.

Both models are of Schechter (1976) form.

MODEL 1
Sebok (1986)

Luminosity function slope: $\alpha = -1.2$
Morphological types: E, Sa, Sc, Im.

	Normalisation ϕ^* $10^{-3}\,\mathrm{Mpc}^{-3}$	$M^*_{R_C}$
E	1.53	−22.32
Sa	1.46	−21.04
Sc	5.26	−20.78
Im	5.00	−19.69

MODEL 2
Durham/AAT, King & Ellis (1985)

Luminosity function slope: $\alpha = -1.0$
Morphological types: E, Sb, Sd.

	Normalisation ϕ^* $10^{-3}\,\mathrm{Mpc}^{-3}$	$M^*_{R_C}$
E	1.786	−22.49
Sb	3.74	−21.98
Sd	3.24	−21.30

of E/S0s, resulting in low–redshift galaxies that are too red (and consequently high–redshift galaxies that are too faint); his stellar spectra generally have zero flux at $\lambda < 2000$Å for types F0 and later, and the giant branch used was too strong at late epochs. Although Bruzual attempted to remedy the situation by adding an *ad hoc* population of horizontal branch stars, Rocca–Volmerange & Guiderdoni (1987) have recently used the *IUE* stellar atlases to analyse the far–UV component in a number of E/S0s, and conclude that the HB contribution at 2000Å is in fact very small; the UV–excess, when it exists at all is produced by current star formation. The models of GRV also include contributions from nebular emission and the effects of internal extinction.

Three parameters describe the course of the evolution: i) the star formation rate (essentially the variation in timescale for the conversion of gas into stars), ii) the IMF, and iii) the galaxy age. GRV adopt Scalo's (1986) observational IMF rather than the steeper model of Salpeter (1955) adopted by Bruzual. The star formation histories are characterised by a star formation rate $\tau_*(t)$, and a timescale of gas consumption t_*. Table 5 shows the star formation laws which GRV associate with each morphological type, where $g(t) = M_{gas}(t)/M_{tot}$, the gas fraction as a function of time. There are two E/S0 models, designed to fit the range of far–UV behaviour seen in low–redshift ellipticals, from the "UV–hot" types characterised by M87 to the "UV–cold" types characterised by NGC 4382.

Using the software kindly made available by the authors we have calculated observed R_C band K– and evolution corrections for a model with a galaxy formation redshift $z_F = 5$: this corresponds to a galaxy age of 16.3 Gyr in the $H_o = 50 \mathrm{km\,s^{-1}\,Mpc^{-1}}, \Omega_o = 0$ cosmology adopted here. For the ellipticals, we have averaged the E(UV–hot) and E(UV–cold) models, a reasonable procedure because these two models straddle the range of properties observed in low–redshift ellipticals. In Table 5 we give the coefficients for the polynomial fits derived for these corrections as a function of redshift. The corrections are

Table 5. K and evolution corrections.

Spectral synthesis models of Guiderdoni & Rocca–Volmerange (1987).
Redshift of formation z_F=5.
$H_o = 50\,km\,s^{-1}\,Mpc^{-1}, \Omega_o = 0$
Age of galaxy: 16.3 Gyr.

Star formation histories:

	$\tau_\star(t)$ Star formation rate	$t_\star$(Gyr) Gas consumption timescale
UV–cold E/S0	1exp–t	1.0
UV–hot E/S0	0.37exp–0.37t	2.7
Sa	$0.3g(t)$	3.0
Sb	$0.2g(t)$	4.5
Sc	$0.1g(t)$	9.1
Sd	0.048	13.2
Im	$4.0.10^{-4}t^2$	16.8

$$g(t) = M_{gas}(t)/M_{tot}$$

Polynomial coefficients:
$R(z) - R(0) = a + bz + cz^2 + dz^3 + ez^4 + fz^5$
Fit good for $0 < z < 1.0$

	E/S0	Sa	Sb	Sc	Sd	Im
a	−0.221	−0.142	−0.038	0.095	−0.093	−0.009
b	5.604	3.462	1.036	−2.324	2.253	−0.145
c	−29.610	−18.814	−4.220	1.229	−11.322	−0.726
d	70.985	50.009	13.883	−2.426	32.368	4.645
e	−69.448	−52.157	−16.185	2.925	−35.456	−6.132
f	24.390	19.040	6.376	−1.212	13.459	2.562

Note:
E/S0 model is the average of the UV–hot and UV–cold models.

given in the form adopted by Bruzual i.e. $R(z) - R(0)$, the difference in absolute magnitude to be assigned to a galaxy at redshift z compared with one at zero–redshift, due to the *combined* effects of the K–correction and evolution. The corrections show several inflections as a function of redshift, necessitating a moderately high order of fit.

5.4 B_{gr} VALUES

In Table 6 we present the A_{gr} values for each object, and the resultant B_{gr} values for each of the two luminosity function models. The errors have been calculated assuming Poisson statistics, where the error on the number of objects assumed to be associated with the radio galaxy (N_t) is $\sqrt{2}\sqrt{N_{bc}}$. This is used to derive an estimate of the error on A_{gr} and consequently on B_{gr} via the conversion function $H(z)$. It is important to note that this error refers only to the galaxy counts, and excludes the error due to uncertainties in our knowledge of $H(z)$. Thus the real errors are likely to be larger than the formal values quoted here. The differences in B_{gr} values for the two models are quite substantial, Model 2 (the Durham/AAT model) tending to produce lower amplitudes than Model 1 (Sebok 1986). The Durham/AAT luminosity function is both flatter than Sebok's, and has brighter characteristic magnitudes ($M^*_{R_C}$). Consequently, at redshift $z = 0.6$, for example, the Durham/AAT luminosity function predicts nearly twice the number of galaxies per unit volume for any given limiting magnitude than Sebok's model, thus reducing the calculated amplitudes.

At this point it is worth examining the effect our chosen cosmology has on the calculated values of B_{gr}, in particular our choice of Ω_o. The two cosmologically dependent factors in the conversion function (equation (9)) are the distance term $(D/1+z)^{3-\gamma}$, and the integrated luminosity function term, Φ. As an illustration, we will compare the size of these terms in $\Omega_o = 1$ and 0 cosmologies (the latter being the chosen cosmology in this present work) at $z = 0.45$. At this redshift, the adoption of $\Omega_o = 1$ results in a distance term which is 13% larger than that

Table 6. B_{gr} values.

IAU	Other	z	A_{gr} /10^{-2}	MODEL 1 B_{gr}	MODEL 1 ΔB_{gr}	MODEL 2 B_{gr}	MODEL 2 ΔB_{gr}
0035+130	3C 16	0.405	2.26	138	59	147	63
0035−023	3C 17	0.220	0.42	11	16	21	30
0051−038	3C 26	0.211	−1.80	−48	29	−70	41
0116+082	PKS	0.594	1.72	334	181	154	104
0211−479	PKS	0.22	4.03	113	33	159	46
0442−184	PKS	0.281	2.78	91	27	157	47
0511−48A	PKS	0.306	1.33	52	21	67	27
0938−014	PKS	0.382	−0.52	−32	35	−29	31
0939+139	3C 225.0B	0.58	0.13	27	115	11	54
0947+145	3C 228	0.55	1.80	290	119	147	58
1137+169		0.204	0.00	0	17	0	30
1140+223	3C 263.1	0.824	0.69	117	130	191	212
1159−104	PKS	0.266	−0.26	−9	20	−12	25
1232+216	3C 274.1	0.422	1.71	83	37	120	53
1239−044	3C 275	0.480	2.70	210	54	184	48
1425−011	3C 300.1	0.308	2.53	103	25	122	30
1452−041	3C 306.1	0.442	2.92	154	37	222	55
1602+014	3C 327.1	0.463	−1.08	−96	48	−80	41
1641+173	3C 346	0.162	0.97	23	16	64	46
1648+050	3C 348	0.154	0.23	5	15	14	38
1934−638	PKS	0.183	0.47	12	21	21	38
2037−029	PKS	0.192	0.15	4	11	10	29
2120+155	3C 434	0.322	0.31	13	29	20	43
2126+073	3C 435	0.471	1.35	97	42	97	43
2309+090	3C 456	0.234	0.14	4	19	9	44
2310+050	3C 458	0.289	−0.76	27	23	−44	37

for $\Omega_o = 0$, and a luminosity function term 20% larger. The calculated B_{gr} scales as the reciprocal of the distance term, and as $1/\Phi$ (equation (4)). Thus an $\Omega_o = 1$ cosmology will produce values of B_{gr} that are $\simeq 30\%$ smaller than those under $\Omega_o = 0$, although the precise difference is a function of redshift.

To get a feel for the strengths of clustering implied by the values of B_{gr} shown in Table 6, we can refer to the amplitudes of the cross–correlation function which PP obtained for a sample of 107 Abell clusters. They derived mean values of B_{gr} for richness classes 0, 1 and 2 of 114, 272 and 388 respectively. Because the Abell clusters are at low redshift, these values will not be strongly dependent on the form of the conversion function ($H(z)$) used, and so provide a good benchmark.

We will discuss the trends in the data as a whole in Section 7 after a brief discussion of the more interesting galaxies.

6 Interesting objects and their morphologies

Greyscale representations of the radio galaxies and their immediate environments are shown in Figs. 1(a)–(z).

6.1 NOTES ON SPECIFIC OBJECTS

Although tentative suggestions of clusters around distant radio galaxies are legion, the basis for these claims has often been founded on evidence no more substantial than the presence of other faint galaxies in the field of view. Here we discuss some of the more interesting objects in our sample.

3C 16. (Fig. 1(a)). This source was identified by Riley, Longair & Gunn (1980) who noted the fainter companion to the south–east. This dumbbell galaxy is in one of the richest environments observed in our sample.

PKS 0116+082. (Fig. 1(d)). Spinrad *et al.* (1975) obtained a deep 4m plate of this galaxy, noting that it is much brighter than the surrounding galaxies and so

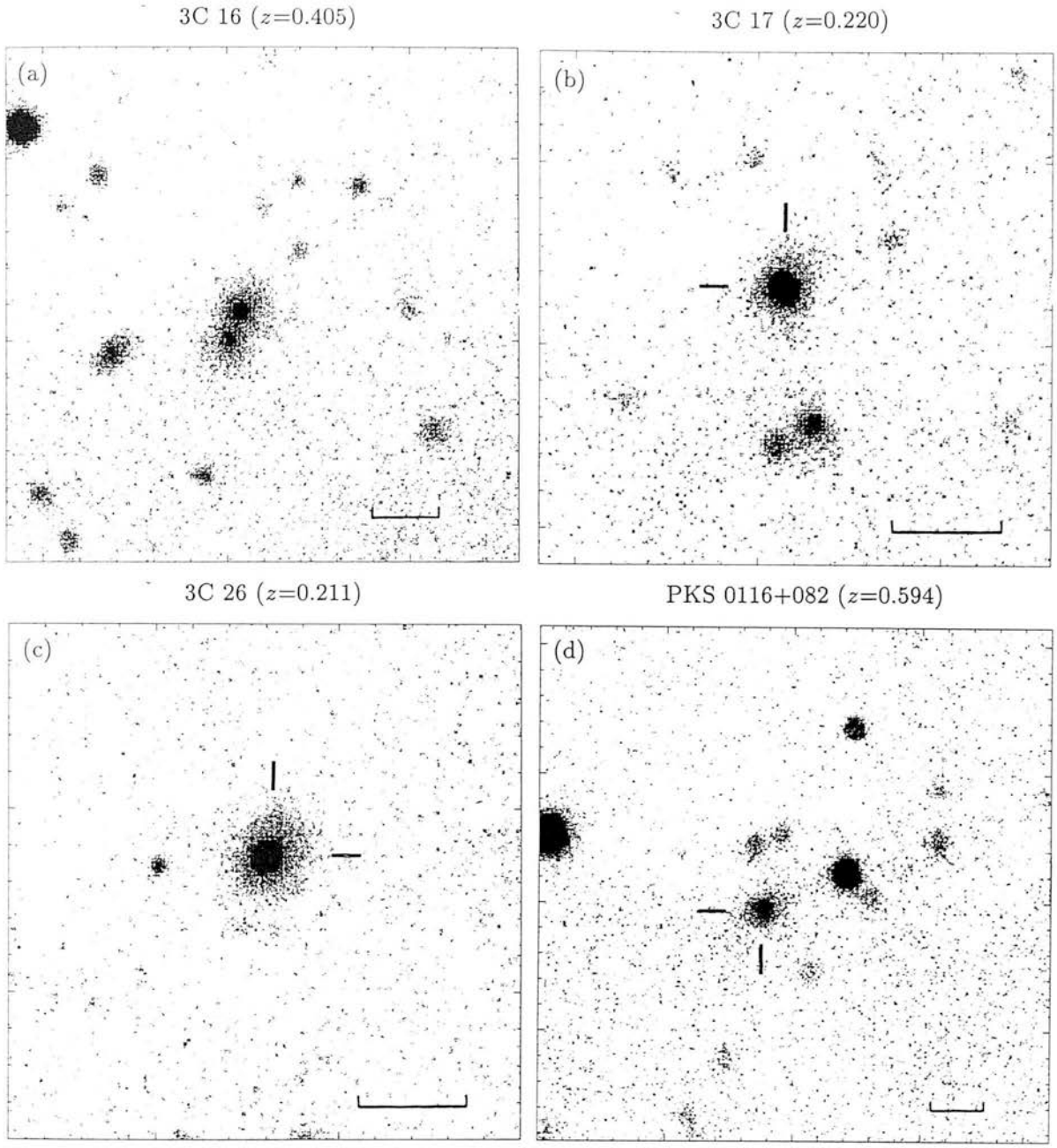

Figure 1 (a)–(z). Greyscale representations of the radio galaxies imaged in this survey. North is at the top and east at the left. The horizontal bar indicates 50 kpc at the redshift of the radio galaxy ($H_o = 50\,\mathrm{km\,s^{-1}\,Mpc^{-1}}$, $q_o = 0$).

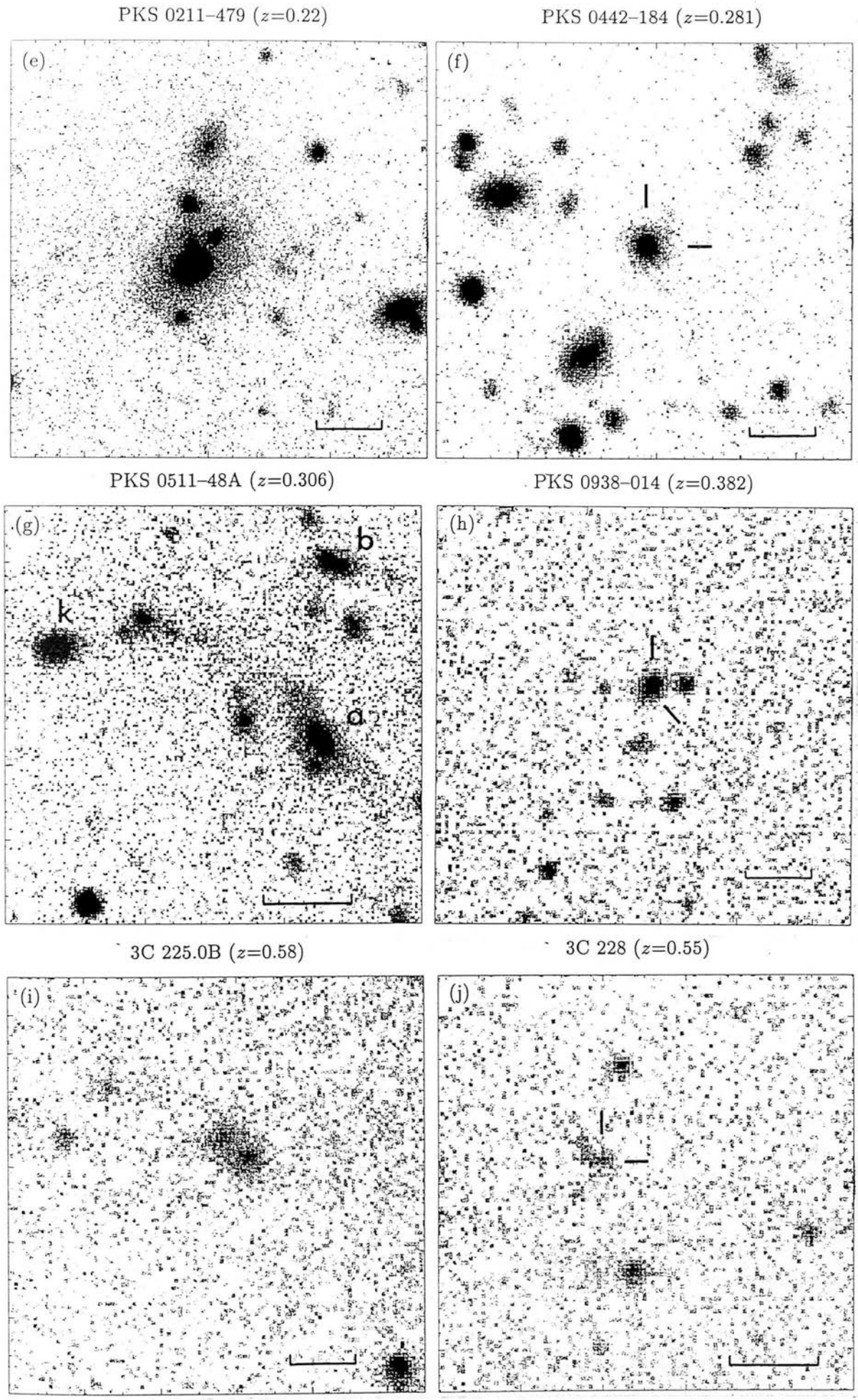

Figure 1 – *continued.*

1137+169 (z=0.204)

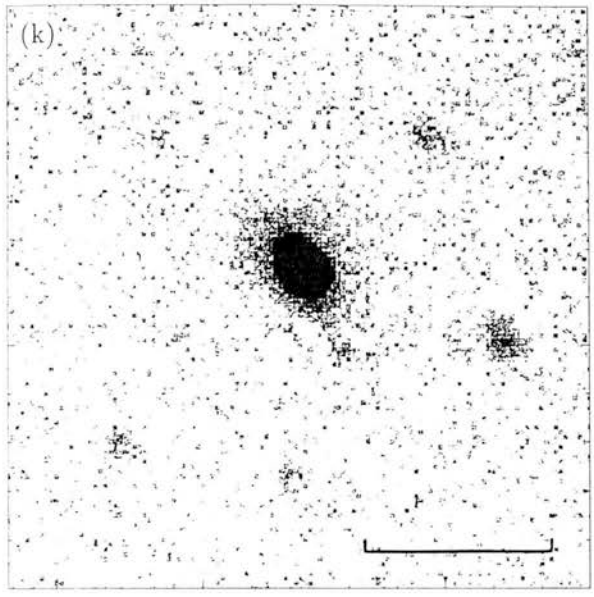

3C 263.1 (z=0.824)

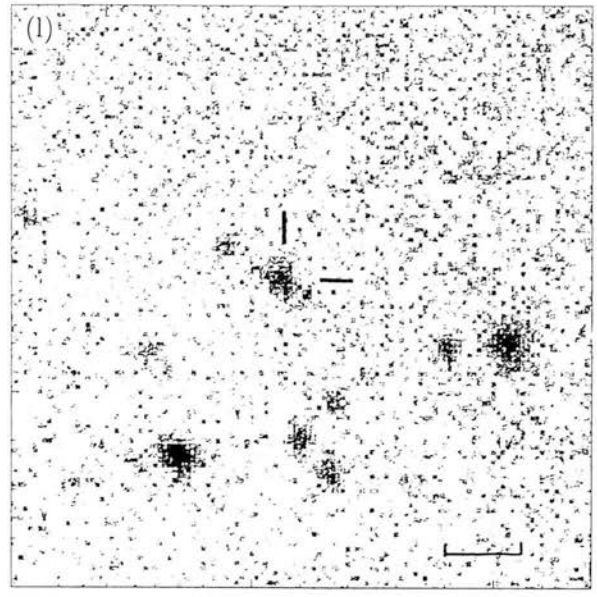

PKS 1159–104 (z=0.266)

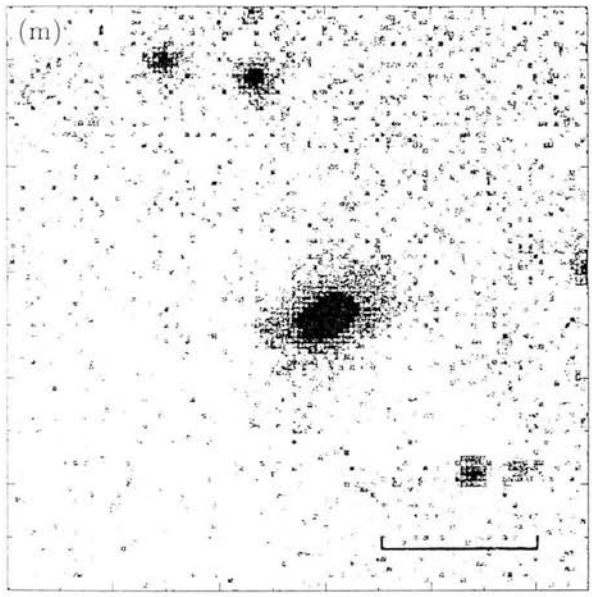

3C 274.1 (z=0.422)

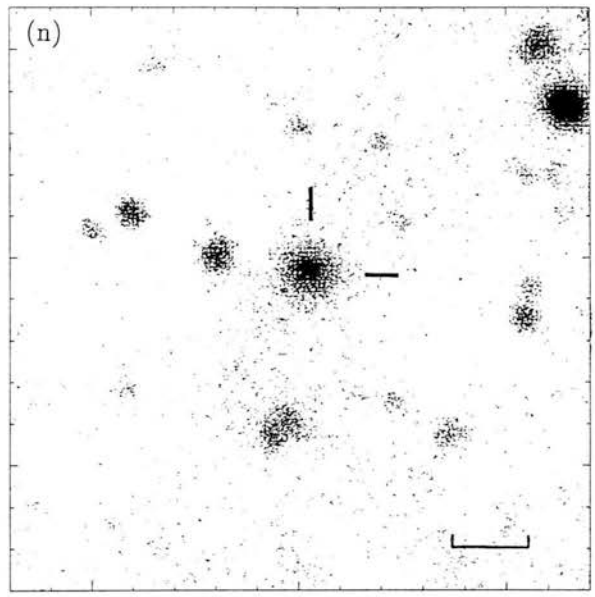

3C 275 (z=0.480)

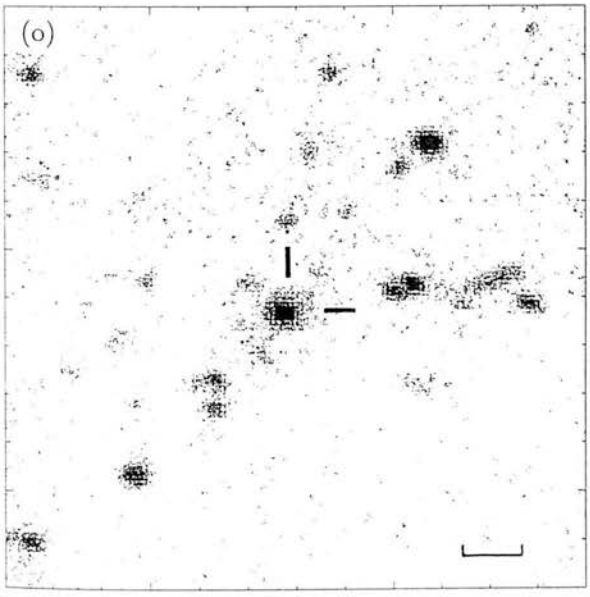

3C 300.1 (z=0.308)

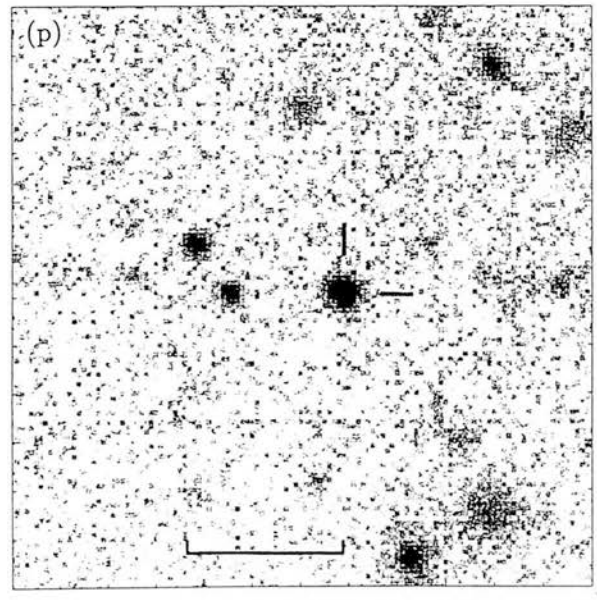

Figure 1 – *continued.*

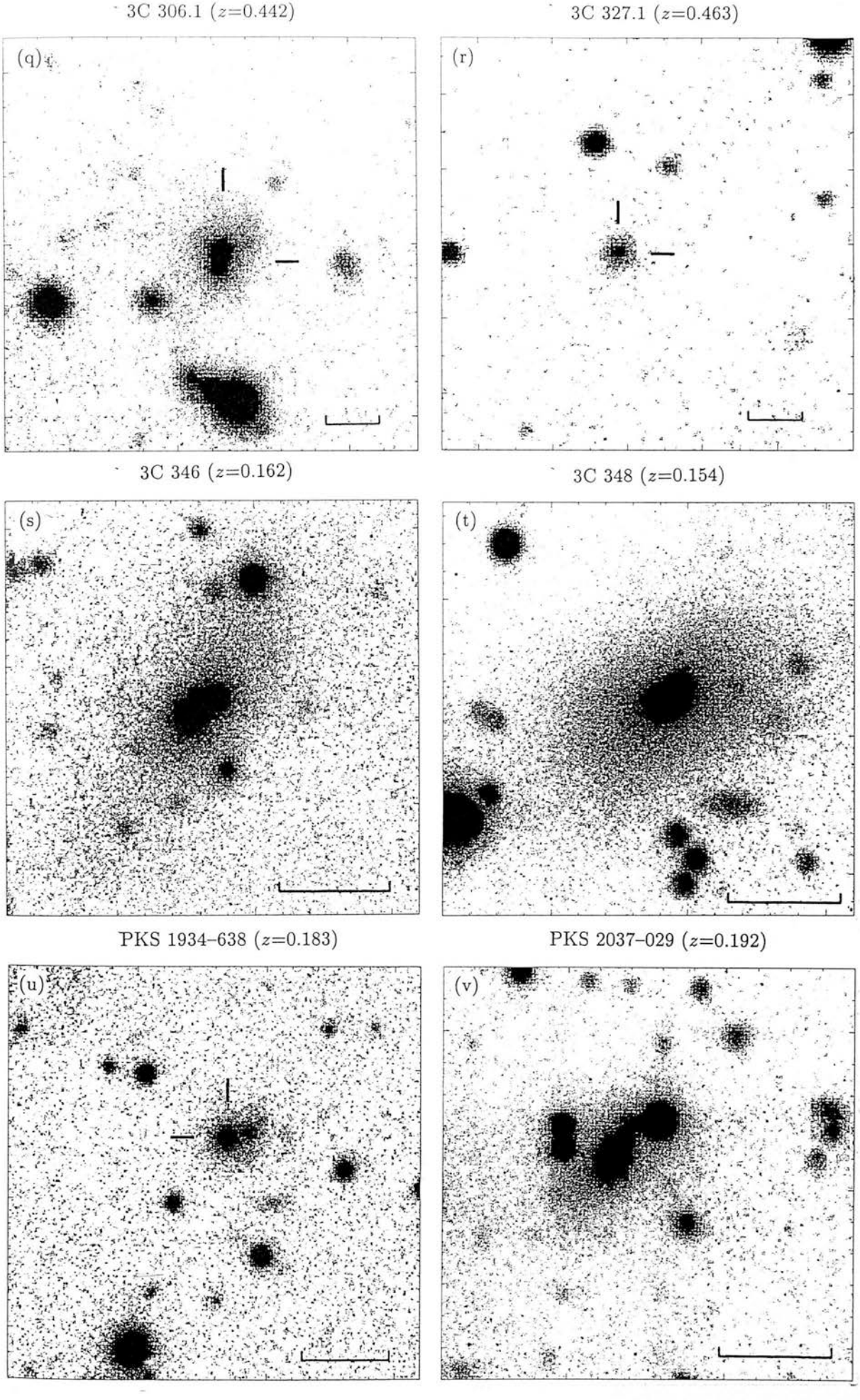

Figure 1 – *continued.*

3C 434 (z=0.322)

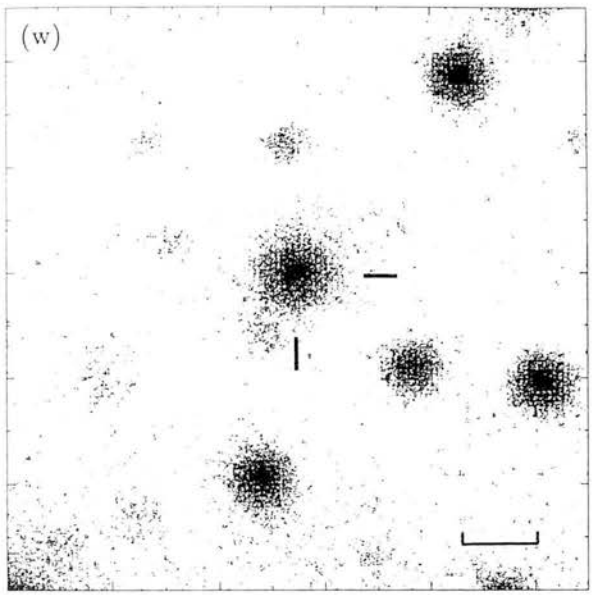

3C 435 (z=0.471)

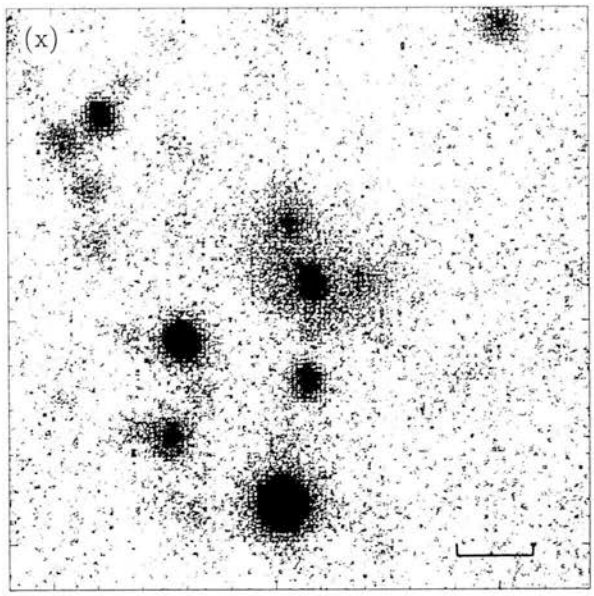

3C 456 (z=0.234)

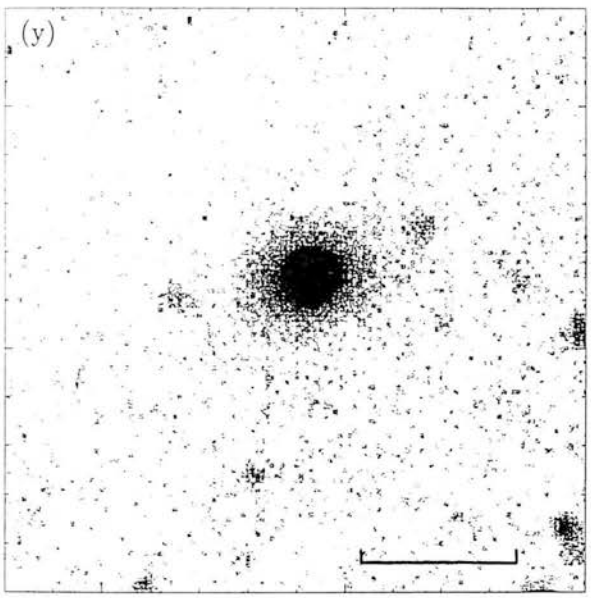

3C 458 (z=0.289)

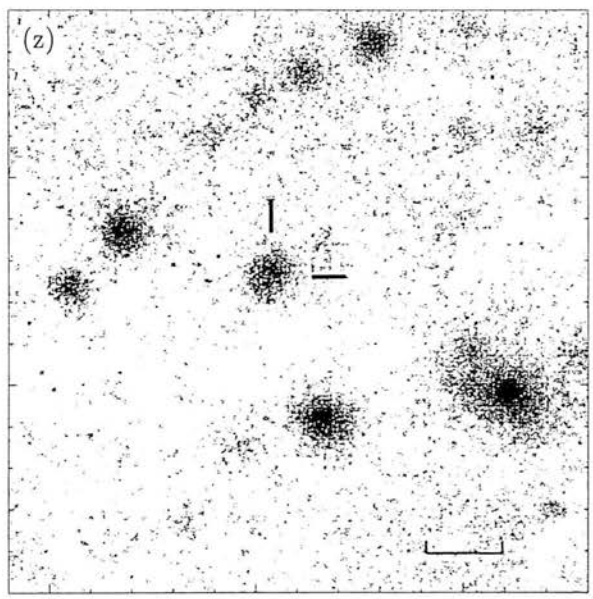

Figure 1 – *continued.*

is presumably in a Bautz–Morgan type I cluster. The cluster is certainly very rich, having having the largest B_{gr} value in our sample.

PKS 0211-47. (Fig. 1(e)). This source was identified by Tritton & Schilizzi (1973) who observed that there are many faint galaxies in the field – its B_{gr} value indicates an Abell class 0 cluster.

PKS 0442-184. (Fig. 1(f)). Spinrad, Kron & Hunstead (1979) first identified this source and noted the presence of a cluster, in agreement with our B_{gr} value of 91 (Model 1).

PKS 0511-48A. (Fig. 1(g)). Smith & Robertson (1985) have made a comprehensive study of this complex source. They proposed that the filament extending from source 'a' is tidal in origin, spectroscopy indicating a rotation velocity of at least $250\,\mathrm{km\,s^{-1}}$ with respect to the parent galaxy. They could not see a double nucleus in their imaging and suggested that the interloper responsible for the disturbance could have already merged or that the nuclei are too small to be resolved – there is an object visible to the south of the main galaxy in our image, although it is not clear whether this is responsible for the observed distortions. Component 'b' (to the north–west) is a late–type spiral at $z = 0.21$ and so is not a member of the cluster. Weak [OIII] $\lambda\lambda 4959, 5007$ and [OII] $\lambda 3727$ emission was detected from the brightest knot 'k' at the end of the tail, and they suggest that the three knots here may be H II regions. The source is in a moderately rich cluster, Abell class 0.

1137+169. (Fig. 1(k)). From an image–tube observation of this source, Wills & Wills (1979) noted a seeing limited nucleus ($\simeq$ 2 arcsecs) with extensions to the north–east and south–west, apparent in our image. This object is in a rather poor environment.

3C 274.1. (Fig. 1(n)). Kristian, Sandage & Katem (1978) obtained a 200–inch red plate of this source, allowing them to make a tentative identification;

they suggested that this source may be in a cluster. Later imaging by Laing *et al.* (1978) (object 'B' in their notation) confirmed this suggested identification. Most of the faint galaxies in our image are invisible on Laing *et al's* 200–inch frame.

3C 275. (Fig. 1(o)). This source was identified by Kristian, Sandage & Katem (1974) who commented that there was clearly a very distant cluster in the area. 4m imaging by Spinrad, Kron & Hunstead (1979) seemed to confirm this claim – our value of $B_{gr} = 210$ (Model 1) is consistent with these assertions, and our image shows confirms that this region is indeed very rich.

3C 327.1. (Fig. 1(r)). First correctly identified by McEwan, Browne & Crowther (1975), although Kristian, Sandage & Katem (1978) were unaware of this and tentatively proposed this object as a new identification, suggesting that it may be in a cluster. Our value of $B_{gr} = -96$ (Model 1) does not support this latter suggestion, and there are few faint galaxies near the radio galaxy in our image.

3C 346. (Fig. 1(s)). Although Wyndham (1966) suggested that many nearby diffuse objects may be cluster members, our value of $B_{gr} = 23$ (Model 1) does not identify this as a particularly rich region. Although there appears to be a contaminating star to the north–west of the nucleus, there is no star apparent on the less saturated Palomar Observatory Sky Survey plate.

3C 348 (=Her A). (Fig. 1(t)). This famous cD has a contaminating star 3.3 arcsecs to the north–west of the galaxy (Maltby, Matthews & Moffett 1963). Greenstein (1962) noted that "the field is rich in much fainter extragalactic nebulae" and Matthews, Morgan & Schmidt (1964), examining the Palomar Observatory Sky Survey (POSS) plates claimed that it was located in a very faint cluster of richness class 2. Our value of $B_{gr} = 5$ (Model 1) indicates that the radio galaxy is not in a particularly rich region. Examination of the POSS does show many faint objects in the area but they are by no means concentrated

towards the radio galaxy.

PKS 1934-638. (Fig. 1(u)). This source was one of the first observed to have a low frequency cut–off due to synchrotron self–absorption (Kellerman 1966). Penston & Fosbury (1978) suggested that the galaxy is crossed by a dust lane, in the manner of Centaurus A. However, Jauncey *et al.* (1986) obtained CCD imaging and spectroscopy of the two components, and argue that they are two separate objects rather than a single one crossed by a dust–lane, an interpretation that our imaging would seem to favour. The compact radio source is unequivocally associated with the brighter eastern component ('A' in their notation) again arguing against the dust–lane hypothesis. Spectroscopy by Fosbury *et al.* (1987) of the two components indicates that they have a velocity difference of $\simeq 900\mathrm{km\,s^{-1}}$, suggesting that a close gravitational encounter is occurring. The radio galaxy is in a region of only average galaxy density, however.

3C 434. (Fig. 1(w)). Longair & Gunn (1975) noted that there were several other galaxies of comparable magnitude to 3C 434 in the field, and that it was probably in a rich cluster. Our value of $B_{gr} = 13$ (Model 1) indicates that although there are faint galaxies visible, the region is not particularly rich.

3C 435. (Fig. 1(x)). This galaxy has two close companions which would appear to share a common envelope with the radio galaxy.

6.2 MORPHOLOGIES AND MULTIPLE NUCLEI

Rather than attempt an over–elaborate zoological classification of our radio galaxies, we have classified them according to one of three broad types: giant ellipticals (gE), dumbbells (dB) and peculiar objects (pec). We classify a galaxy as a giant elliptical if it is generally characteristic of the E and D types defined by Matthews, Morgan & Schmidt (1964) – Her A (3C 348) imaged in this present study is a classic example. All cD type galaxies are included in this category. For the moment we ignore all low–surface brightness features such as wisps and

tails (c.f. Heckman *et al.* 1986) and faint companions if they do not appear to drastically alter the basic elliptical morphology of the primary. Dumbbell galaxies are characterised by two components of fairly comparable luminosity sharing a common envelope (Matthews, Morgan & Schmidt 1964). 3C 16 is a good example in this present study. Finally, objects which do not fit into either of these two categories (such as 3C 435 which is clearly an object consisting of three components) are classified as peculiar. Table 3 shows the class assigned to each galaxy in our sample. We have adopted this broad classification in order to realistically test the claim of Heckman *et al.* (1986) that many powerful radio galaxies are not normal ellipticals.

In addition, we have re–considered those galaxies broadly classified as gE and looked for any evidence of low–surface brightness tails, wisps, and other peculiarities. The presence of such features is indicated by a ($\surd$) sign in Table 3. Because of the large redshift range encompassed by our sample, this classification must be extremely subjective since there will be a strong bias towards the detection of low surface brightness features in the low–redshift objects. We have also examined the galaxies for multiple nuclei, and in Table 3 indicate the number of secondary nuclei within a projected radius of 19.2 kpc at the radio galaxy. This fiducial sampling radius (γ) was chosen by Gunn & Oke (1975) to measure their structural parameter α (the slope of the logarithmic growth curve of integrated luminosity at radius γ) and has also been used in the study of multiple nuclei by Hoessel (1980) and Lilly & Prestage (1987) amongst others. We discuss the general morphological trends in Section 7.4.

7 Discussion

7.1 GENERAL TRENDS

In Figs. 2 (a) and (b) we plot values of B_{gr} against redshift for our 26 radio galaxies, using Models 1 and 2 respectively. In Figs. 3 and 4 we plot B_{gr} against

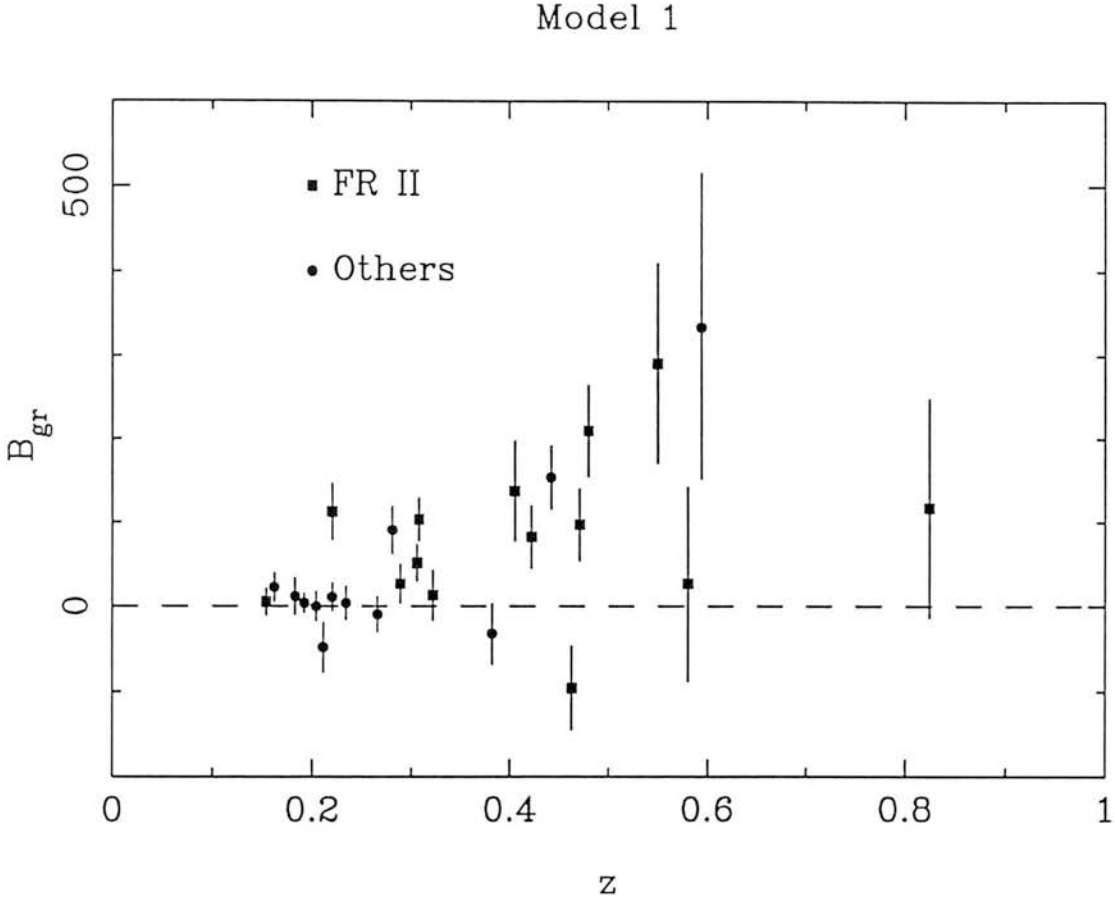

Figure 2(a). The amplitude of the cross–correlation function, B_{gr}, calculated under Model 1 (Sebok 1986), against redshift.

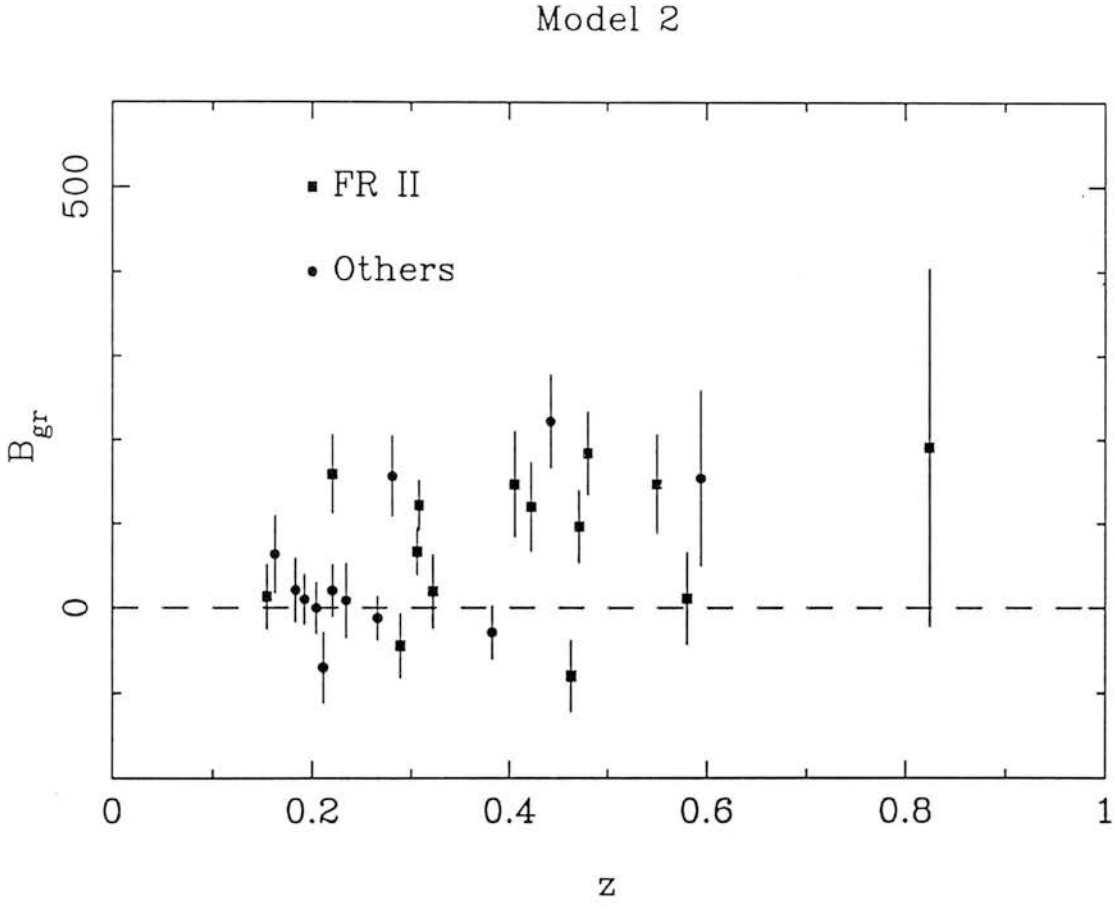

Figure 2(b). The amplitude of the cross–correlation function, B_{gr}, calculated under Model 2 (King & Ellis 1985), against redshift.

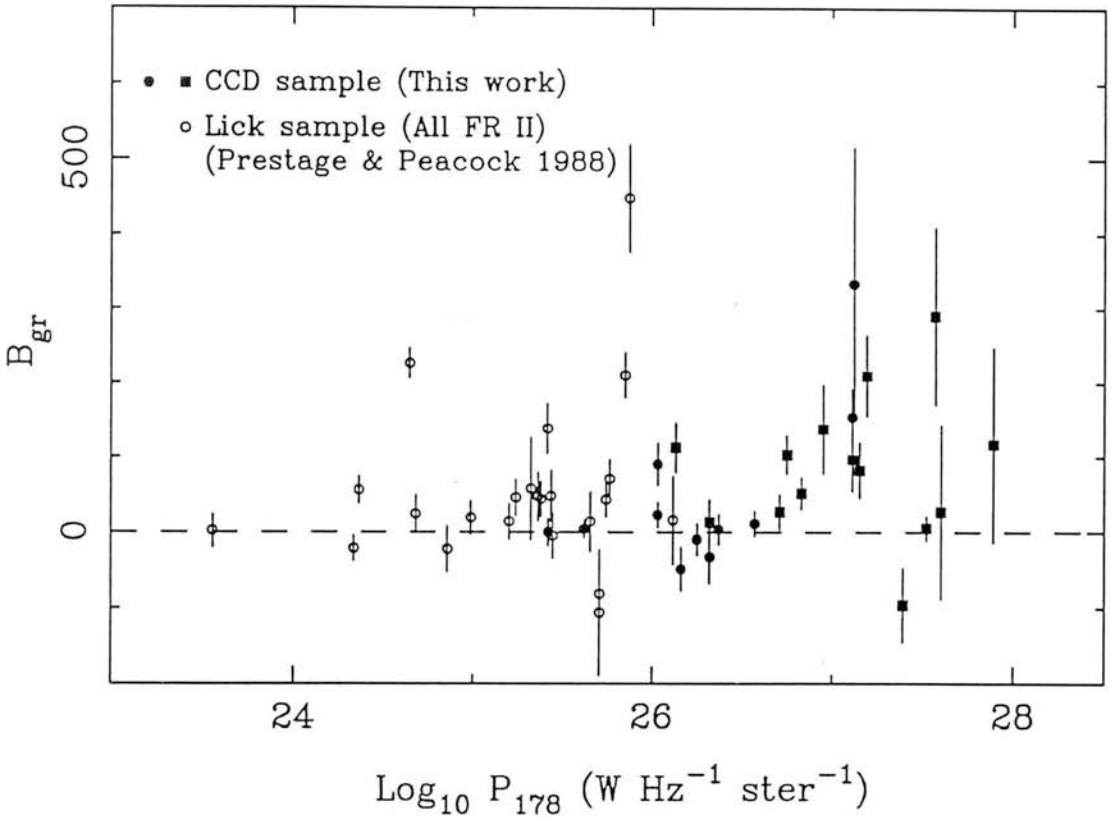

Figure 3. B_{gr} (Model 1) against radio luminosity at 178 MHz for our 26 galaxy sample, and 23 low–redshift FR IIs from the work of Prestage & Peacock (1988). Members of the CCD sample which are of FRII type are shown as filled squares, and those which are FRIs or of unknown type as filled circles.

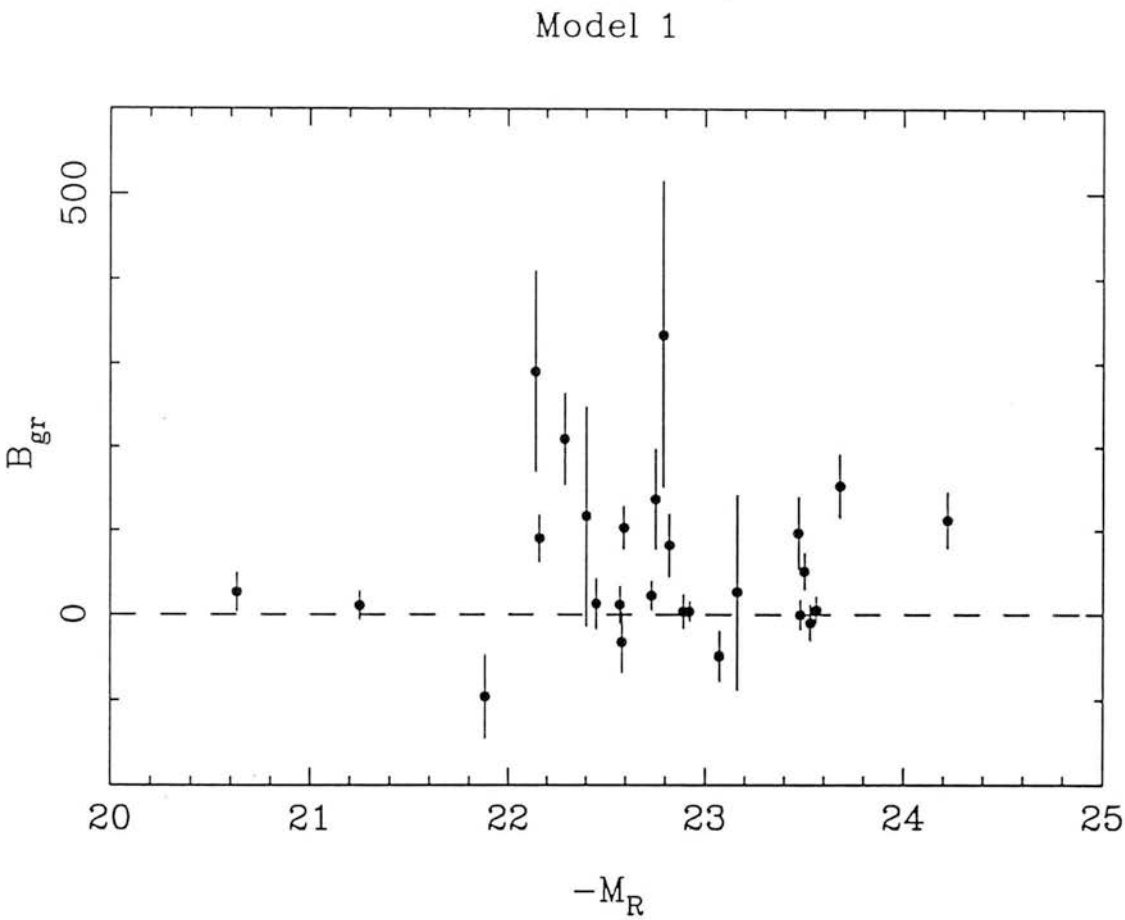

Figure 4. B_{gr} (Model 1) against absolute magnitude.

radio–power and absolute magnitude for our 26 galaxies, using Model 1 alone. Absolute R_C magnitudes were calculated for the radio galaxies using the K– and evolution corrections for the E/SO model shown in Table 5. In Fig. 3 we have added 23 radio galaxies from the Lick composite sample of PP. This sample was constructed primarily from the the 2.7 GHz catalogues of Wall & Peacock (1985) and Peacock & Wall (1981), with additions from three other bright samples. These 23 galaxies plotted are all FR II types and have $z < 0.1$, allowing us to compare a sample of weaker classical double sources with our more powerful sample. Although PP employed a slightly different luminosity function, and K– and evolution corrections to those used in this present study, their objects are at a low enough redshift as to ensure that the differences in their model and ours are minimal, and so a reasonable comparison should be possible. Although the error bars are large, it is apparent that our high–redshift galaxies tend to lie in richer environments than those at lower redshift, and that the more radio–powerful galaxies tend to lie in environments richer than the weaker ones. There seems to be little correlation of environment with the absolute magnitude of the radio galaxy.

To study the trends in environment in more detail, we have divided the sample of 26 galaxies into high and low–redshift groups, high and low radio luminosity groups, and bright and faint groups. Table 7 presents the mean values of B_{gr} for these groups and an estimate of the error: in this analysis we have used the iterative technique discussed in Appendix II of PP which allows one to calculate the weighted mean of a set of measurements (each with individual measurement errors) in the presence of an initially unknown amount of cosmic scatter.

The average values of B_{gr} confirm the trends apparent in Figs. 2–4: galaxies in the high–redshift group (average $z = 0.47$) and the high radio–power group inhabit environments 4–5 times as rich as those galaxies at low–redshift ($\langle z \rangle =$

Table 7. Average values of B_{gr}

All 26 galaxies included.

	Low redshift	**High redshift**
	$z < 0.3$	$z \geq 0.3$
	$(\langle z \rangle = 0.22)$	$(\langle z \rangle = 0.47)$
Lum. function model	B_{gr}	B_{gr}
1	16 ± 11	71 ± 15
2	23 ± 19	77 ± 16

	Low power	**High power**
	$\mathrm{Log_{10}\,P_{178}} < 26.75$	$\mathrm{Log_{10}\,P_{178}} \geq 26.75$
	$(\langle \mathrm{P} \rangle = 26.21)$	$(\langle \mathrm{P} \rangle = 27.29)$
Lum. function model	B_{gr}	B_{gr}
1	21 ± 12	73 ± 17
2	28 ± 18	78 ± 15

	Faint	**Bright**
	$M_{R_C} > -22.75$	$M_{R_C} \leq -22.75$
	$(\langle M_{R_C} \rangle = -22.14)$	$(\langle M_{R_C} \rangle = -23.27)$
Lum. function model	B_{gr}	B_{gr}
1	38 ± 16	42 ± 17
2	45 ± 16	55 ± 21

0.22), or those with weaker radio powers. Comparison with the mean B_{gr} values for Abell clusters, noted in Section 5.4, indicates that our high–redshift and high radio luminosity galaxies occupy environments at least as rich as Abell class 0. There is no difference in cluster environment between the bright and faint radio galaxies.

Whilst it is clear that the strength of clustering is greater at high redshifts, the flux limited nature of the sample ensures that there is an implicit relationship between redshift and radio luminosity: the most distant objects are also the most radio luminous. In order to try to discover the underlying trend in the clustering strength, i.e. to answer the question of whether the trends are the result of an increase in clustering as a function of redshift or radio–power (or both) we have performed a partial–rank analysis, in the manner described by Macklin (1982). To test for example, a correlation between B_{gr} and radio–power (P) with redshift held constant, we form the statistic

$$r_{B_{gr}P,z} = \frac{r_{B_{gr}P} - r_{B_{gr}z}\, r_{Pz}}{[(1 - r^2_{B_{gr}z})(1 - r^2_{Pz})]^{1/2}} \tag{11}$$

where $r_{B_{gr}P,z}$ is the partial correlation coefficient for B_{gr} and P at constant redshift, and $r_{B_{gr}P}$, $r_{B_{gr}z}$ and r_{Pz} are the Spearman rank correlation coefficients between B_{gr} and P, B_{gr} and z, and P and z respectively. The significance levels of the partial correlations are calculated using the Student's t test (see Yates, Miller & Peacock 1986). This partial rank analysis was used in our earlier work to reveal that for the 3CR radio galaxies, the correlation between radio power and infrared luminosity was the fundamental one, rather than that between radio power and redshift.

We have performed such a test for our 26 member sample and the coefficients and the significance levels of the correlations are shown in Table 8 (denoted as sample 'A'). The partial–rank correlation between radio–power and redshift ($r_{Pz,B_{gr}}$) is so strong that the correlations between B_{gr} and redshift ($r_{B_{gr}z,P}$) and

Table 8. Partial rank coefficients.

Sample	n	$r_{B_{gg}P,z}$		$r_{B_{gg}z,P}$		$r_{Pz,B_{gg}}$	
A	26	0.067	$(< 1\sigma)$	0.415	(2σ)	0.626	(2.5σ)
A+P	49	0.074	$(< 1\sigma)$	0.030	$(< 1\sigma)$	0.899	$(> 3\sigma)$
A+Q	61	−0.171	$(< 1.5\sigma)$	0.399	(2.5σ)	0.603	$(> 3\sigma)$
Q	35	−0.170	$(< 1\sigma)$	0.331	(2σ)	0.649	$(> 3\sigma)$

Key to samples:

A: 26 radio galaxies observed in this work.

P: 23 FRII radio galaxies from Prestage & Peacock (1988).

Q: 35 radio–loud quasars from Yee & Green (1987) and Green & Yee (1984).

B_{gr} and radio–power ($r_{B_{gr}P,z}$) are rather overwhelmed, neither of them resulting in a very significant correlation by themselves. There is a suggestion that the correlation between redshift and B_{gr} is stronger than that between radio power and B_{gr}, but the former correlation is only significant at the 2σ level. To increase the sample size, we then added the 23 FR II galaxies from PP to the analysis (denoted as sample 'P'). The coefficients are shown in Table 8. Again, no strong correlations were found other than that between radio–power and redshift, and indeed, the correlation between B_{gr} and redshift is now rather weaker than it was for the 26 member sample alone.

Thus with this present data set, it is not possible to firmly establish whether the strength of clustering about radio–galaxies is primarily determined by the redshift (and thus epoch) or the radio luminosity of the sources. However, the work of Yates, Miller & Peacock (1986) suggests that radio power is in fact the fundamental parameter. The most effective way to disentangle the effects of radio power and redshift on the strength of clustering would be to image a number of radio galaxies within a narrow range of redshift, but with widely differing radio fluxes (and thus radio powers).

7.2 A COMPARISON OF THE CLUSTER ENVIRONMENTS OF QUASARS AND RADIO GALAXIES

The comprehensive CCD imaging survey of YG provides an excellent opportunity to compare the environments of radio galaxies and quasars to $z \simeq 0.5$, a comparison that may provide important clues about the relationship between these two types of active galaxy. A cursory examination of the amplitudes of the quasar–galaxy cross–correlation function (B_{gq}) for the quasars in YG shows that the amplitudes generally appear to be much greater than our values. Six of their quasars have $B_{gq} > 500$. Given the model dependence of the B_{gr} and B_{gq} values (particularly with respect to the conversion function $H(z)$) it is worth considering in some detail the differences between the models employed by YG

and ourselves before attempting a comparison of clustering strengths.

The two major differences between the conversion function $H(z)$ used by YG and ourselves are in the normalization of the luminosity function, and in the parameterization of the evolution applied. To estimate the former parameter, YG first construct a number–magnitude plot of galaxies from their control fields. They then obtain scaling factors such that the luminosity functions of Sebok (1986) and King & Ellis (1985) give good fits to their observed counts at $r = 20.0$. This exercise is carried out for three values of q_o and for each of the two luminosity function models. Finally, to determine which of these six models best describes the data, they compare the predicted counts for each model at a fainter magnitude ($r \simeq 23$) with the observed counts. Their preferred model is the Sebok (1986) luminosity function with $q_o = 0.50$, and this is the one they use to calculate the conversion function $H(z)$ and thus the values of B_{gq} which they tabulate. However, the scaling factor which they derive results in values of ϕ^* for the E+SO, Sa+Sb, Sc and Sdm+Irr morphological groups of 6.73×10^{-4}, 6.42×10^{-4}, 2.31×10^{-3} and $2.2 \times 10^{-3}\,\mathrm{Mpc}^{-3}$ respectively. These values are generally much smaller than those used in Models 1 and 2. For example, YG's normalization for the E+SO group is a factor $\simeq 2.3$ times smaller than in our Model 1 (Sebok 1986) and $\simeq 2.7$ times smaller than in Model 2 (King & Ellis 1985).

Thus, if one adopts the self–consistent normalization for the Sebok (1986) luminosity function employed by YG, a concomitant assumption is that the average number of galaxies per unit volume (regardless of redshift) is $\simeq 2.3$ times smaller than that commonly observed at zero–redshift. Because B_{gr} (and B_{gq}) $\propto 1/\Phi$ (equations (4) and (9)) YG will thus derive amplitudes that are $\simeq 2.3$ times *larger* than those which would be obtained under our own models. In principal, self–consistently derived values of ϕ^* are preferable to the approach that we have adopted here, namely that the zero–redshift values of ϕ^* are valid at

all redshifts. However, the large discrepancy between the normalization derived by YG and that actually observed at low–redshift (from high signal–to–noise data) is rather worrying, and we believe that our approach is the safer one to take at present. Even with a large number of offset fields from which to construct the number–magnitude relation, it is probable that an accurate determination of the normalization from CCD data alone is rather difficult, and could easily lead to errors of a factor of two and possibly even larger. Well studied examples of galaxy number–magnitude counts are those derived in the photographic (b_J) band (see Ellis 1987 for a recent review) and differences in the normalization between the various studies at $b_J = 20$, for example commonly amount to factors of 3–5.

The second major difference between our evaluation of $H(z)$ and that of YG is that they derive self–consistent estimates of the evolution of the luminosity function (described by the evolution of M^*), whereas we simply employ the models of GRV. The precise effects that the differences between these two approaches will have on $H(z)$ is hard to quantify because YG do not specify the amount of evolution actually applied in calculating $H(z)$ for any specific object. Rather, they present values of the evolution in M^* for the six models (the two luminosity functions with three values of q_o each) for three redshift bins, $\langle z \rangle = 0.24$, 0.42 and 0.61 respectively. The self–consistently derived values are not a smooth function of redshift and have large errors. For example, their values of $M_r^*\,(observed) - M_r^*\,(model)$, the amount of evolution in M_r^*, for their preferred model (that of Sebok 1986, with $q_o = 0.5$) are -0.44 ± 0.44, -0.93 ± 0.52 and -0.94 ± 0.51 mags. for the redshift bins $\langle z \rangle = 0.24$, 0.42 and 0.61 respectively.

It is apparent that a straightforward comparison of our radio galaxy B_{gr} values with the B_{gq} values derived by YG for their quasars is inappropriate, owing principally to the significant difference between the normalizations of

the luminosity functions employed. We have therefore re–calculated our B_{gr} values using parameters in the $H(z)$ function such that this function is directly equivalent to that used by YG. Determination of the requisite $H(z)$ was done by taking the galaxy count data provided for the quasars in Table 5 of YG, calculating the values of A_{gq}, and then adjusting our $H(z)$ function so as to be able to closely reproduce the B_{gq} values obtained by YG for each quasar. This adjustment principally involved the above mentioned difference in ϕ^*, and the adoption of $q_o = 0.5$ rather than the $q_o = 0$ cosmology used in our Models 1 and 2. Rather than attempt to extract the the evolution component from the above noted values for the evolution in M^* we have continued to employ evolution based on the GRV models. In practice it was found that it was possible to derive an $H(z)$ function that could satisfactorily reproduce the B_{gq} values obtained by YG, solely by the modification of ϕ^* and q_o. This indicates that the galaxy evolution employed by YG (and derived self–consistently by them) must be in broad agreement with that modelled by GRV.

Having determined the $H(z)$ function which is appropriate for comparison with the data of YG, we then used it to calculate new B_{gr} values for our sample of 26 radio galaxies. We will denote this modified $H(z)$ function as Model 3. It is important to note that because the difference between Models 1 and 3 is primarily one of scaling, the conclusions of Section 7.1 (based on Models 1 and 2) will be unchanged, as will be demonstrated shortly. Furthermore, we intend to explore Model 3 only in the context of a comparison of our radio galaxies with the quasars of YG. We believe that Models 1 and 2 are more suitable as absolute measures of the strength of clustering, given the rather low normalization implicit in Model 3. Fig. 5 plots values of B_{gr} and B_{gq} against redshift for our 26 radio galaxies (calculated under Model 3) and 35 radio–loud quasars from YG and Green & Yee (1984). The B_{gq} values for the quasars were either taken from Table 5 of YG, or calculated from the values of A_{gq} plotted in Figure 1 of Yee & Green (1984). For convenience, we will denote the two types

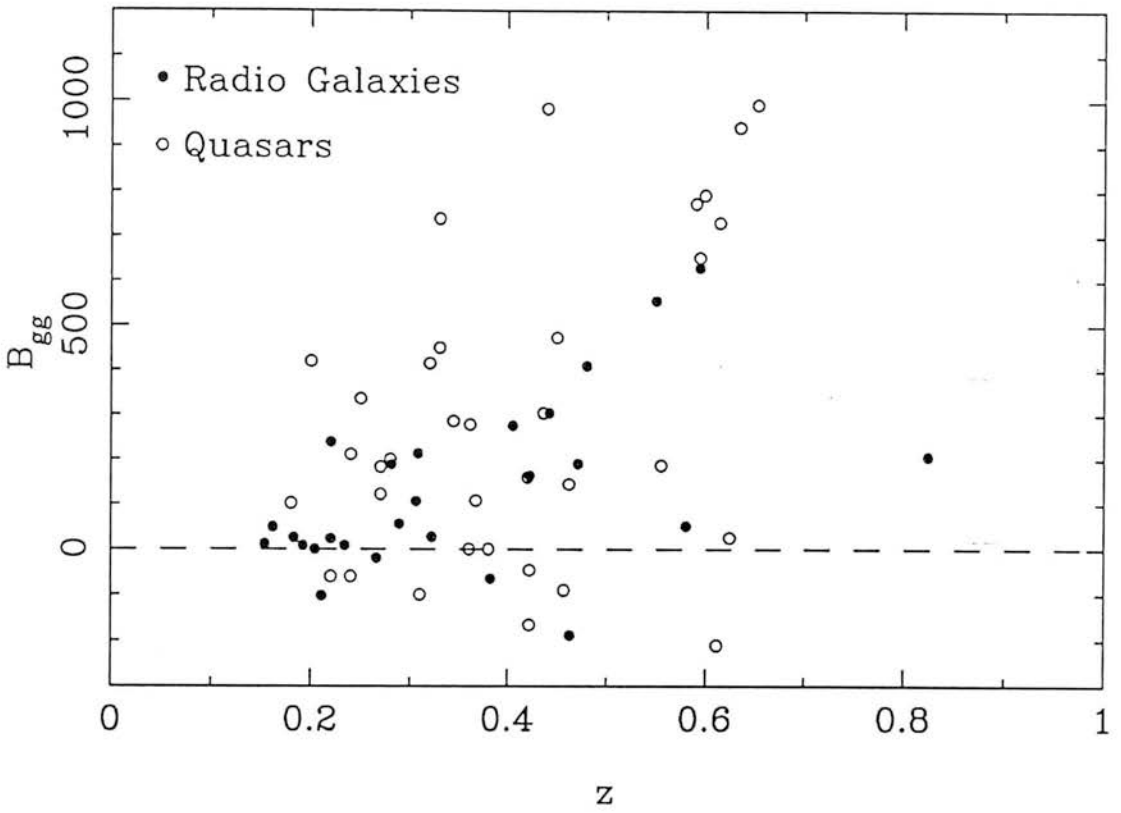

Figure 5. The amplitude of the cross–correlation function (denoted as B_{gg}) against redshift for the 26 radio galaxies studied here (filled circles), and 35 radio–loud quasars (open circles) from YG and Green & Yee (1984). The error bars are omitted for clarity. Both sets of data employ approximately the same conversion function ($H(z)$) and cosmology (Model 3) in the calculation of B_{gg} as YG ($H_o = 50\,\mathrm{km\,s^{-1}\,Mpc^{-1}}$, $q_o = 0.5$).

of cross–correlation amplitude (B_{gr} and B_{gq}) generally as B_{gg}.

In order to compare the strength of clustering between the two types of active galaxy as a function of redshift, we have divided each sample into three groups, a low–redshift one ($z < 0.35$), an intermediate–redshift one ($0.35 \leq z \leq 0.50$), and a high–redshift one ($z > 0.50$). Table 9 compares the mean values of B_{gr} and B_{gq} for these groups. As was apparent from the previous analysis of the radio galaxies in Section 7.1, those at $z \geq 0.35$ lie in richer environments than those at low ($z < 0.35$) redshift, and the adoption of Model 3 rather than our preferred Models 1 and 2 has not changed this conclusion. It is apparent that the radio galaxies and quasars at intermediate and high–redshift lie in environments of similar richness, although our high–redshift ($z > 0.5$) radio galaxy group is rather small. However, there is a large difference between the mean B_{gr} and B_{gq} values at low–redshift ($z < 0.35$), in that the quasars lie in richer environments. Indeed, the average value of B_{gq} for the quasars at $z < 0.35$ is greater than that in the intermediate–redshift bin ($0.35 \leq z \leq 0.50$), a trend that is also apparent in YG's analysis. It should be noted that the low–redshift quasars do not really form a homogeneous data set with the intermediate and high–redshift ones, in that those at $z < 0.35$ were observed with a vidicon camera rather than a CCD. It is possible that there is some systematic difference between the $z \geq 0.35$ and $z < 0.35$ quasar data sets.

This combined radio galaxy and quasar data set provides an opportunity to re–examine the relationship between radio power, richness of environment and redshift, discussed in Section 7.1. Fig. 6 plots B_{gg} against radio power for the 61 member 'active galaxy' sample, and we have calculated a partial rank analysis for this combined 'active galaxy' sample as a whole. Table 8 presents the partial rank coefficients and confidence levels for this 61 member sample (denoted as sample 'A+Q'). The correlation between radio power and redshift is still very strong ($> 3\sigma$). That between B_{gg} and redshift is significant at the 2.5σ level

Table 9. Comparison of the environments of radio galaxies and quasars.

	Radio galaxies[a]			Quasars[b]		
			Model 3			
	$\langle z \rangle$	n	$\langle B_{gr} \rangle$	$\langle z \rangle$	n	$\langle B_{gq} \rangle$
$z < 0.35$	0.24	15	50 ± 22	0.27	14	234 ± 62
$0.35 \leq z \leq 0.50$	0.44	7	151 ± 78	0.41	12	161 ± 93
$z > 0.50$	0.64	4	312 ± 124	0.61	9	438 ± 140

Notes:
(a): The mean B_{gr} values for the radio galaxies have been calculated under Model 3 and assume a conversion function ($H(z)$) and cosmology equivalent to that used for the quasars in YG.
(b): Quasars from YG and Green & Yee (1984).

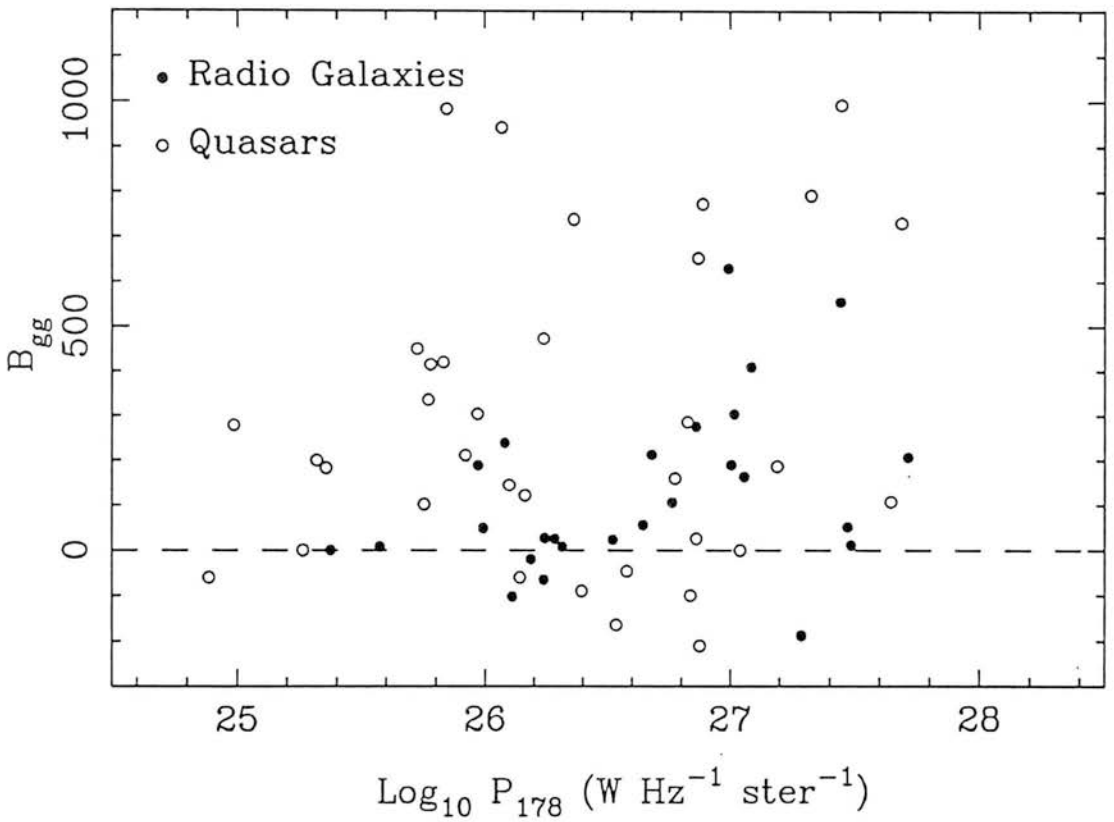

Figure 6. B_{gg} (Model 3) against radio power at 178 MHz (cosmology as in Fig. 5) for the 26 radio galaxies (filled circles) and 35 radio–loud quasars (open circles).

and is therefore stronger than the correlation found for the radio galaxies alone (sample 'A'). The correlation between B_{gg} and radio power is very weak ($< 2\sigma$). Thus there is a tendency for the richness of environment of active galaxies in general to be more dependent on redshift than radio power, but the significance of the former correlation is not overwhelming.

As a final exercise, we have carried out a partial rank analysis for the quasars alone (sample 'Q'). Table 8 presents the coefficients and significance levels. As was the case for the radio galaxies, the correlation between cluster richness and redshift is stronger than that between cluster richness and radio power. However, this former correlation is only significant at the 2σ level. Thus the evidence that the evolution in the environment of quasars is primarily epoch dependent (as advocated by YG) rather than radio luminosity dependent is not strong.

7.3 THE RELATIONSHIP BETWEEN CLUSTER ENVIRONMENT AND RADIO STRUCTURE

In view of the well–established result of LS and PP, namely that FR II sources are generally found in poor environments, perhaps the most surprising result of this present work is that many of our FR II sources do in fact lie in very rich environments. Of our sample of 14 galaxies known to be FR IIs, 6 have values of B_{gr} in excess of 100 (Model 1). In the picture discussed by PP, it is proposed that the gas pressures in the cores of rich clusters will be higher than the minimum pressures in the hotspots of the weaker FR IIs, thus preventing formation of the classical double structures seen in these sources and accounting for the general absence of these types in rich environments at $z \leq 0.1$. X–ray measurements of the intergalactic medium (IGM) in rich clusters of galaxies typically yield pressures $\sim 5.10^{-12}\,\mathrm{N\,m^{-2}}$ (Jones & Forman 1984), higher than the minimum pressures in the hotspots of relatively weak FR II sources ($\sim 10^{-12} - 10^{-13}\,\mathrm{N\,m^{-2}}$, Miller *et al.* 1985). However, our high–redshift sample is likely to include many very powerful sources where the ram pressure in the

jets is powerful enough to overcome the static pressure in rich clusters, allowing the formation of classical–double FR II type structures, even in these rich environments. Cygnus A, a powerful FR II source, is estimated to have a minimum hotspot pressure $\sim 10^{-9}\,\mathrm{N\,m^{-2}}$ (Hargreave & Ryle 1976), easily sufficient for the formation of classical–double structure even in the presence of a dense IGM. 3C 295 ($z = 0.458$) is the archetypal powerful FR II galaxy which lies in a rich environment. However, this object is at low–redshift compared with the active galaxies in the very richest environments ($B_{gg} > 500$), principally the $z > 0.5$ quasars of YG. This supports the hypothesis that it is the radio luminosity rather than the redshift which is the fundamental factor determining the richness of environment. We suggest that many of our high–redshift FR IIs are of a similar nature to 3C295.

Alternatively, given that we observe several FR IIs in rich environments at earlier epochs it is relevant to ask whether there could be real evolution of the IGM, encouraging the formation of classical–double type structure in clusters of galaxies at high–redshift. X–ray studies of very distant clusters are at a rather rudimentary stage: Henry *et al.* (1982) studied a small number of clusters to $z \simeq 0.5$ and concluded that there was no evidence for evolution in their X–ray properties. Miley (1987) has recently studied the radio structures of a sample of high–redshift radio galaxies and claims that they are more crooked and smaller than low–redshift ones, a result he ascribes to interaction with a denser and clumpier IGM at earlier epochs. If this is indeed the case, then this would tend to inhibit the formation of classical–double structures at high–redshift rather than encourage them. Kaiser (1986) discusses the possible evolution of cluster X–ray properties using dimensional arguments. The characteristic X–ray luminosity (L_X^*) scales like $L_X^* \propto M^* \rho^* T^{1/2}$ where M^*, ρ^*, and T are the mass, density and temperature respectively. Kaiser (1986) argues that L_X^* remains approximately constant with redshift, thus the temperature evolution is the main factor which will determine the density ρ^* for a cluster of mass M^*.

The clear difference in cluster environment between low–redshift FR Is and IIs has been used as evidence that it is unlikely that the two types of galaxy have a common origin, and that FR IIs are unlikely to evolve into FR Is. This argument clearly breaks down for our high–redshift FR IIs which do appear to lie in rich environments at early epochs; were they to evolve into FR Is at later epochs they would then occupy the rich environments commonly observed around these relaxed sources at low–redshift.

7.4 RADIO GALAXY MORPHOLOGIES AND GALAXY MERGERS

There has been a recent revival of interest in the role that galaxy interactions and mergers may play in the promotion and sustenance of all types of active galaxy. Whilst the richness of environment is a good indicator of the likelihood of significant dynamical friction in clusters of galaxies (Hausman & Ostriker 1978), the structures of the radio galaxies themselves are excellent probes of cannibalism actually in progress, or having taken place only just prior to the epoch of observation. In Table 10 we present a few statistics on the morphologies of the galaxies in the sample, and also present percentages for the FR IIs alone. Note that there are likely to be significant biases in these percentages, particularly as regards the detection of low–surface brightness features at high–redshift: these particular percentages are therefore likely to be lower limits.

Heckman *et al.* (1986) have imaged a sample of 43 powerful, low–redshift radio galaxies and find that one quarter to one third of the sample are peculiar. This fraction is similar to the number of galaxies in our sample which could *not* be broadly classified as giant–ellipticals (31%). Whilst 23% of our galaxies do have low–surface brightness features (wisps, tails, fans etc.), there are only two of these objects where the galaxy could not still be broadly classified as a gE or dB. We believe that it is the high surface brightness structure (which is likely to trace the bulk of the mass) that is the most relevant in this discussion, and at least for this sample of radio galaxies, significant morphological peculiarities are definitely

Table 10. Morphological statistics.

	26 galaxy sample	FR IIs only (14)
giant ellipticals	18 (70%)	9 (65%)
peculiar	4 (15%)	3 (21%)
dumbbells	4 (15%)	2 (14%)
multiple nuclei	7 (27%)	4 (29%)
LSB features	6 (23%)	2 (14%)

not a major feature; 18/26 are giant–ellipticals. More specifically, Heckman *et al.* argue that FR IIs generally have peculiar morphologies, whereas the FR Is are more likely to be gE or cD galaxies. For our sample, the majority of FR IIs are in fact gEs. It is possible that this apparent difference in FR II morphologies between the two studies is connected with the fact that we see several FR IIs in rich environments. Our discussion above indicates that our high–redshift FR IIs must be particularly special in that they are powerful enough to support double–lobe structures despite the presence of a dense IGM suggested by the rich environments, and in this respect, our high–redshift FR II population is different from that at low–redshift ($z < 0.1$) imaged by Heckman *at al.* Another factor to bear in mind is the subjective nature of galaxy classifications – whilst Heckman *et al.* may regard faint tails and wisps as evidence of abnormality, comparison must be made with a sample of 'normal' ellipticals that have been imaged in a comparable manner to the radio galaxies, in order to determine how different their peculiar objects really are from the radio–quiet elliptical galaxy population. For example, Ebneter, Djorgovski & Davis (1988) have recently imaged a sample of 159 generally radio–quiet 'nearly normal' E and S0 galaxies, and note that $\sim 50\%$ of their ellipticals have features of some kind, including dust and stellar disks.

Lilly & Prestage (1987) obtained surface photometry of 31 powerful radio galaxies with $z < 0.25$, and found that FR Is were more likely to have multiple nuclei than FR IIs. After allowing for the possibility of chance projections, they estimated that possibly none of their FR IIs had true multiple nuclei. Our sample has only 2 FR Is, and so we can not make a meaningful comparison between the incidence of multiple nuclei in FR Is and IIs. However, it is worth noting that 4/14 of our FR IIs do have multiple nuclei. In order to estimate how many of these multiple systems are true physical systems rather than projection effects, we need to calculate the expected frequency of apparent companions for galaxies in general. More specifically, we can use our knowledge of the observed surface

density of galaxies as a function of magnitude (Section 5.3) to estimate the probability that, on placing a radio galaxy at random in the field, an unrelated field galaxy will appear to lie within a projected radius of 19.2 kpc of that radio galaxy. For a limiting magnitude of $R_C = 22.5$ (typical for this present work) the probability that an unrelated galaxy will lie within a projected radius of 19.2 kpc is 5% at $z = 0.25$ and 2% $z = 0.5$. This calculation assumes that the observed surface density of galaxies is smoothly distributed. In order for the probability of a chance companion to be as large as 50% (at $z = 0.25$) the radio galaxy must lie in a region with a galaxy surface density ten times that of the field on average. It is probably not unreasonable to assume that at least 2/4 of our multiple nuclei are genuine multiple systems.

Lilly & Prestage (1987) also note that multiple nuclei are extremely rare for galaxies with low cross–correlation amplitudes: only 1/13 of their galaxies with an amplitude less than 80 had any possible multiple nucleus. We find 4/15 galaxies with $B_{gr} < 80$ have possible multiple nuclei, in broad agreement with this observation. Study of the structures of their radio galaxies on the $(M_V - \alpha)$ plane (Hoessel 1980), revealed that the FR Is were of similar luminosity to Abell cluster first–ranked galaxies, and had high values of α, whilst the FR IIs were of lower optical luminosities and had smaller α values. The work of Hausman & Ostriker (1978) demonstrated that as giant galaxies undergo cannibalism, they tend to move across the $(M_V - \alpha)$ plane towards bright values of M_V and large values of α. Lilly & Prestage suggest that if some process such as cannibalism has acted on Abell first–ranked galaxies then it is also likely to have been operative on the FR Is. Thus FR Is have probably undergone more merging than FR IIs. This result seemed to contradict that of Heckman *et al.* (1986) where it was claimed that FR IIs show *more* signs of merging activity than the FR Is. Only 1 of our gE FR IIs has any low–surface brightness features, and a further 5 FR IIs are peculiar or multiple systems, perhaps suggesting that most of our FR IIs have not had particularly violent histories, in accord with Lilly & Prestage's

observations. Alternatively, one could argue that the FR IIs studied here are in fact at a more advanced stage of merging than those of Heckman *et al.* (1986), the initial violent and spectacular morphological peculiarities having been erased long before the epoch of observation. A way to test this hypothesis would be to measure α values for the FR IIs, although this would be difficult for our higher redshift objects of small angular extent.

7.5 THE RELATIONSHIP BETWEEN CLUSTER ENVIRONMENT AND RADIO GALAXY LUMINOSITY

As noted above, Lilly & Prestage (1987) found that their FR I galaxies tended to be more optically luminous than the FR IIs, in parallel with the former's tendency to lie in richer environments. Schneider, Gunn & Hoessel (1983) have shown that a similar, although rather weak relation exists for Abell cluster first brightest members – the more luminous brightest cluster members tend to occur in the richest Abell clusters. In this present work we find that the environments of the bright and faint members of our sample are indistinguishable, mean values of B_{gr} for these two groups (Model 1) being 42 ± 17 and 38 ± 16 respectively. A possible problem is that Lilly & Prestage derived total magnitudes for their galaxies extrapolated from their metric magnitudes by assuming a $r^{1/4}$ de Vaucouleurs law, and as they note, this will not be strictly correct for any galaxy that does not follow this law. For their dumbbell systems, they did derive total magnitudes by summing the enclosed light within a large radius, a similar procedure to that employed in this present work. Dividing their radio galaxy sample into two groups, one with $B_{gr} \geq 80$ and the other with $B_{gr} < 80$, and considering their *metric* absolute magnitudes (the total magnitudes are not tabulated), one obtains mean values of $-23.04(\pm 0.39)$ and $-22.46(\pm 0.66)$ respectively. Application of the Mann–Whitney U–test (two tailed) indicates that the probability that these samples are in fact distinguishable is only 2σ.

It is likely that our sample, and the range of cluster environments encoun-

tered are too small to address this question properly. Besides, the evidence for a correlation between the magnitude of the brightest members in clusters and the richness is not overwhelming. Schneider, Gunn & Hoessel (1983) studied the brightest members of 83 Abell clusters and found values for the mean reduced absolute magnitudes (RAM) of the brightest members in Abell classes 0 and 2 of 23.3($\pm$0.8) and 23.7($\pm$0.5), barely distinguishable. Similarly, the comprehensive study of the brightest members in 103 clusters by Schombert (1987) could only produce weak support for a correlation between brightest cluster member magnitude and richness, and there is no evidence at all for such a relation over the richness range 0–2.

7.6 IMPLICATIONS FOR THE HIGH-REDSHIFT EVOLUTION OF POWERFUL RADIO GALAXIES

The result that these high–redshift radio galaxies ($\langle z \rangle = 0.47$) inhabit environments on average as rich as Abell class 1 clusters has important implications for the interpretation of the evolution of very distant and powerful radio galaxies. One of the motivations for this present study was to try to examine the possible relationship between the environments and radio luminosities of the most distant 3CR galaxies, those seen to be undergoing luminosity evolution on the Hubble diagram. Although we definitely see an increase in clustering at high redshift (or high radio–luminosity) it was not possible to determine unequivocally whether the epoch dependence or radio–luminosity dependence is the driving factor. There is a slight ($\sim 2\sigma$) suggestion that it is the redshift that is the fundamental correlation with richness of environment, but data for a more tightly defined sample is needed in order to test this possibility, and firmly rule out a correlation with radio–luminosity. This is particularly important in that the work of Yates, Miller & Peacock (1986) on the 3CR sample suggested that radio luminosity might in fact be the fundamental parameter, rather than redshift. However, whatever the underlying cause, because the objects observed

to be undergoing luminosity evolution are of both higher redshift and radio luminosity than the objects studied here, it is probable that they continue the trend seen in our $z < 1$ sample, and generally lie in environments at least as rich as Abell class 0–1 clusters.

There is now a substantial body of evidence that many of the high–redshift ($z > 1$) 3CR galaxies are undergoing massive bursts of star formation (see Djorgovski (1988) for a review), possibly fuelled by highly dissipative mergers of gas–rich galaxies (Djorgovski *et al.* 1987). Naturally, the probability of merging taking place is greatly increased if the radio galaxy lies in a rich environment, and if the $z > 1$ members of the 3CR sample continue the behaviour seen in our $z < 1$ galaxies, the conditions would seem to be very favourable for substantial interaction and merging activity at these early epochs.

8 Conclusions

We have imaged a sample of 26 powerful radio galaxies in the redshift range $0.15 < z < 0.82$, and have derived amplitudes of the cross-correlation function (B_{gr}) about each source, enabling us to reach the following conclusions:

1) Powerful radio galaxies at $z \simeq 0.5$ generally occupy environments as rich as Abell class 0–1 clusters of galaxies, 4–5 times richer than radio galaxies at lower redshift, $z \simeq 0.2$. Similarly, the most powerful radio galaxies in our sample ($P_{178} = 10^{27.3}\,W\,Hz^{-1}\,ster^{-1}$) occupy richer environments than the weaker objects ($P_{178} = 10^{26.2}$). Because of the limited size of our sample, we are unable to determine whether the underlying cause of this difference in clustering properties is primarily epoch dependent, or radio–luminosity dependent. There may be a slight suggestion ($\sim 2\sigma$) that the epoch dependence is the dominant correlation. There is no correlation between the absolute magnitudes of the radio galaxies and the richness of environment.

2) The trend in clustering properties with redshift observed in our radio galaxies

broadly mimics that seen in radio–loud quasars over the same redshift range (Yee & Green 1987). The environments of our radio galaxies at $z \simeq 0.5$ are as rich as those observed around radio–loud quasars at this redshift.

3) Roughly half of our FR II sources occupy environments at least as rich as Abell class 0 clusters, having B_{gr} values in excess of 100 (Model 1). We suggest that these objects, which are amongst the most powerful in our sample are the analogues of Cygnus A and 3C 295, and are powerful enough to support classical double–lobed structures despite the presence of a dense intracluster medium. This result contrasts with the tendency for weaker FR II galaxies at low–redshift ($z < 0.1$) to lie poor environments.

4) Nearly three–quarters of our sources can be adequately classified as giant–elliptical galaxies, and significant high surface–brightness morphological peculiarities only occur in a minority of cases.

5) About one quarter of our sample have multiple nuclei (true or apparent), and multiple nuclei are very rare for objects in poor environments ($B_{gr} < 80$ Model 1).

Acknowledgments

We are grateful to Bruno Guiderdoni and Brigitte Rocca–Volmerange for allowing us to use their spectral evolution programs to calculate K–corrections, and to James Dunlop for advice on their use. Richard Prestage and Andrew Mead supplied various useful items of software. MGY was a visiting astronomer at the Cerro Tololo Inter–American Observatory, National Optical Astronomy Observatories which are operated by AURA Inc., under contract with the NSF, and a Visiting Astronomer at the European Southern Observatory, La Silla, Chile. In addition to these two facilities, we are grateful to PATT for allocation of time at the AAT and to Ray Sharples and Tony Marston for assistance. This data was reduced using the STARLINK facilities at ROE. MGY was supported by a

research studentship from the Science and Engineering Research Council during the course of this work.

References

Bahcall, J.N. & Soneira, R.M., 1981. *Astrophys. J. Suppl.*, **47**, 357.

Bessell, M.S., 1986. *Publ. astr. Soc. Pacific*, **98**, 1303.

Bruzual, G.,A., 1983. *Astrophys. J.*, **273**, 105.

Burstein, D. & Heiles, C., 1982. *Astr. J.*, **87**, 1165.

Djorgovski, S., 1988. *Astr. J.*, submitted.

Djorgovski, S., Spinrad, H. & Dickinson, M., 1988. *Astrophys. J.*, in press.

Djorgovski, S., Spinrad, H., Pedelty, J., Rudnick, L. & Stockton, A., 1987. *Astr. J.*, **93**, 1307.

Ellis, R.S., 1987. *Observational Cosmology, IAU Symp. No. 124*, p.367, eds. Hewitt, A., Burbidge, G. & Fang, L.Z., Reidel, Dordrecht.

Ebneter, K., Djorgovski, S & Davis, M., 1988. *Astr. J.*, in press

Fosbury, R.A.E., Bird, M.C., Nicholson, W. & Wall, J.V., 1987. *Mon. Not. R. astr. Soc.*, **225**, 761.

Graham, J.A., 1982. *Astr. J.*, **94**, 244.

Green, R.F. & Yee, H.K.C., 1984. *Astrophys. J. Suppl.*, **54**, 495.

Greenstein, J.L., 1962. *Astrophys. J.*, **135**, 679.

Groth, E.J. & Peebles, P.J.E., 1977. *Astrophys. J.*, **217**, 385.

Guiderdoni, B. & Rocca–Volmerange, B., 1987. *Astr. Astrophys.*, **186**, 1.

Gunn, J.E. & Oke, J.B., 1975. *Astrophys. J.*, **195**, 255.

Gunn, J.E., Hoessel, J.G. & Oke, J.B., 1986. *Astrophys. J.*, **306**, 30.

Hargreave, P.J. & Ryle, M., 1976. *Mon. Not. R. astr. Soc.*, **175**, 481.

Hausman, M.A. & Ostriker, J.P., 1978. *Astrophys. J.*, **224**, 320.

Heckman, T.M., Smith, E.P., Baum, S.A., van Breugel, W.J.M., Miley, G.K., Illingworth, G.D., Bothun, G.D. & Balick, B., 1986. *Astrophys. J.*, **311**, 526.

Henry, J.P., Soltan, A., Briel, U. & Gunn, J.E., 1982. *Astrophys. J.*, **262**, 1.

Hoessel, J.G., 1980. *Astrophys. J.*, **241**, 493.

Jauncey, D.L., White, G.L., Batty, M.J. & Preston, R.A., 1986. *Astr. J.*, **92**, 1036.

Jones, C. & Forman, W., 1984. *Astrophys. J.*, **276**, 38.

Kaiser, N., 1986. *Mon. Not. R. astr. Soc.*, **222**, 323.

Kellerman, K.I., 1966. *Austr. J. Phys.*, **19**, 195.

King, C.R. & Ellis, R.S., 1985. *Astrophys. J.*, **288**, 456.

Koo, D.C. & Kron, R.G., 1987. *Observational Cosmology, IAU Symp. No. 124*, p.388, eds. Hewitt, A., Burbidge, G. & Fang, L.Z., Reidel, Dordrecht.

Kristian, J., Sandage, A. & Katem, B., 1974. *Astrophys. J.*, **191**, 43.

Kristian, J., Sandage, A., & Katem, B., 1978. *Astrophys. J.*, **219**, 803.

Laing, R.A., Longair, M.S., Riley, R.M., Kibblewhite, E.J. & Gunn, J.E., 1978. *Mon. Not. R. astr. Soc.*, **183**, 547.

Laing, R.A., Riley, J.M., & Longair, M.S., 1983. *Mon. Not. R. astr. Soc.*, **204**, 151.

Le Fèvre, O., Hammer, F., Nottale, L., Mazure, A. & Christian, C., 1988. *Astrophys. J.*, **324**, L1.

Lilly, S.J. & Longair, M.S., 1984. *Mon. Not. R. astr. Soc.*, **211**, 833.

Lilly, S.J. & Prestage, R.M., 1987. *Mon. Not. R. astr. Soc.*, **225**, 531.

Longair, M.S. & Gunn, J.E., 1975. *Mon. Not. R. astr. Soc.*, **170**, 121.

Longair, M.S. & Seldner, M., 1979. *Mon. Not. R. astr. Soc.*, **189**, 433.

MacGillivray, H.T. & Stobie, R.S., 1984. *Vistas Astr.*, **27**, 433.

Macklin, J.T., 1982. *Mon. Not. R. astr. Soc.*, **199**, 1119.

Maltby, P., Matthews, T.A. & Moffett, A.T., 1963. *Astrophys. J.*, **137**, 153.

Matthews, T.A., Morgan, W.W. & Schmidt, M., 1964. *Astrophys. J.*, **140**, 35.

McEwan, N.J., Browne, I.W.A. & Crowther, J.H., 1975. *Mem. R. astr. Soc.*, **80**, 1.

Miley, G.K., 1987. *Observational Cosmology, IAU Symp. No. 124*, p.267, eds. Hewitt, A., Burbidge, G. & Fang, L.Z., Reidel, Dordrecht.

Miller, L., Longair, M.S., Fabbiano, G., Trinchieri, G., & Elvis, M., 1985. *Mon. Not. R. astr. Soc.*, **215**, 799.

Peacock, J.A. & Wall, J.V., 1981. *Mon. Not. R. astr. Soc.*, **194**, 331.

Peebles, P.J.E., 1980. *The Large Scale Structure of the Universe*, Princeton University Press.

Penston, M.V. & Fosbury, R.A.E., 1978. *Mon. Not. R. astr. Soc.*, **183**, 479.

Prestage, R.M. & Peacock, J.A., 1988. *Mon. Not. R. astr. Soc.*, **230**, 131.

Rieke, G.H. & Lebofsky, M.J., 1985. *Astrophys. J.*, **288**, 618.

Riley, J.M., Longair, M.S. & Gunn, J.E., 1980. *Mon. Not. R. astr. Soc.*, **180**, 233.

Rocca–Volmerange, B. & Guiderdoni, B., 1987. *Astr. Astrophys.*, **175**, 15.

Salpeter, E.E., 1955. *Astrophys. J.*, **121**, 161.

Scalo, J.M., 1986. *Fund. of Cosmic Phys.*, **11**, 1.

Schechter, P., 1976. *Astrophys. J.*, **203**, 297.

Schneider, D.P., Gunn, J.E. & Hoessel, J.G., 1983. *Astrophys. J.*, **268** , 476.

Schombert, J.M., 1987. *Astrophys. J. Suppl.*, **64**, 643.

Sebok, W.L., 1986. *Astrophys. J. Suppl.*, **62**, 301.

Seldner, M. & Peebles, P.J.E., 1978. *Astrophys. J.*, **225**, 7.

Smith, R.M. & Robertson, J.G., 1985. *Mon. Not. R. astr. Soc.*, **212**, 809.

Spinrad, H. & Djorgovski, S., 1987. *Observational Cosmology, IAU Symp. No. 124*, p.129, eds. Hewitt, A., Burbidge, G. & Fang, L.Z., Reidel, Dordrecht.

Spinrad, H., Djorgovski, S., Marr, J. & Aguilar, L., 1985. *Publ. astr. Soc. Pacific*, **97**, 932.

Spinrad, H., Kron, R.G. & Hunstead, R.W., 1979. *Astrophys. J. Suppl.*, **41**, 701.

Spinrad, H., Liebert, J., Smith, H.E. & Hunstead, R., 1976. *Astrophys. J.*, **206**, L79.

Tritton, K.P. & Schilizzi, R.T., 1973. *Mon. Not. R. astr. Soc.*, **165**, 245.

Véron–Cetty, M.P. & Véron, P., 1983. *Astr. Astrophys. Suppl.*, **53**, 219.

Wall, J.V. & Peacock, J.A., 1985. *Mon. Not. R. astr. Soc.*, **216**, 173.

Wills, B.J. & Wills, D., 1979. *Astrophys. J. Suppl.*, **41**, 689.

Wyndham, J.D., 1966. *Astrophys. J.*, **144**, 459.

Yates, M.G., Miller, L. & Peacock, J.A., 1986. *Mon. Not. R. astr. Soc.*, **221**, 311.

Yee, H.K.C. & Green, R.F., 1984. *Astrophys. J.*, **280**, 79.

Yee, H.K.C. & Green, R.F., 1987. *Astrophys. J.*, **319**, 28.

Yee, H.K.C., Green, R.F. & Stockman, H.S., 1986. *Astrophys. J. Suppl.*, **62**, 681.

Postscript at February 1988.

The preceding paper is only a first step in the study of the structure and environments of powerful high redshift galaxies. An obvious question to answer is what happens at $z \geq 0.8$? As is apparent from the error bars on our clustering strengths, the search for clusters at these high redshifts is likely to be exceedingly difficult with current ground–based technology, and until the new generation of 10m class telescopes comes on–line I would venture to say that only the brave (or foolish) should try to extend the experiment to $z > 0.8$. As well as the difficulty in obtaining deep enough imaging, the estimate of the clustering strength (B_{gr}) is rather model dependent, and assumes a knowledge of the galaxies' spectral evolution, the evolution of the luminosity and cross–correlation functions, and a knowledge of the pertinent cosmology. All these factors are uncertain, and their true nature may be so far in error from our current best–bet values for $z > 1$, that no meaningful experiment is possible.

Perhaps the most unsatisfactory aspect of this present work was that it was not possible to completely extricate the effects of radio luminosity and redshift (epoch) on the cluster strength. An attempt to address this problem is currently being made by Hill at the University of Hawaii who is imaging a number of radio galaxies in a small redshift range at $z \simeq 0.5$, but with widely differing radio fluxes (and thus radio luminosities). This programme nicely complements our more redshift orientated project, and we look forward to seeing the first results from Hill's survey. Both types of survey are necessary in order to satisfactorily uncover the underlying trend in clustering

strength, thus I do not think that we were incorrect to adopt the redshift dependent approach.

Another fruitful line for future work is the study of the stellar populations of the clusters themselves, via the use of multi–waveband imaging. Originally we had proposed to image in more than one band (thus obtaining colour information) but this would have doubled or trebled the amount of telescope time needed to survey a reasonable number of radio galaxies. Early on, I suspected that it would be better to concentrate purely on the cluster detection part of the experiment (thus imaging in R alone), and leaving the multiwaveband work until later. In as much as it has taken two years to complete the R band work alone, I believe that this policy was fully justified. Oemler at Yale University is currently attempting a multi–wavelength study of a number of radio galaxies at $z \simeq 0.5$ with the aim of comparing their cluster populations with "radio–quiet" clusters at similar redshifts. Some preliminary results suggest that the radio–loud clusters tend to have bluer galaxies than the radio–quiet ones. Oemler also notes an evolution in the environments of powerful radio galaxies similar to that found in our own work, but his survey is not yet complete and so we await more specific conclusions from this project.

Chapter 4

Deep *IRAS* observations of 3C radio galaxies.

Mon. Not. R. astr. Soc., in press.

Prologue to *"Deep IRAS observations of 3C radio galaxies".*

In this and the following paper we change tack, and focus closely on the astrophysics of very low redshift ($z < 0.2$) active galaxies. The 3C galaxies have been studied in virtually all the regions of the electromagnetic spectrum, but until the launch of the IRAS satellite, they had not yet succumbed to scrutiny in the $12 - 100\,\mu$m region. The ultimate aim of these multi–wavelength studies is to be able to account for all the sources and sinks of the energy associated with the active galaxy phenomenon. For example, energy originating in the ultraviolet can be reprocessed by dust into infrared radiation. By observing across the entire electromagnetic spectrum, one hopes to be able to calculate the total energy budget of these active galaxies, and move closer to a resonable understanding of the active galaxy phenomenon.

This work was done in collaboration with Simon Lilly (University of Hawaii) and Malcolm Longair (Royal Observatory, Edinburgh). I was responsible for extracting the numbers from the raw data, but we take equal responsibility for the interpretation.

Summary

Deep IRAS Additional Observations of the fields of 18 3C radio galaxies with $0.01 < z < 0.2$ have resulted in detections of 6 galaxies, comprising the broad line radio galaxies (BLRG) 3C234 and 3C382, the anomalous narrow line radio galaxy (NLRG) 3C433 and the three closest NLRGs, 3C31, 3C293 and 3C449. The overall spectral energy distributions between X–ray and radio wavelengths are constructed and compared. As found earlier for the BLRG 3C390.3, the BLRGs have 12.5 μm flux densities that follow the power–law established at near–infrared wavelengths, but show a peak at 25 μm. Most of the luminosity of the BLRGs is radiated in this 25 μm component. The three normal NLRGs detected have large far infrared luminosities of typically 10^{37} W at 100 μm, despite having no detectable non–stellar continua at either 3000Å or 3.5 μm and only weak optical emission lines. This far–infrared component has a much greater luminosity than either the X–ray or the radio components. There is no evidence for the 25 μm peak seen in the BLRGs. Two of the NLRGs may be involved in an interaction with another galaxy. The peculiar 3C433, which is known to have BLRG–like near–infrared properties but a narrow–line optical spectrum and no non–stellar radiation detected at 3000Å, has a BLRG–like IRAS spectral energy distribution, peaking at 25 μm. A search for 3C sources in the IRAS Point Source Catalogue shows that, in addition to the well–known infrared sources M82, M84, M87, NGC1275 and the recently studied 3C390.3, 3C321 and Cygnus A are also luminous in the far–infrared.

1 Introduction

The powerful radio galaxies in the 3C catalogue have been extensively studied over a wide range of the electromagnetic spectrum and, for those galaxies with $z < 0.2$, there is a large amount of data in the form of multi–frequency radio maps, near–infrared photometry, optical images, photometry and spectroscopy, and broad–band X–ray flux densities from the Einstein observatory. As part of the Infrared Astronomical Satellite (IRAS) Additional Observations (AO) programme, we have observed many of these radio galaxies in the $10 - 100\,\mu$m spectral region for the first time, and this paper reports the results of these observations.

3C radio galaxies are almost invariably giant elliptical galaxies. They often show narrow optical emission lines although these are rather weak in some cases. In a few instances, broad permitted lines are also seen, usually accompanied by a strong featureless continuum that gives rise to the N–type morphology of these broad line radio galaxies (BLRG). At X–ray wavelengths, the BLRGs are more luminous than the narrow line radio galaxies (NLRG), but almost all the 3C galaxies with $z < 0.2$ were detected by the Einstein satellite observatory (Fabbiano *et al.* 1984). In the near–infrared $1 - 2\,\mu$m region, Lilly & Longair (1982, 1984) showed that, with few exceptions, the NLRGs have stellar spectral energy distributions while the BLRGs have substantially enhanced infrared flux densities, presumably associated with the non–stellar optical component. At $3.5\,\mu$m, Lilly, Longair & Miller (1985) found that while the NLRGs with weak optical emission lines continued to have stellar spectral energy distributions, those with stronger optical lines had redder $(K - L')$ colours and contained a steeply rising non–stellar component.

IRAS observations of the BLRG 3C390.3 at $10 - 100\,\mu$m have been reported by Miley *et al.* (1984) who presented its spectrum between X–ray and radio wavelengths. They observed that, unlike most other active galactic nuclei

(AGN), this source showed a pronounced peak at 25 μm superposed on a second smooth component. This 25 μm component was responsible for most of the luminosity of the source.

In order to study the far–infrared properties of a large number of 3C radio galaxies we requested Deep Survey mode observations of a sample of 38 sources. By the end of the mission, 16 NLRGs and 2 BLRGs had been observed. This set of objects is an unbiassed subset of the complete compilation of Laing, Riley & Longair (1983) with $0.01 < z < 0.2$ and $\delta < 55°$.

In the next section we describe these observations and their reduction and in Section 3 we discuss our results, including a brief discussion of other 3C sources detected in the IRAS All–Sky survey. Our conclusions are presented in Section 4. We have adopted a standard Friedmann cosmology with $H_o = 50\,km\,s^{-1}\,Mpc^{-1}$ and $\Omega_o = 1$.

2 Data

2.1 OBSERVATIONS AND REDUCTION

In addition to the all sky survey carried out by IRAS (Neugebauer *et al.* 1984a) provision was made for a number of Additional Observations. The observations described in this paper were made by the satellite operating in Deep Survey mode, allowing almost simultaneous observations in the four passbands at 12, 25, 60 and 100 μm to a sensitivity level about 4–5 times deeper than the all sky survey. A total of 18 radio fields were observed in our programme. In most cases repeat observations were made shortly after the initial observation.

The data were made available to us after initial processing by the Jet Propulsion Laboratory. For each scan of the radio source field an 'intensity grid' and a 'flux grid' had been produced. In the former, no filtering was done, thus preserving the the total flux information (in units of $W\,m^{-2}\,ster^{-1}$). The latter

grids were filtered with a zero–sum bandpass filter centered on the point source frequency, thereby suppressing extended information. In uncrowded fields such as ours, these provide greater sensitivity for the detection of unresolved sources. The flux grid was in units of $W\,m^{-2}$.

For each field observed, contour maps of flux density were produced from the flux grids using the STARLINK IRAS Data Analysis Package which allowed the radio source position and a coordinate grid to be superposed on the maps. Information on suitable search radii was taken from recent identification work using IRAS data. The compilation of Catalogued Galaxies and Quasars Observed in the IRAS survey (Lonsdale *et al.* 1985) employed search radii of 90, 120 and 180 arcsec depending on the accuracy of the catalogued positions. Typical errors in the IRAS positions of galaxies with accurately known positions (appropriate for our accurately known radio galaxy positions) were 15 arcsec and 4 arcsec in the directions parallel and perpendicular to the satellite scan direction respectively. Wolstencroft *et al.* (1986) find that 95% of their identifications of IRAS sources on UK Schmidt plates lie within an ellipse with semi–major and semi–minor axes of 30 and 6 arcsec. With these figures in mind, we chose a generous search radius of 1 arcminute. In actual fact, all our proposed identifications have positional discrepancies smaller than this and none lie close to the boundary of this error circle. We are therefore confident that we have not missed any possible detections.

Positional discrepancies in the perpendicular direction to the scan averaged 10–20 arcsec, and in the parallel direction about 30–40 arcsec. It was found that the brightest detections showed the least positional discrepancy, often lying within 10 arcsec of the radio galaxy position. The typical number density of IRAS sources was ~ 0.2 per square arcminute and in no case were there two candidate IRAS detections at a given radio source position. A signal to noise threshold of 4.5σ was chosen.

Following the precepts of the Explanatory Supplement to the IRAS Catalogue the following operations were carried out. For each detection, the 'inband flux' ($\mathrm{W\,m^{-2}}$) measurements were converted to a flux density (Jy) by multiplying by the bandwidth terms for the four bands ($7.91 \times 10^{12}, 2.00 \times 10^{13}, 3.93 \times 10^{13}, 9.92 \times 10^{13}$ respectively) and by multiplying by additional correction terms (1.20, 1.15, 1.22 and 1.01). For those fields observed during Satellite Operations Plan (SOP) numbers > 404, the first correction term was taken to be 1.09. Finally, the measured fluxes have been colour–corrected according to the tables in the Explanatory Supplement. These corrections are in general less than 5%. Most of the radio galaxies that were detected above the 4.5σ threshold had signal to noise ratios $5 < S/N < 10$ and, taking account of the systematic uncertainty of the IRAS calibration, we estimate that a total uncertainty of about 20% should be adopted for the flux density measurements presented in this paper.

2.2 NOTES ON INDIVIDUAL SOURCES

Seven radio galaxies (3Cs 31, 234, 293, 382, 388, 433 and 449) were identified in this way in at least one of the four IRAS passbands. 3C388 was subsequently rejected because, although the positional agreement of the single detection in band 1 was excellent (7 arcsec in each direction), the 'detection' was 7 times brighter than the upper limit of an earlier observation that had not detected this source. Brief notes on the details of the detections of the remaining 6 sources are as follows.

3C31. This source was detected in bands 3 and 4 in two different observations. All 4 detections are within the ± 25 arcsec box, and the mean positional discrepancy is less than 10 arcsec. The flux densities in the two observations agree to within 7% for both wavebands.

3C234. This source was detected on two occasions in bands 1, 2 and 3. The positional agreements worsen at the longer wavelengths, from 10 arcsec in band

1 to 45 arcsec in band 3. The flux densities of the detections in each band agree to within 8% in all three bands. The mean positional discrepancy is 4 arcsec perpendicular and 17 arcsec parallel.

3C293. This source was detected in bands 3 and 4 on two occasions; the positional agreement was best in band 3 (about 20 arcsec). The flux densities are also in close agreement (7%).

3C382. This is the most problematic source in our programme. It was observed twice and is clearly detected in band 1 on both occasions with positional discrepancies of about 20 arcsec. However, the flux densities are only consistent at the 36% level. In band 2, there is a detection with a large parallel displacement of about 1 arcmin in the second observation, and this source was not detected in band 2 in the earlier observation, indicating a flux density discrepancy of 60%. We do not include this band 2 identification in our subsequent discussion.

3C433. Only one observation of this source was made towards the end of the mission. The source is certainly detected in bands 1, 2 and 3 with positional discrepancies of $\sim$ 20 arcsec.

3C449. Again, only one observation was possible of this galaxy. In band 3 a detection with a positional discrepancy of about 40 arcsec, principally in the parallel direction, was found.

For the IRAS wavebands where no detection was found we have listed in Table 1 upper limits, and for the remaining 12 radio galaxies for which no detection was found in any waveband we have listed in Table 2 the detection limits in each passband. These upper limits are simply the 4.5σ noise threshold levels used in the source detection algorithm.

3 Discussion

The set of six radio galaxies that were detected in one or more of the IRAS

Table 1. Colour corrected flux densities (mJy) for the galaxies detected in one or more bands. The number of observations is indicated for each source.

ID	z	n	12.5 μm	25 μm	60 μm	100 μm
31	0.017	2	< 85	< 140	494	2025
234	0.185	2	176	312	240	< 400
293	0.054	2	< 82	106	275	767
382	0.059	2	161	< 127	< 118	< 270
433	0.102	1	81	215	324	< 480
449	0.017	1	< 81	< 94	142	< 480

Table 2. Upper limits to flux densities (mJy) for galaxies not detected in any of the bands.

ID	z	n	12.5 μm	25 μm	60 μm	100 μm
28	0.195	2	< 84	< 138	< 137	< 403
35	0.067	2	< 82	< 97	< 149	< 630
192	0.059	2	< 81	< 120	< 112	< 200
219	0.174	2	< 92	< 120	< 160	< 620
223	0.136	2	< 90	< 150	< 134	< 429
236	0.099	2	< 91	< 163	< 135	< 415
277	0.086	2	< 85	< 122	< 57	< 530
315	0.108	2	< 68	< 81	< 98	< 348
319	0.192	2	< 84	< 87	< 150	< 520
346	0.161	2	< 65	< 77	< 97	< 380
381	0.161	2	< 92	< 71	< 132	< 371
388	0.091	2	< 94	< 72	< 148	< 351

bands (3C31, 234, 293, 382, 433 and 449) comprise the following classes of radio galaxy. Both the BLRGs in the sample observed, 3C234 ($z = 0.185$) and 3C382 ($z = 0.059$) were detected. The three NLRGs detected (3C31, 293 and 449) are the closest NLRGs in the sample observed by IRAS, all three galaxies having $z < 0.05$. The sixth galaxy detected is the peculiar radio galaxy 3C433 ($z = 0.102$) which Lilly, Longair & Miller (1985) noted had a spectral energy distribution in the $1.0 - 3.5\,\mu$m waveband similar to that of a BLRG. This entirely reasonable set of identifications of these IRAS sources gives additional confidence that the proposed associations are correct.

The BLRGs and 3C433 were most readily detected in the shorter wavelength bands, while the three NLRGs were detected principally at longer wavelengths. This indicates that the $10 - 100\,\mu$m spectra of the two classes of object must be different. To examine the spectral energy distributions of these galaxies over a wide wavelength baseline, the new IRAS data are combined with data at other wavelengths. In Figures 1 and 2 we plot the total energy fluxes (νL_ν, units of Watts) from X–ray to radio wavelengths for the two BLRGs and four NLRGs detected in this programme. Near–infrared data are taken from 7.5 arcsec aperture $JHKL(L')$ photometry of Lilly, Longair & Miller (1985) for all sources except 3C293 which was observed by Lilly & Longair (1984). These data are approximately contemporaneous with the IRAS data. X–ray flux densities at 2 keV have been taken from Fabbiano *et al.* (1984) and were measured between 1979 and 1981. Radio flux density measurements for both nuclear and extended radio components are taken from a variety of sources (Burch 1979, Bridle, Fomalont & Cornwell 1981, van Breugel *et al.* 1983, and the compilations by Laing, Riley & Longair 1983 and Fabbiano *et al.* 1984).

While the differences in epoch of the various measurements at different wavelengths introduce some uncertainty in constructing the overall spectral energy distribution, there is no evidence for significant variability in the non–BLRG

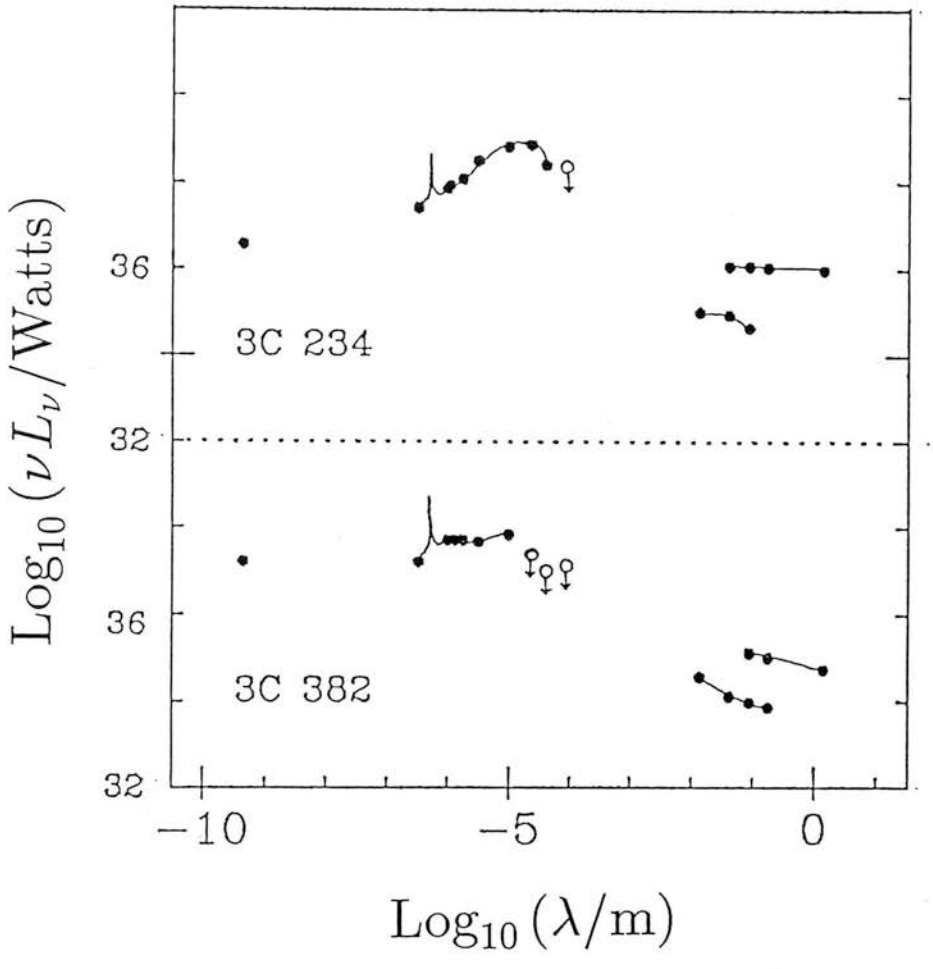

Figure 1. The luminosity per decade of wavelength, in units of $\log \nu L_\nu$ (Watts), for the two detected BLRGs as a function of $\log \lambda$ (metres) between 2keV X–ray energies and 178MHz radio frequencies. In each case the two radio luminosities that have been plotted refer to the compact nucleus and the whole source respectively.

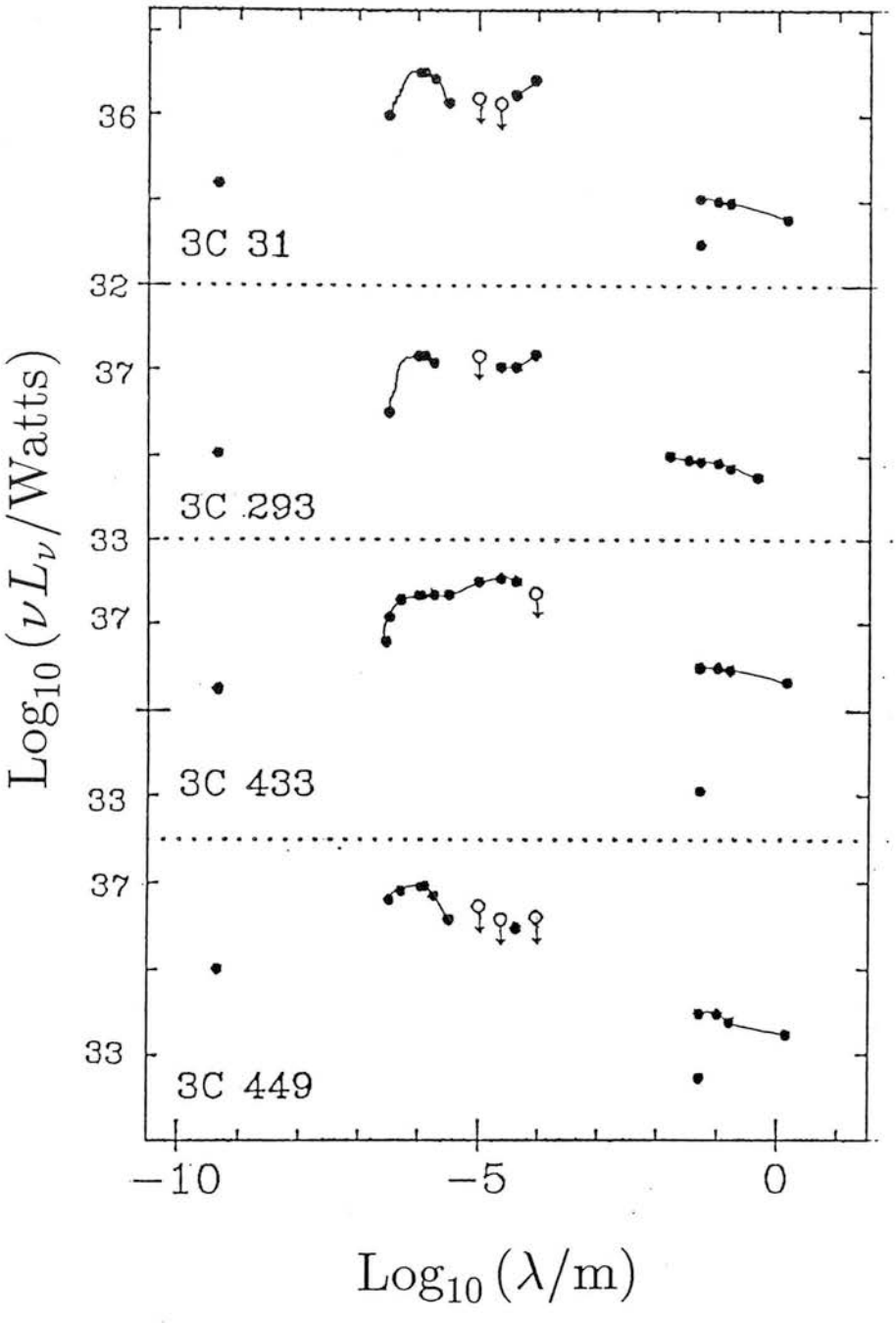

Figure 2. The luminosity per decade of wavelength for the four NLRGs detected in this programme. 3C 293 is dominated by a complex core whose integrated luminosity is shown. A flat spectrum nuclear component has not been detected in this source.

sources. Similar uncertainties arise from the different apertures used for the photometry at different wavelengths. This is most serious in the optical and near–infrared wavebands where the contamination of the nuclear emission by starlight from the host galaxy is inevitable. This stellar component dominates in most NLRGs. Some of the X–ray flux may be associated with a hot cluster gas component (Fabbiano *et al.* 1984).

3.1 THE BLRGS 3C234 AND 3C382

The 12.5 μm flux densities of both the BLRGs lie close to the extrapolation of the powerlaw–like behaviour established between 1 and 4 μm. However, like the BLRG 3C390.3 studied by Miley *et al.* (1984), both 3C234 and 3C382 have pronounced peaks in their observed flux densities around 25 μm, with effective spectral indices between 25 μm and 60 μm of 0.22 and > 0.24 respectively with uncertainties of ~ 0.15. These positive spectral indices are comparable to the $\alpha \sim 0.40$ found in 3C390.3 by Miley *et al.* (1984) and hence, as pointed out by Miley *et al.*, quite different to those found in IRAS galaxies ($\alpha \sim -0.8$) and other AGN ($-0.7 > \alpha > -1.2$). In shape, the peak in flux density in 3C234 closely resembles that in 3C390.3 although it is an order of magnitude more luminous ($10^{38.8}$ W for 3C234 compared with $10^{37.8}$ W for 3C390.3). The spectral curvature index, $\alpha(60,25) - \alpha(25,12)$, is 0.99 for 3C234 compared with 1.7 for 3C390.3 (Miley *et al.* 1984), indicating that the peak is less pronounced in 3C234. For comparison, the mean values of this index for six galaxies with measurements at 25, 60 and 100 μm (Soifer *et al.* 1984, Young *et al.* 1984) is -1.3 ± 0.4 and for five quasars (Neugebauer *et al.* 1984b) is 0.1 ± 0.2. In the case of 3C382 the peak probably occurs between 10 and 25 μm and appears to be broader than in the other BLRGs, although this may be due simply to 3C382 having a shallower overall spectrum between 1 and 25 μm.

Unlike 3C390.3, no upturn in the flux density between 60 μm and 100 μm was seen in the IRAS data for either 3C234 or 3C382, indeed neither source was

detected in the 100 μm waveband. If this long wavelength negative spectral–index component seen in 3C390.3 is associated with the flat–spectrum nuclear radio component, as suggested by Miley *et al.* (1984), then a similar component would probably not have been detected in 3C234 or 3C382 because the shortest wavelength radio flux density measurements at $\lambda \sim 2$ cm are already below the 100 μm detection threshold of about 300 mJy and because, unlike 3C390.3, there is evidence for a steepening of the radio spectral index ($\alpha < 0.0$) between 2 and 6 cm in both 3C234 and 3C382.

The nature of the 25 μm peak in 3C390.3 has been discussed by Miley *et al.* (1984) who mentioned both a thermal ($T \sim 180$ K) source and a variable self–absorbed non–thermal source possibly associated with a recent burst of nuclear activity. The fact that such a similar peak is found in both the BLRGs studied in the current programme suggests that the former explanation may be the correct one. Recent $1 - 20\,\mu$m observations of 3C234 by Elvis *et al.* (1984) and a measurement of the Pa α flux in this galaxy also apparently favour the thermal model, although a comparison of the Elvis *et al.* data with earlier photometry by Lilly & Longair (1982) and Lilly, Longair & Miller (1985) suggests that the $1 - 4\,\mu$m luminosity of this galaxy may have varied by 50% on a 2–3 year timescale. This would not be consistent with a thermal model.

If we do assume that the 25 μm component is thermal at a temperature of 180K, and that $A_V \sim 2.6$ (Carleton *et al.* 1984), then we can estimate the size of the emitting region following the analysis of Miley *et al.* (1984). This yields a size between 60 and 120 pc, which may be compared with the 180 pc derived for 3C390.3 by Miley *et al.* (1984). Miley & de Grijp (1986) note that several Seyfert galaxies in their survey show clear peaks in their IRAS spectral energy distributions, similar to those seen in the BLRGs. With a model in which the reradiating dust is optically thin and located at a distance R from a single nuclear source of heating, they estimate typical sizes in the range 15–150pc,

comparable to the BLRGs discussed here.

Whatever the cause of the 25 μm peak in the BLRGs, the luminosity distributions of Figure 1 clearly show that this component contains most of the energy output of these radio galaxies. It is also interesting to note the smooth extrapolations of their spectra from the optical to the X–ray, a feature not seen in the NLRGs.

3.2 THE NLRGS 3C31, 3C293 AND 3C449

In contrast to the BLRGs, which have substantial non–stellar components at all wavelengths 3000Å to 3.5 μm, the spectral energy distributions of the NLRGs are generally dominated by the integrated starlight of the galaxies. This is particularly true for those radio galaxies that have only weak, or even entirely absent, emission lines (i.e. Hine & Longair, HL 1979, class B sources). Apart from the anomalous 3C433, the three NLRGs detected in this programme are all HL class B galaxies. In a sample of HL class B galaxies observed by Lilly, Longair & Miller (1985), which included both 3C31 and 3C449, none showed evidence for a non–stellar radiation component at 3.5 μm. 3C31 and 3C293 were observed spectrophotometrically by Yee & Oke (1978) and, as with other class B galaxies, these galaxies show no excess of ultraviolet radiation relative to a normal giant elliptical galaxy.

The luminosity distributions of the three NLRGs 3C31, 3C293 and 3C449 are shown in Figure 2. The contrast with the BLRGs is apparent. The spectra show no sign of the peak at 25 μm found in the BLRGs and have a much cooler infrared spectrum.

The upper limits to the apparent spectral indices between 60 and 100 μm, $\alpha(60,25)$ are $< -1.42, < -1.04$ and < -0.47 for 3C31, 3C293 and 3C449 respectively. The $\alpha(100,60)$ values are -2.7, -1.9 and < -2.4. These spectral indices may be compared with mean $[\alpha(60,25) : \alpha(100,60)]$ values of $[-1.0{:}1.1]$

and [−1.2:−0.8] for Seyfert 1 and Seyfert 2 galaxies (Miley, Neugebauer & Soifer 1985), and about [−3.2:−1.8] (with considerable scatter) for normal IRAS galaxies. The shape of the far–infrared spectral energy distributions of the NLRGs are rather steeper than typically found in Seyfert galaxies and are similar to the coolest Shapley–Ames galaxies observed by de Jong *et al.* (1984).

In terms of luminosity, the far infrared sources in these three normal NLRGs are unremarkable when comparison is made with other IRAS sources. The 60 μm luminosities (νf_ν) of 3C31, 3C293 and 3C449 are $3 \times 10^{36}, 8 \times 10^{35}$ and 1.6×10^{37} W compared with a median Seyfert luminosity of around 10^{37} W (Miley, Neugebauer & Soifer 1985). The Shapley–Ames spiral galaxies studied by de Jong *et al.* (1984) typically have a 60 μm luminosity of 4×10^{36} W. The ratios of 80 μm far–infrared luminosity to optical (B band) luminosity, ($\log(L_{IR}/L_B)$, see e.g. de Jong *et al.* 1984) for the NLRGs are −1.1 and −0.6 for 3C31 and 3C293 and, based on the 60 μm luminosity, about −1.5 for 3C449. These values may be compared with typical spiral galaxy values of −0.4 (de Jong *et al.* 1984) and that of M31 of −1.4 (Habing *et al.* 1984).

Nevertheless it should be appreciated that in terms of the energy output from the active nucleus, the luminosity of this far infrared component is very large, and exceeds in every case the luminosities of the non–thermal X–ray and radio components, the latter including both the extended lobes and the compact core. If the ultimate energy source for the 100 μm component is the central nuclear engine, then most of the radiative output of the engine is in this 100 μm component. Rees *et al.* (1982) have discussed the overall energetics of the radio galaxy phenomenon, emphasising their apparent efficiency in producing collimated jets that transport considerable amounts of kinetic energy out of the nucleus (of order 10^{38} W) without a comparable radiation luminosity. The detection of substantial 100 μm components may mean that the radiation output of the nucleus is substantially higher than hitherto believed. If this radiation

is indeed nuclear in origin, then it could result from either degraded radiation initially produced at much higher frequency or directly from the central engine itself (see e.g. the models of ion–supported tori constructed by Rees *et al.* 1982 that predict substantial far–infrared radiation from a non–radiation supported accretion disk). The steepness of the 60 to 100 μm spectra, and the fact that the IRAS flux densities are greater than those of the flat spectrum radio core makes it unlikely that the far infrared component has the same origin as the radio core.

An important question, however, is whether the far–infrared emission is indeed associated with the active nucleus, or whether it is produced by processes taking place in the body of the galaxy. The colour temperatures of approximately 30K are the same as the cool dust in spiral galaxies that reradiates a small fraction of the general interstellar radiation field. Although few elliptical galaxies have been detected by IRAS (e.g. the Shapley–Ames sample studied by de Jong *et al.* 1984) dust may play an important role in these galaxies. Sadler & Gerhard (1985) have recently presented evidence that dust lanes are a common feature of nearby elliptical galaxies (about 40% have features that are interpreted as dust lanes with diameters of a few kpc) and a similar incidence of dust features has been found by Sparks *et al.* (1985). Jura (1986) has examined IRAS fluxes for a sample of elliptical and related galaxies and noted that 30–50% of the optically brightest galaxies have significant dust. He argues that within 3 kpc of the nucleus in many ellipticals, there often appears to be more cold matter than hot gas.

In this context the three normal NLRGs detected by IRAS and discussed in this section are quite interesting optically. 3C31 consists of a close pair of elliptical galaxies, NGCs 382 and 383, which clearly show a common envelope (Blandford & Icke 1978) and have a differential radial velocity of 268 $\mathrm{km\,s^{-1}}$ (Humason, Mayall & Sandage 1956) and are presumably undergoing some kind

of encounter. 3C293 is a flattened system and is somewhat spiral in appearance (Argue, Riley & Pooley 1978). Battistini *et al.* (1980) noted that it appeared to have dust lanes along the major axis. A compact object is located some 40 arcsec away from the nucleus along the major axis, but the relationship of this to the radio galaxy is not known. As with 3C31, a pair of galaxies is also identified with 3C449 (Longair & Gunn 1975) which may also be interacting, although there is at present no evidence that they are. The role of interactions in the production of starbursts in the nuclei of galaxies has been recently reviewed by Joseph (1986). Dust absorbs the hard stellar radiation and reradiates it at wavelengths longer than 30 μm. Whilst the most infrared luminous starbursts have been observed in gas rich systems (Joseph *et al.* 1984) it is possible that interacting elliptical galaxies may undergo similar bursts of lesser strength. Jura (1986) argues that even for his sample of non–interacting elliptical galaxies the IRAS data are fully consistent with significant amounts of continuing star formation.

However it would be premature to attribute the 100 μm luminosities in these NLRGs to particular peculiarities of these galaxies, and in particular to their location in possibly interacting systems. These three radio galaxies have the lowest redshifts in our sample and generally have low radio luminosities. It will be shown in Section 3.5 that the non–detections of the remainder of the NLRGs (most of which are definitely not in dumbbell systems) are consistent with them having much stronger 100 μm components. Lilly & Prestage (1987) show that dumbbell and other multiple nuclei radio galaxies are generally associated with low luminosity radio sources.

3.3 THE ANOMALOUS OBJECT 3C433

The NLRG 3C433 ($z = 0.102$) is anomalous in a number of ways. It is a powerful radio source with $P_{178} = 10^{27.5}$ W Hz^{-1} ster^{-1}, yet has a complex and diffuse radio structure (see e.g. van Breugel *et al.* 1983) that is more typical of radio sources less luminous by an order of magnitude or more. The optical spectrum is more

normal, being typical of a strong narrow–lined radio galaxy with unremarkable line widths (Koski 1978), and the reddening that may be inferred from the Balmer decrement $E(B-V) = 0.14$ is typical for this class of galaxy. The continuum as measured through a small aperture by Koski (1978) appears to be quite red, an impression supported by the earlier photometry of Sandage (1972) who measured Galactic reddening corrected colours of $(U-B) = 0.49$ and $(B-V) = 1.49$. Van Breugel *et al.* (1983) reported that 3C433 had an extended region of somewhat bluer colour that appeared to be in the form of a disk. The galaxy has a companion some 10 arcsec to the northeast, but there is no evidence for an interaction from the broad band images. Relative velocities have not yet been measured.

In the near–infrared $1-2\,\mu$m waveband, 3C433 was the only galaxy in the survey of Lilly & Longair (1984) that had significantly non–stellar JHK colours. Lilly, Longair & Miller (1985) showed that, as with the BLRGs, the excess continued approximately in power–law form to $3.5\,\mu$m. The reason why this NLRG should have a BLRG–like $1-4\,\mu$m spectral energy distribution remained a mystery.

The far–infrared spectrum of 3C433 is shown in Figure 2. As with the BLRG 3C234, the $12.5\,\mu$m flux density lies close to the extrapolation of the near–infrared spectrum measured between 1 and $4\,\mu$m. The $10-100\,\mu$m spectrum is distinctly curved and the energy output of 3C433 peaks at $25\,\mu$m like the BLRGs 3C234 and 3C390.3.

While the $1-60\,\mu$m continuum of this object is more similar to the BLRGs than to the other NLRGs it is clear that 3C433 does not possess the non–stellar ultraviolet continuum (or the broad emission lines) usually found in BLRGs. Lawrence & Elvis (1982) have suggested that there may be sufficient obscuration associated with the emission line regions of some active galactic nuclei so as to extinguish broad emission lines at optical wavelengths, thus making a BLRG

look like a NLRG in the optical. It would be interesting to set limits on the strength of Paα in the near–infrared to see whether this may be the case in 3C433.

3.4 OTHER 3C RADIO GALAXIES DETECTED IN THE IRAS POINT SOURCE CATALOGUE

The average sensitivities of the All-Sky IRAS survey (Neugebauer *et al.* 1984a) are comparable to the flux densities measured for the brightest sources in our Additional Observations programme. Consequently a search was made to determine which 3C radio galaxies in a much larger statistical sample appeared in the IRAS Point Source Catalogue (IRPS). The fields of all 118 3C radio galaxies in the statistical sample of Laing, Riley & Longair (1983) were examined. These sources have $S_{178} > 10\,\mathrm{Jy}, \delta > 10°$, and $|\mathrm{b}| > 10°$. These galaxies have redshifts ranging from 0.0009 to at least 1.79. A generous search radius of 1 arcmin was used, but in practice it was found that all the subsequent associations lay within the error ellipses given for each source in the IRPS.

Six members of this sample, all at low redshift, were detected in the all–sky survey. These were 3C84, 3C231, 3C272.1, 3C274, 3C321 and 3C390.3. The colour corrected flux density measurements for these galaxies are listed in Table 3. We have also listed in Table 3 the flux densities of 3C405 (Cygnus A), which was detected by IRAS but is not in the Laing, Riley & Longair (1983) sample on account of its low galactic latitude.

Four of these galaxies are well–known infrared sources (see e.g. Rieke & Lebofsky 1978) – 3C84 is NGC1275, 3C231 is M82, and 3C272.1 and 3C274 are M84 and M87 respectively. M82, M84 and M87 represent all the 3C radio galaxies in the Laing, Riley & Longair (1983) sample that have $z < 0.01$. In contrast, in the redshift interval $0.01 < z < 0.1$ less than 10% of the radio galaxies appear in the IRPS, and at $z > 0.1$, there are no IRPS detections.

Table 3. Colour corrected flux densities (Jy) for 3CR radio galaxies in the sample of Laing, Riley & Longair (1983) observed in the IRAS All Sky Survey.

ID		z	12.5 μm	25 μm	60 μm	100 μm
84	NGC1275	0.0172	1.21	3.60	7.57	7.61
231	M82	0.0009	62.63	279.59	1215.84	1107.57
272.1	M84	0.0031	< 0.43	< 0.50	0.50	< 1.36
274	M87	0.0043	< 0.48	< 0.34	0.46	< 1.15
321		0.096	< 0.25	0.38	1.06	1.03
390.3		0.0569	< 0.25	0.29	< 0.40	< 1.00
405	Cyg A	0.0567	< 0.25	1.20	2.18	< 8.11

M84 and M87 were both detected at 60 μm only, thus little can be said about their far–infrared spectral energy distributions from these data. The four sources with $0.01 < z < 0.1$ are 3C84, the BLRG 3C390.3 discussed in Section 3.1, and the very strong–lined NLRGs 3C321 and 3C405. The overall spectral energy distribution of 3C84 has been studied by Longmore *et al.* (1984). This source has a flat spectrum for $\lambda > 30\,\mu$m, and Longmore *et al.* (1984) argued that the dominant radiation mechanism for this source is non–thermal synchrotron. 3C321 has an infrared spectrum that is very similar to that of 3C84, with $\alpha(100,60) = 0.06$ and $\alpha(60,25) = -1.7$, and is also, like 3C84, a flat spectrum radio source although with classical double structure (Jenkins, Pooley & Riley 1977). In view of these similarities, the far–infrared radiation detected by IRAS is probably also produced by the non–thermal synchrotron mechanism. 3C405, Cygnus A, has a spectrum that appears intermediate between the BLRGs and the NLRGs and is reminiscent of the anomalous object 3C433. The luminosity of Cygnus A peaks at about 60 μm, and at this wavelength is second only to 3C234 in luminosity in our sample.

3.5 THE UNDETECTED SOURCES

Two thirds of the sample observed in our AO programme were not detected in any of the four IRAS wavebands, and it is of interest to determine to what extent these non–detections constrain the properties of these galaxies relative to the galaxies that were detected. This is particularly true for the strong–lined (HL class A) NLRGs, for which only the peculiar 3C433 was detected.

In Figure 3 we have plotted the 60 μm luminosities (νL_ν) of the detected sources and upper limits for the remainder, as a function of redshift. Three lines of constant observed flux density are also shown.

It is clear that 3C234 and 3C433 must have luminosities that are considerably above average for the sample, but that those for the nearby NLRGs, 3C31, 3C293

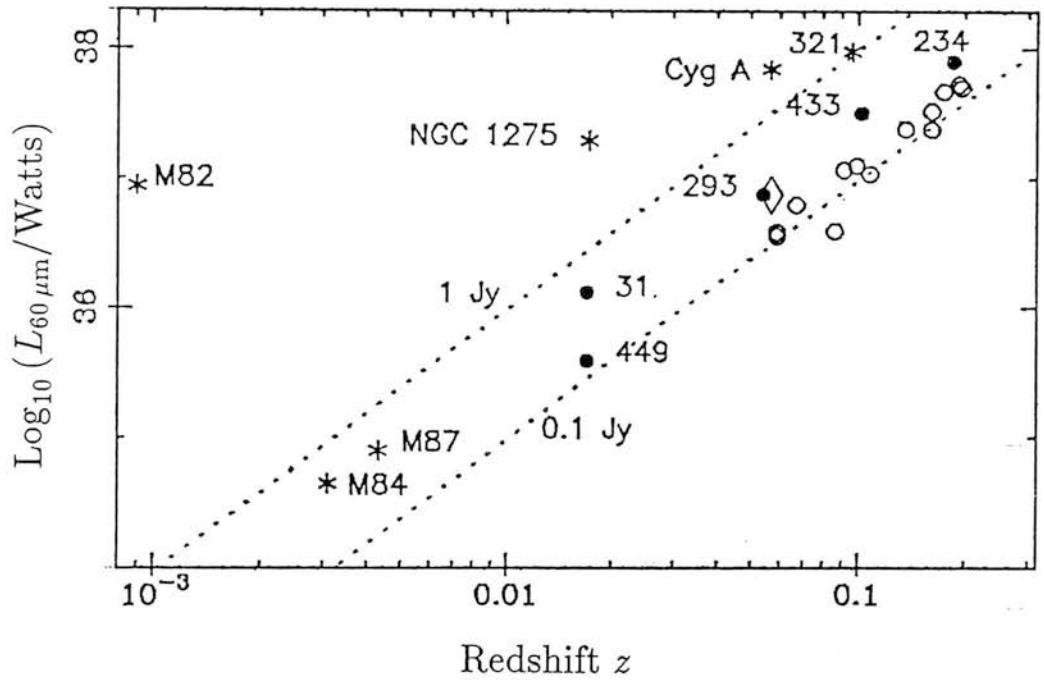

Figure 3. The luminosity per decade of wavelength (Watts) at $60\,\mu m$, (five detections plotted as filled circles and 13 upper limits plotted as open circles) as a function of redshift for all 18 galaxies observed by IRAS in our Additional Observations programme. Also shown, as asterisks, are the $60\,\mu m$ luminosities for the 3C galaxies observed by IRAS in the All Sky Survey and included in the sample of Laing, Riley & Longair (1983). Cygnus A (excluded from this sample) is also shown for comparison. 3C390.3 only has an upper limit at $60\,\mu m$ in the All Sky Survey but was observed by Miley *et al.* (1984) with the satellite operating in Deep Survey Mode: the resulting $60\,\mu m$ luminosity is plotted here as an open diamond.

and 3C449, are probably not unusually large. The upper limits to the 60 μm luminosities are in almost all cases consistent with at least the luminosity of 3C293.

4 Conclusions

The fields of 18 3C radio galaxies with $0.01 < z < 0.2$ have been observed using the Deep Survey mode of IRAS. Only six galaxies were detected, comprising the two BLRGs, the three nearest NLRGs and the anomalous object 3C433. Construction of the spectral energy distributions of these sources between X-ray and radio wavelengths have enabled the following conclusions to be reached.

1) Both the BLRGs have far-infrared spectral energy distributions that peak at around 25 μm and decline to longer wavelengths. This peak is the same as has been seen earlier in the BLRG 3C390.3 and this suggests that this is not a transient phenomenon and is probably associated with a warm ($T \sim 180K$) dust component, which in the case of 3C234 might also account for the reddening inferred from the hydrogen line ratios in this galaxy. This 25 μm peak contains most of the luminosity of these objects.

2) The three NLRGs that were detected have $z < 0.05$ and are associated with relaxed double radio sources. They have at most weak optical emission lines and no detectable non-stellar component at either 3000Å or 3.5 μm, but nevertheless have substantial far-infrared luminosities of order 10^{36} Watts at 60 μm. These dominate the luminosity output of the galaxies. The NLRGs do not appear to have the 25 μm component seen in the BLRGs. Two of the NLRGs show some evidence for having undergone an interaction with companion galaxies, but it is not known to what extent this may have contributed to the infrared luminosity.

3) The NLRG 3C433 which had previously been shown to have an anomalous BLRG-like near-infrared spectral energy distribution has a $10 - 100\,\mu$m spectrum that is also similar to the BLRGs.

A systematic search of the IRAS All Sky Survey has also been made in the fields of a complete sample of 118 3C sources extending to redshifts in excess of unity. A further six sources, all with $z < 0.1$, were identified. These comprise the well–known infrared sources 3C231, 3C272.1 and 3C274 (M82, M84 and M87 respectively), 3C84 (NGC1275) and 3C321 and 3C390.3. Consideration of these, together with 3C405 (outside the complete sample), shows that the strong NLRGs 3C321 and 3C405 have high 60 μm luminosities comparable to the BLRGs and 3C433 detected in the main programme.

Acknowledgments

We are grateful for the opportunity to have participated in the IRAS mission and appreciate the efforts of those who made it a success. SJL was supported by a SERC/NATO Overseas Research Fellowship at Princeton University at the start of this research. MGY is grateful for an SERC Research Studentship.

References

Argue, A.N., Riley, J.M. & Pooley, G.G., 1978. *Observatory*, **98**, 132.

Battistini, P., Bonoli, F., Silvestro, S., Fanti, R., Gioia, I.M. & Giovannini, G., 1980. *Astr. Astrophys.*, **85**, 101.

Blandford, R.D. & Icke, V., 1978. *Mon. Not. R. astr. Soc.*, **185**, 527.

Burch, S.F., 1979. *Mon. Not. R. astr. Soc.*, **186**, 293.

Bridle, A.H., Fomalont, E.B. & Cornwell, T.J., 1981. *Astr. J.*, **86**, 1294.

Carleton, N.P., Willner, S.P., Rudy, R.J. & Tokunaga, A.T., 1984. *Astrophys. J.*, **284**, 523.

de Jong, T., Clegg, P.E., Soifer, B.T., Rowan–Robinson, M., Habing, H.J., Houck, J.R., Aumann, H.H. & Raimond, E., 1984. *Astrophys. J.*, **278**, L67.

Elvis, M., Willner, S.P., Fabbiano, G., Carleton, N.P., Lawrence, A. & Ward, M., 1984. *Astrophys. J.*, **280**, 574.

Fabbiano, G., Miller, L., Trinchieri, G., Longair, M. & Elvis, M., 1984. *Astrophys. J.*, **277**, 115.

Habing, H.J., Miley, G., Young, E., Baud, B., Boggess, N., Clegg, P.E., de Jong, T., Harris, S., Raimond, E., Rowan–Robinson, M., Soifer, B.T., 1984. *Astrophys. J.*, **278**, L59.

Hine, R.G. & Longair, M.S., 1979. *Mon. Not. R. astr. Soc.*, **188**, 111.

Humason, M.L., Mayall, N.U. & Sandage, A.R., 1956. *Astr. J.*, **61**, 97.

Jenkins, C.J., Pooley, G.G. & Riley, J.M., 1977. *Mem. R. astr. Soc.*, **84**, 61.

Joseph, R.D., 1986. *New Light on Dark Matter, Proc. of 1st Int. IRAS Conf.*, p.447, ed. Israel, F.P., Reidel, Dordrecht.

Joseph, R.D., Meikle, W.P.S., Robertson, N.A. & Wright, G.S., 1984. *Mon. Not. R. astr. Soc.*, **209**, 111.

Jura, M., 1986. *Astrophys. J.*, **306**, 483.

Koski, A.T., 1978. *Astrophys. J.*, **223**, 56.

Laing, R.A., Riley, J.M. & Longair, M.S., 1983. *Mon. Not. R. astr. Soc.*, **204**, 151.

Lawrence, A. & Elvis, M., 1982. *Astrophys. J.*, **256**, 410.

Lilly, S.J. & Longair, M.S., 1982. *Mon. Not. R. astr. Soc.*, **199**, 1053.

Lilly, S.J. & Longair, M.S., 1984. *Mon. Not. R. astr. Soc.*, **211**, 833.

Lilly, S.J., Longair, M.S. & Miller, L., 1985. *Mon. Not. R. astr. Soc.*, **214**, 109.

Lilly, S.J. & Prestage, R.M., 1987. *Mon. Not. R. astr. Soc.*, **225**, 531.

Longair, M.S. & Gunn, J.E., 1975. *Mon. Not. R. astr. Soc.*, **170**, 121.

Longmore, A.J., Sharples, R.M., Tokunaga, A.T., Rudy, R.J., Robson, E.I., Ade, P.A.R. & Radostitz, J., 1984. *Mon. Not. R. astr. Soc.*, **209**, 373.

Lonsdale, C.J., Helou, G., Good, J.C. & Rice, W., 1985. *Catalogued Galaxies and Quasars Observed in the IRAS Survey*, Jet Propulsion Laboratory.

Miley, G., Neugebauer, G., Clegg, P.E., Harris, S., Rowan–Robinson, M., Soifer, B.T. & Young, E., 1984. *Astrophys. J.*, **278**, L79.

Miley, G.K., Neugebauer, G. & Soifer, B.T., 1985. *Astrophys. J.*, **293**, L11.

Miley, G.K. & de Grijp, R., 1986. *New Light on Dark Matter, Proc. 1st Int. IRAS Conf.*, p.471, ed. Israel, F.P., Reidel, Dordrecht.

Neugebauer, G., Habing, H.J., van Duinen, R., Aumann, H.H., Baud, B., Beichman, C.A., Beintema, D.A., Boggess, N., Clegg, P.E., de Jong, T., Emerson, J.P., Gautier, T.N., Gillett, F.C., Harris, S., Hauser, M.G., Houck, J.R., Jennings, R.E., Low, F.J., Marsden, P.L., Miley, G., Olnon, F.M., Pottasch, S.R., Raimond, E., Rowan–Robinson, M., Soifer, B.T., Walker, R.G., Wesselius, P.R. & Young, E., 1984a. *Astrophys. J.*, **278**, L1.

Neugebauer, G., Soifer, B.T., Miley, G., Young, E., Beichman, C.A., Clegg, P.E., Habing, H.J., Harris, S., Low, F.J., Rowan–Robinson, M., 1984b. *Astrophys. J.*, **278**, L83.

Rees, M.J., Begelman, M.C., Blandford, R.D. & Phinney, E.S., 1982. *Nature*, **295**, 17.

Rieke, G.H. & Lebofsky, M.J., 1978. *Astrophys. J.*, **220**, L37.

Sadler, E.M. & Gerhard, O.E., 1985. *Mon. Not. R. astr. Soc.*, **214**, 177.

Sandage, A., 1972. *Astrophys. J.*, **178**, 25.

Soifer, B.T., Rowan–Robinson, M., Houck, J.R., de Jong, T., Neugebauer, G., Aumann, H.H., Beichman, C.A., Boggess, N., Clegg, P.E., Emerson, J.P., Gillett, F.C., Habing, H.J., Hauser, M.G., Low, F.J., Miley, G. & Young, E., 1984. *Astrophys. J.*, **278**, L71.

Sparks, W.B., Wall, J.V., Thorne, D.J., Jorden, P.R., van Breda, I.G., Rudd, P.J. & Jorgensen, H.E., 1985. *Mon. Not. R. astr. Soc.*, **217**, 87.

van Breugel, W., Balick, B., Heckman, T., Miley, G. & Helfand, D., 1983. *Astr. J.*, **88**, 40.

Wolstencroft, R.D., Clowes, R.G., Kalafi, M., Leggett, S.K., MacGillivray, H.T., & Savage, A., 1986. *New Light on Dark Matter, Proc. of 1st Int. IRAS Conf.*, p.425, ed. Israel, F.P., Reidel, Dordrecht.

Yee, H.K.C. & Oke, J.B., 1978. *Astrophys. J.*, **226**, 753.

Young, E., Soifer, B.T., Low, F., Neugebauer, G., Rowan–Robinson, M., Miley, G., Clegg, P.E., de Jong, T. & Gautier, T.N., 1984. *Astrophys. J.*, **278**, L75.

Postscript at February 1988.

The main factor which hampered this work was the comparatively poor sensitivity of the IRAS satellite, even with the use of pointed Additional Observations. The small number of positive detections that were obtained (even for $z < 0.1$) does not yet allow a wholly representative discussion of the $12 - 100\,\mu$m spectra of the most powerful radio galaxies. Even so, it was encouraging that we were able to distinguish between the IRAS spectra of the narrow– and broad–line galaxies notwithstanding the small sample. A more effective study of the far–infrared spectra of powerful radio galaxies should be possible with the Infrared Space Observatory (ISO) which will have a sensitivity in the $12 - 100\,\mu$m region approximately 100 times better than was possible with IRAS.

Chapter 5

Near–simultaneous optical and infrared spectrophotometry of active galaxies.

To be published in *Mon. Not. R. astr. Soc.*

Prologue to *"Near-simultaneous optical and infrared spectrophotometry of active galaxies."*

This paper tackles broadly the same problem as the previous one, namely the energetics of active galaxies, and the possible role that dust plays in the reprocessing of their radiation. However, here we concentrate on optically bright quasars (although including a lone broad–line radio galaxy, 3C120) and utilize more accessible regions of the spectrum, namely the optical and the near–infrared. The presence or absence of dust in active galaxies has been fiercely debated for the last fifteen years or so, and my feeling is that not much progress has been made, and that the various protagonists have become rather entrenched. This is a pity, because if we are to ever understand the physics of active galaxies, it is vital to understand how the line–emission that we observe is reprocessed. There are some, such as Grandi, who will argue vehemently that spectroscopy of active galaxies is virtually useless as a physical probe, with our knowledge of the photoionization processes that may be involved in the line–emitting regions being far too scanty at present. At the other extreme, some tend to treat any reasonable departure from a predicted unreddened spectrum as evidence for dust.

Our aim in this present work was to try to obtain data of a higher quality than was possible in 1980, when the two previous attempts at optical–infrared spectrophotometry of bright quasars were made. We were also very keen to try to approach the problem of dust in active galaxies from a rather more neutral standpoint than has been adopted by many workers in this field in the past.

This project was done in collaboration with Ron Garden (University of California, Berkeley) who was responsible for the reduction of the infrared spectra. The rest of the paper, and its conclusions are solely my responsibility.

Summary

We present optical and infrared spectrophotometry for a sample of eight optically bright quasars, and the broad–line radio galaxy (BLRG) 3C120. The optical and infrared spectrophotometry is separated by only five weeks, thus we have been able to minimise uncertainties due to variations in the objects. We compare our observed Paα/Hα and Hα/Hβ ratios with a large number of current photoionization models. We find that none of these models are able to reproduce our observed values of Paα/Hα in any of the active galaxies except 3C273. Generally, the predicted values of Paα/Hα are too low, although the predicted values of Hα/Hβ are in good agreement. Our observed ratios are not even well modelled by *reddened* photoionization models. We present evidence to suggest that any reddening in 3C273 is minimal, and compare the observed line ratios for the rest of our sample with 3C273 ratios which are subject to various amounts of reddening. Three of our quasars have 1–2 mag. of dust with respect to 3C273, and data at other wavelengths (e.g. *IRAS*) supports this conclusion. Two quasars are not well modelled by a reddened 3C273 spectrum, but their Paα/Paβ and Brγ/Paα ratios suggest that they too are subject to reddening. The BLRG 3C120 has 1–2 mag. of reddening with respect to 3C273, but the evidence from other wavelengths is inconclusive.

1 Introduction

The aim of this paper is to use optical and infrared hydrogen–recombination line ratios to probe the conditions of the line–emitting regions of optically bright quasars. In particular, we aim to address the complex problem regarding the presence or absence of dust in these regions. An important aspect of this present work is that in all cases we have obtained the optical and infrared line measurements within five weeks of each other, thus considerably reducing the inherent problems of variability encountered in much of the longer time–baseline optical–infrared spectrophotometry reported until now (e.g. Puetter *et al.* 1981, Soifer *et al.* 1981). The main motivation behind this work is that quasar emission lines are one of the prime diagnostics that will help us to understand the quasar phenomenon, but before any progress can be made it is necessary to understand to what extent our observed quasar spectra are different from the intrinsic emitted spectra, both as a result of physical conditions in the broad and narrow–line regions of quasars, and from the presence of intervening dust.

The advantage of using optical and infrared line ratios (as opposed to purely optical line ratios such as the Balmer decrement) is that Paα($\lambda = 1.875\,\mu$m, $n = 4 \rightarrow 3$) and Hβ($n = 4 \rightarrow 2$), the main diagnostics to be used in this present work, arise from the same upper level. Thus they are likely to be less sensitive to high electron densities and the effects of collisional excitation and de–excitation than Balmer lines alone. This is an advantage in that the densities in the broad–line region (BLR) may be high enough to produce significant changes in the intrinsic line–ratios, making it difficult to disentangle the effects of reddening from high density recombination. In addition, a long wavelength baseline is useful for determining the differential reddening.

Another useful ratio is that between Brγ ($\lambda = 2.165\,\mu$m, $n = 7 \rightarrow 3$) and Paα. The two lines have a small wavelength separation and lie in a region where galactic dust extinction is small, thus total or selective extinction will not have

a large effect. The two lines arise in different levels, so there is hope that density and optical depth dependent effects may be extricable, and that the ratio can be used as a test of non–standard recombination.

There has been more than one previous attempt to use optical and infrared hydrogen recombination line ratios to study the role that dust might play in the reprocessing of the line emission in quasars (Puetter *et al.* 1981, Soifer *et al.* 1981) and in Seyferts (e.g. McAlary *et al.* 1986, Lacy *et al.* 1982). However, it would be fair to say that no clear consensus has been reached, except to confirm that pure case B recombination theory is not a good description of the line ratios in bright active galactic nuclei. Given that there are good reasons (discussed in Section 6) to expect that case B theory is invalid at the high densities likely to be encountered in the BLR of active galaxies, the most fruitful starting point would appear to be a comparison of the observed ratios with the many sophisticated photoionization models, incorporating collisional processes and contributions from non–hydrogenic electrons amongst other refinements (Kwan 1984, Hubbard & Puetter 1985, Collin–Souffrin *et al.* 1986, and references therein). These models have been calculated for a wide range of densities, temperatures and optical depths and thus allow one to study a good fraction of the likely parameter space.

However, Grandi (1983) has cast doubt that, in the absence of a firm knowledge of the *intrinsic* ratios, hydrogen recombination lines will ever tell us anything useful about the conditions in active galaxies, and urges caution in assuming that the photoionization models are even approximately correct. There are several grounds for optimism though: In general, the regions on the Paα/Hβ – Hα/Hβ plane covered by the many models noted above is very small, despite the wide range of physical conditions involved. McAlary *et al.* (1986) obtained hydrogen recombination line ratios for a sample of Seyfert 1 galaxies and found that the array of models that they considered (principally those of Krolick &

McKee 1978, Kwan & Krolick 1981, Canfield & Puetter 1981 and Drake & Ulrich 1980) was well bounded on this plane by a triangle consisting of low–density case B with zero reddening, infinite density case B with zero reddening and infinite density case B with 0.4 mag. reddening. Thus the available models could only mimic up to 0.4 mag. of reddening, and then only if at infinite density. They concluded that the galaxies above this triangular region, and in particular those close to the low–density case B model *must* be reddened regardless of the physical conditions.

Even if one accepts Grandi's (1983) pessimism in full (which we do not), this present study is still of value. Even if we can not discover the physical conditions of the line–emitting regions in quasars, we will at least be able to make a firm statement about the ability of the present models to reproduce the observed line ratios, and thereby suggest further regions of parameter space that must be explored, and the range of observed parameters that must be reproduced. Our starting point will be a more optimistic one in that we will assume that the models *may* produce approximately the correct ratios for the physical conditions they claim to model, and we will first consider any departures from the models in the light of this assumption; then we will examine whether there is any evidence to reject the validity of the models altogether.

Early studies of the infrared–optical hydrogen recombination line ratios in quasars tended to make the initial assumption that the intrinsic line–emission obeys case B recombination theory, and then examined ways of producing any observed departures from the predicted values (for example by the addition of reddening). Puetter *et al.* (1981) studied Paα/Hβ with respect to Hβ/Hα ratios for 14 quasars and noted that several had ratios inconsistent with case B theory, but that the trend was in a sense opposite to that expected in the presence of reddening. The Paα/Hα ratios showed little or no reddening, and in some cases were depressed below case B values. In addition, they explored

the photoionization models of Kwan & Krolick (1979) and Canfield & Puetter (1981) to some extent, obtaining a fair agreement between the models and the observations. However, there were several notable discrepancies in that the Kwan & Krolick (1979) model predicted Balmer decrements that were too steep and Balmer continua that were too weak. This was in contrast to the Canfield & Puetter (1981) calculations which tended to produce Balmer continua that were too strong. Despite these discrepancies, Puetter *et al.* (1981) concluded that dust does not dominate the BLR of quasars. Similarly, Soifer *et al.* (1981) found that the Paα/Hβ and Hβ/Hα ratios for a sample of 16 quasars tended to cluster around case B values and so they concluded that the evidence was broadly against dust being important.

Little attempt at simultenaity between the optical and infrared observations was made in either of these two programmes. Many active galaxies, including quasars, are known to vary on a wide range of timescales, and for Seyferts in particular, variations are known to occur on timescales shorter than one month (e.g. Peterson 1987). Zheng *et al.* (1987) present good quality spectrophotometric data for 5 low–redshift quasars obtained over a period of several years and significant variations in the line fluxes are apparent on timescales at least as short as a year – shorter periods could not be studied owing to a lack of time resolution, and periods as short as those seen in Seyferts can not be ruled out. Thus it is imperative that the optical and infrared work be as near contemporaneous as possible.

This present work therefore aims to offer an improvement over the earlier quasar studies of Puetter *et al.* (1981) and Soifer *et al.* (1981) by obtaining near–simultaneous optical and infrared spectrophotometry, better quality infrared data, and by comparing the resultant line–ratios with the most recent models. In Section 2 we describe the sample and in Section 3 the infrared and optical spectrophotometry. Section 4 discusses the derivation of the line parameters and

Section 5 presents a detailed discussion of the reliability of our new data. Section 6 discusses the trends in the data as a whole and finally, Section 7 presents our conclusions.

2 The sample

The main criterion for inclusion in our sample is that the quasar is optically bright ($V < 16.5$), and our sample contains both radio–loud and radio–quiet objects. The main infrared line of interest is Paα which lies in the K window ($1.9\,\mu$m $- 2.5\,\mu$m) for the redshift range $0.00 \leq z \leq 0.24$. For those objects with $z < 0.1$, Brγ is also accessible in this window, and for objects with $z > 0.2$ Pa$\beta(\lambda = 1.282\,\mu\text{m}, n = 5 \rightarrow 3)$ is accessible in the H window ($1.45\,\mu$m$-1.8\,\mu$m).

Our primary source list was the optical catalogue of Hewitt & Burbidge (1987) and our sample consists of 8 quasars selected from this compilation according to the above noted magnitude and redshift constraints. It is otherwise unbiassed with respect to any other property. In addition to this sample of optically bright quasars, we also observed the well–known broad–line radio galaxy 3C 120 ($z = 0.0325$). Table 1 gives details of the 10 objects observed. The magnitudes shown are taken from the literature and in most cases are rather uncertain owing to the objects' possible variability.

3 Observations

3.1 INFRARED SPECTROSCOPY

Infrared spectra were obtained for all the objects in our sample (except 3C273) using UKT9 and the circular variable filter (CVF) on the United Kingdom Infrared Telescope (UKIRT) during the nights of 1987 January 31 – February 3. An aperture of 19.6 arcsec diameter was used in the majority of cases (12.4 arcsec for the remainder) and a beam throw of 35 arcsec in an optimal direction. K and H window scans typically covered $0.2\,\mu$m of the window, fully sampled at

Table 1. The sample.

IAU	Other	z	b°	mag.[(a)]
0736+017	PKS	0.191	+11	16.47* (V)
0837−120	3C206	0.198	+17	15.76* (V)
0953+414	PG	0.239	+52	15.05 (B)
1001+054	PG	0.161	+45	16.13 (B)
1151+117	PG	0.176	+69	15.51 (B)
1211+143	PG	0.085	+74	14.63 (B)
1226+023	3C273	0.158	+64	12.86* (V)
1229+204	Ton1542	0.064	+82	15.6 (B)
0430+052	3C120	0.033	−27	13.9* (V)

Note:
(a): An asterisk denotes known variability.

a resolution of $R \sim 150$ (about 3000 $\mathrm{km\,s^{-1}}$) and total co–added integration times of $\sim$ 10s per point. Spectra of featureless late–type stars were used to flux–calibrate the object spectra. Conditions were generally photometric although mitigated by high winds: however, our large aperture ensured that any consequent loss of flux was minimal.

3C273 was observed at UKIRT by Dr T.R. Geballe on the night of 1987 January 4 using the same instrumental set–up as in our own work, although employing a smaller aperture (7.8 arcsec), and he has kindly allowed us to use the resultant Paα flux.

Table 2 presents a log of the observations and the infrared lines observed in each case. Fig. 1(a)–(f) shows examples of the infrared spectra obtained for five of the quasars and the BLRG 3C120.

3.2 OPTICAL SPECTROSCOPY

3.2.1 Observing procedure

Optical spectra were obtained using the Durham/RGO Faint Object Spectrograph (FOS) on the Isaac Newton 2.5m telescope (INT) at La Palma during the nights of 1986 December 22–23. The FOS is a fixed format system employing a transmission grating with a cross–dispersing prism, providing two spectral orders encompassing the wavelength range 4000–10500Å. The first order covers 5000–10500Å and the second order 4000–5500Å, thus there is some overlap. The spectra are imaged onto a GEC CCD at a dispersion of 10.7Å per pixel (first order) and 5.4Å per pixel (second order). Although the resolution is comparatively low, $\sim 400\,\mathrm{km\,s^{-1}}$ at 7876Å (the wavelength of Hα at $z = 0.2$) this was more than adequate for the broad Balmer lines encountered in the quasars, which typically have FWHM $> 3000\,\mathrm{km\,s^{-1}}$. The wide wavelength range comfortably included all the main lines of interest in a single exposure for the entire redshift range of our sample. Each spectrum consists of adjacent columns of

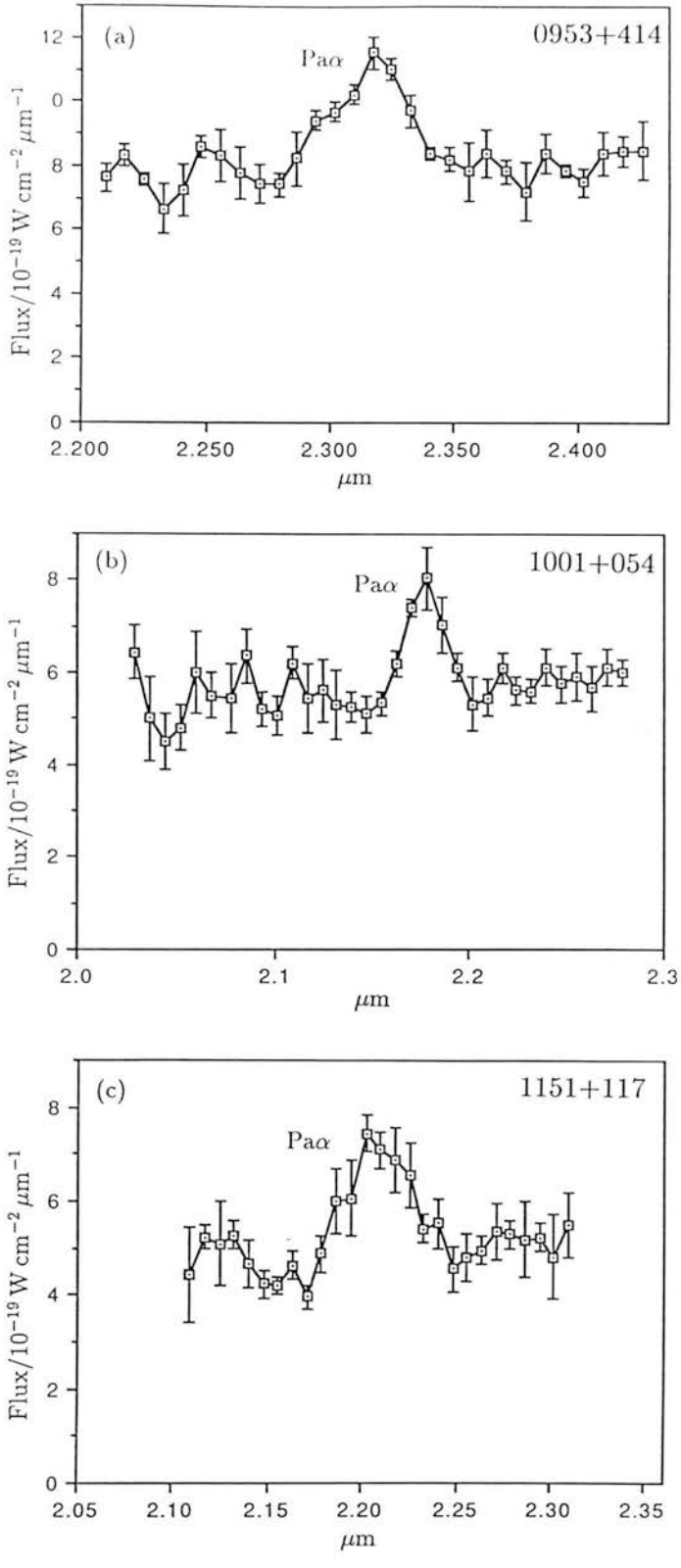

Figure 1. Infrared spectra, obtained with the CVF at UKIRT, of five quasars and one broad-line radio galaxy (3C120): (a) 0953+414; (b) 1001+054; (c) 1151+117; (d) 1211+143; (e) 1229+204; (f) 3C120.

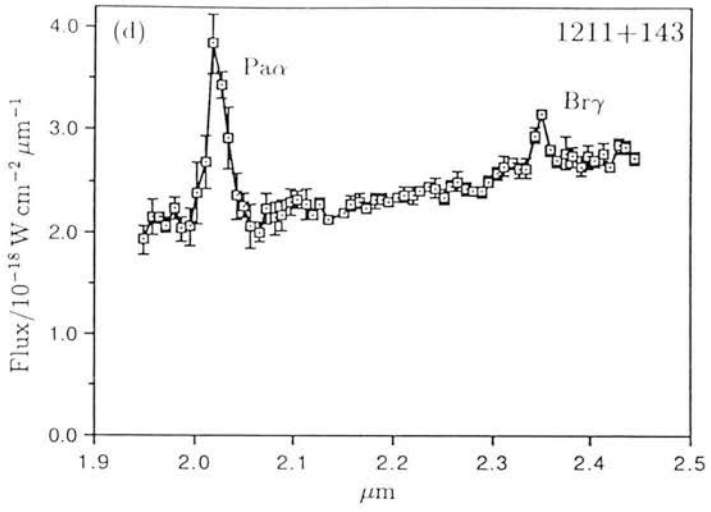

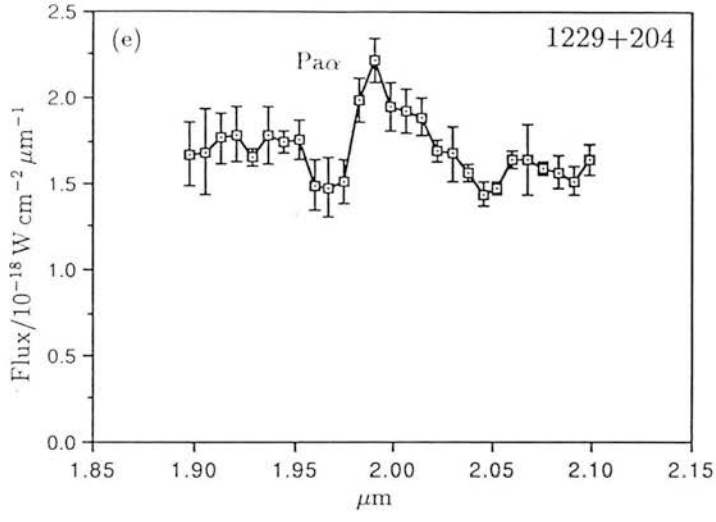

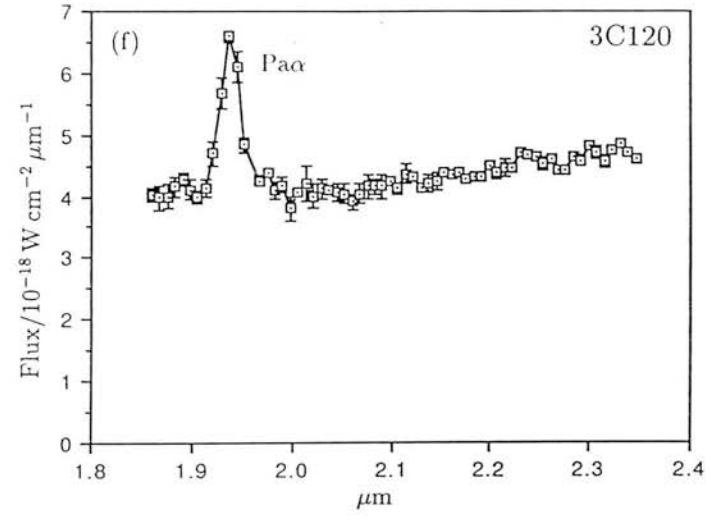

Figure 1 – *continued.*

sky and object spectra (typically three columns of sky flux on either side of 10 columns of object flux).

A slit width of 5.0 arcsec was used so as to sample as much of the object flux as possible, and all object spectra were obtained at the parallactic angle (i.e. perpendicular to the horizon, and thus reducing the effects of atmospheric diffraction). Integration times ranged from 100s for 3C273 to 2000s for the faintest objects. White dwarfs from the list of Oke (1974) were used as flux–calibrators and were taken throughout each night so as to well sample the range of airmasses encountered for the various quasar spectra. 80% of the quasar spectra were taken at airmasses less than 1.25, and the remaining 20% at less than 1.75. In addition to Cu–Ar and Cu–Ne arc spectra for wavelength calibration, dark and bias frames were obtained each night, and 10s exposures of a tungsten lamp imaged through the slit so as to provide a uniform and high signal to noise flat–field calibrator. Several quasars were observed twice during the course of the run, and some three times. Table 2 indicates the dates of the respective optical and infrared observations of each object.

3.2.2 Spectrum reduction

Mean bias frames were derived for each night's observation and used to de–bias all the data frames – no secular trend in the bias level was found during either of the two nights. The dark frames indicated that the dark current was effectively zero. The FOS produces images of the spectra with significant curvature transverse to the wavelength direction, and as a function of wavelength; before flat–fielding, the first and second order spectra were straightened using standard FIGARO software. This procedure was applied to all the data (including the arcs and tungsten lamp exposures). The spectra were then flat–fielded by fitting a polynomial to the respective first and second order tungsten lamp exposures, normalising, and dividing these fits into the first and second order object spectra. The tungsten exposures were collapsed in the direction transverse to the wave-

Table 2. Observing Log.

Object	Infrared (UKIRT)		Optical (INT)
	Dates (UT)	Lines	Dates (UT)
0736+017	1987 Feb. 3	Paα	1986 Dec. 23
3C206	1987 Feb. 3,4	Paα	1986 Dec. 23
0953+414	1987 Feb. 3	Paα, Paβ	1986 Dec. 23
1001+054	1987 Feb. 3,4	Paα	1986 Dec. 24
1151+117	1987 Feb. 4	Paα	1986 Dec. 24
1211+143	1987 Feb. 3	Paα, Brγ	1986 Dec. 24
3C273	1987 Jan. 5	Paα	1986 Dec. 24
1229+204	1987 Feb. 4	Paα	1986 Dec. 24
3C120	1987 Feb. 3	Paα	1986 Dec. 23

length before fitting the polynomial, thus the flat–field correction achieved was purely in the wavelength direction i.e. only row to row (equivalent to wavelength bin to bin) sensitivity variations were accounted for.

Sky and object spectra were extracted for each spectrum, and sky subtracted spectra derived. The spectra were then wavelength calibrated and re–binned to a linear scale in wavelength. The spectra were flux–calibrated using the white dwarf spectra, matching the airmasses of the object and calibration spectra as closely as possible. Our spectra encompass several atmospheric features (in particular the 7600Å band of O_2), and an attempt was made to correct for this by dividing the object spectra near the affected regions with a normalised stellar spectrum. Some of our lines are close to, or overlie the 7600Å feature and this will reduce the accuracy of the derived fluxes. Finally the first and second order spectra were merged in wavelength so as to provide the full spectral coverage (4000–10500Å). Fig.2 (a)–(e) shows spectra of four of the quasars and the BLRG 3C120.

4 Line parameters

In this section we discuss the derivation of the line fluxes, widths and ratios, and tabulate the results.

4.1 INFRARED LINES

Line fluxes were derived for the optical lines by making a least squares fit to selected continuum segments about the line of interest, integrating over the line interval, and subtracting the interpolated continuum. Many of the lines show asymmetric profiles and so it was not appropriate to model them with a Gaussian. Errors were derived by calculating the deviation between individual data points for the $\sim$ 10 spectra which were co–added together to produce each final object spectrum. In addition, an estimate of the uncertainty in the continuum level is included.

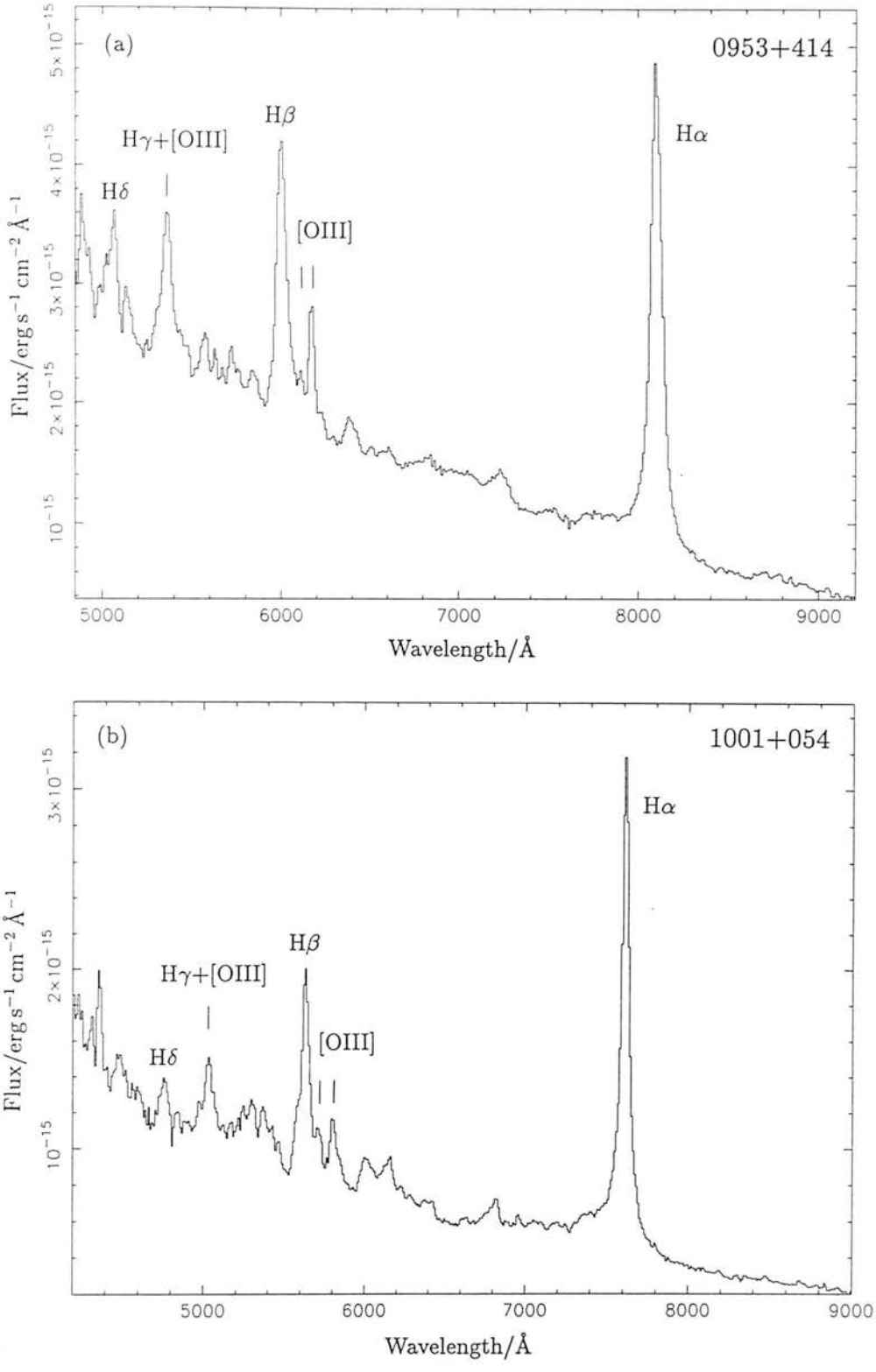

Figure 2. Optical spectra, obtained with the FOS at the INT, of four quasars, and one broad–line radio galaxy (3C120): (a) 0953+414; (b) 1001+054; (c) 1151+117; (d) 3C273; (e) 3C120

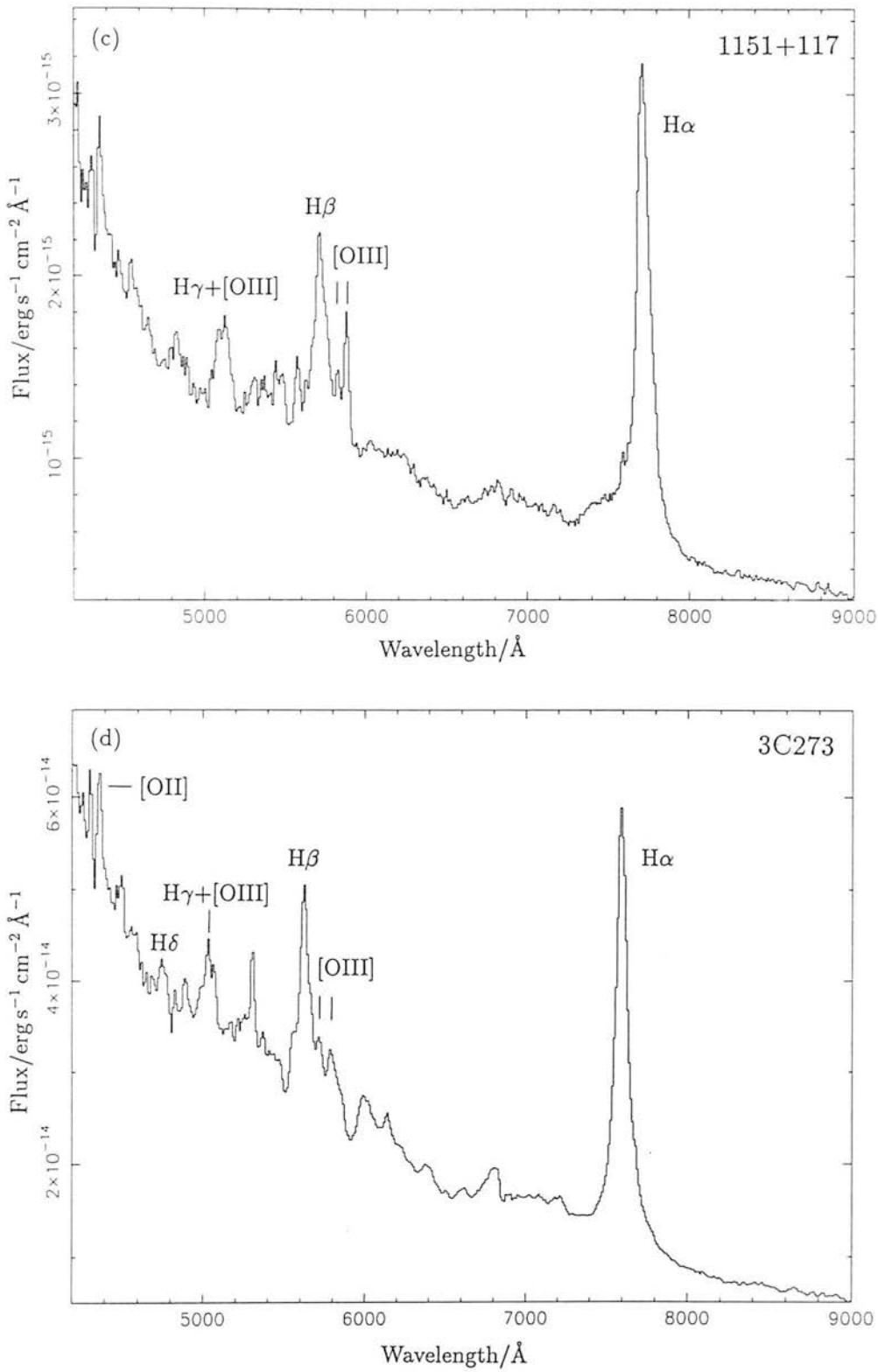

Figure 2 – *continued.*

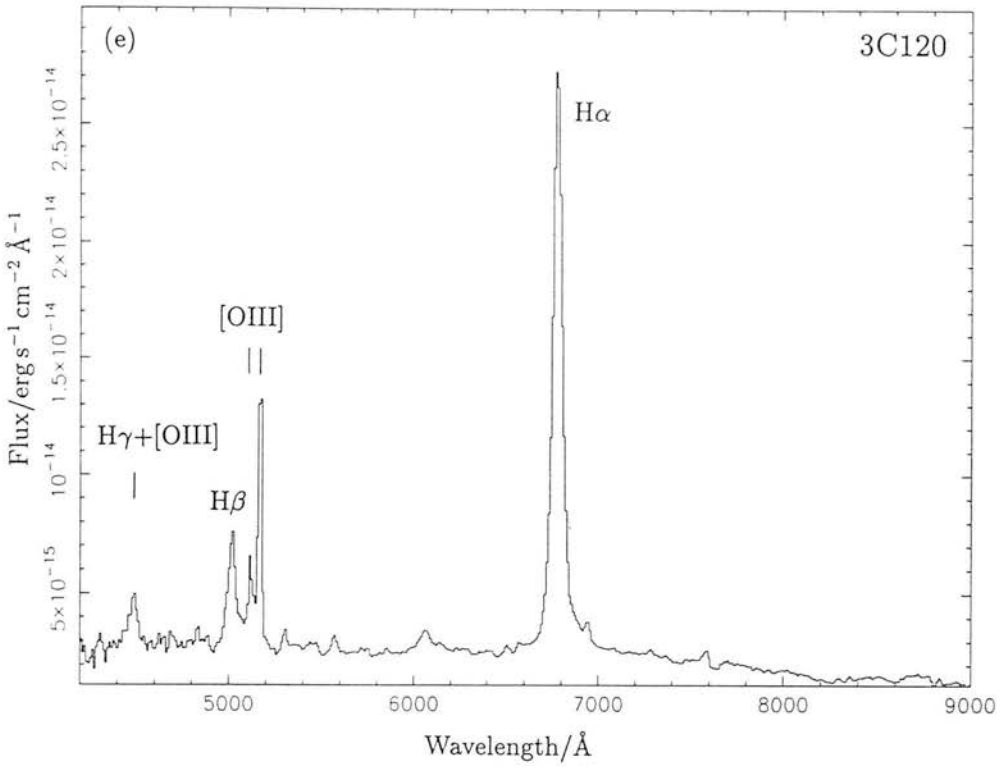

Figure 2 – *continued.*

The observed fluxes were corrected for Galactic extinction by estimating the colour excess, $E(B-V)$, to each object using the HI maps of Burstein & Heiles (1982) and employing the Rieke & Lebofsky (1985) reddening curve with a ratio of total to selective extinction of 3. For lines in the infrared, this extinction correction is very small ($\sim$ 1%) for all of our objects. Table 3 presents the resultant line fluxes and full–width half–maxima for the objects, both parameters expressed in the observer's frame. The errors given for each line are purely those associated with the line–fitting, and thus do not include the error in the absolute flux calibration.

4.2 OPTICAL LINES

Line fluxes were derived for the optical lines in a similar manner to that employed for the infrared lines. The estimate of the continuum level is likely to be the largest error in the derivation of the optical line fluxes, owing to the rich emission–line nature of the objects under study. The derived line fluxes were corrected for Galactic extinction in the same manner as for the infrared lines; the corrections are substantially larger in the optical. Table 4 presents details of the observed line fluxes (corrected for Galactic extinction), and an estimate of the rest–frame equivalent widths of the lines. Because our prime interest is in the Balmer lines and our integration times were fairly short, we have not attempted an exhaustive line analysis for each object and have derived parameters only for the principal lines. Comprehensive study of the non–Balmer emission line systems of these objects (e.g. a study of the FeII λ4570 line, a frequently discussed diagnostic) really requires a higher signal to noise than that available here, and could only be obtained at the expense of saturating the Balmer lines.

Unfortunately we were unable to obtain an unsaturated observation of Hα for the quasar 1211+143 and so we have taken a recent flux measurement for this line from the work of Bechtold *et al.* (1987). They obtained a spectrum of 1211+143 on 1985 June 25, some 18 months prior to our own optical work.

Table 3. Infrared line parameters.

		Flux[(a)] 10^{-21} W cm^{-2}	FWHM[(b)] km s^{-1}
0736+017	Paα	4 ($\pm$1)	< 5000
3C206	Paα	7 ($\pm$3)	8000
0953+414	Paα	10 ($\pm$2)	5000
	Paβ	5 ($\pm$3)	–
1001+054	Paα	5 ($\pm$1)	< 4500
1151+117	Paα	9 ($\pm$4)	5000
1211+143	Paα	46 ($\pm$13)	< 4500
	Brγ	9 ($\pm$3)	–
3C273	Paα	61 ($\pm$6)	–
1229+204	Paα	19 ($\pm$9)	< 5500
3C120	Paα	76 ($\pm$9)	< 4000

Notes:
(a): Observer's frame, corrected for Galactic extinction.
(b): Observer's frame.

Table 4. Optical line parameters.

	0736+017 $A_V = 0.39$		3C206 $A_V = 0.12$		0953+414 $A_V = 0.00$		1001+054 $A_V = 0.00$	
	Flux	EW	Flux	EW	Flux	EW	Flux	EW
Hα	30.0	386	27.9	955	41.8	421	23.7	457
[OIII]$\lambda\lambda$4959, 5007	–	–	5.7	116	6.1	27	3.1	31
Hβ	8.4	50	5.0	99	17.6	74	7.3	71
Hγ + [OIII]λ4363	3.6	18	3.1	49	10.0	34	2.5	20
Hδ	2.7	13	–	–	3.4	10	0.9	7
Hϵ + [NeIII]λ3967	–	–	–	–	2.7	7	–	–
[OII]λ3727	–	–	–	–	–	–	1.3	8

	1151+117 $A_V = 0.03$		1211+143 $A_V = 0.09$		3C273 $A_V = 0.00$		1229+204 $A_V = 0.09$	
	Flux	EW	Flux	EW	Flux	EW	Flux	EW
Hα	36.3	568	153.0†	227†	517.6	392	81.0	532
[OIII]$\lambda\lambda$4959, 5007	4.2	31	21.3	28	94.9	29	11.7	44
Hβ	10.7	78	62.6	77	182.0	58	24.5	90
Hγ + [OIII]λ4363	4.3	27	26.5	28	56.9	15	10.7	34
Hδ	1.7	9	7.8	7	–	–	6.4	18
Hϵ + [NeIII]λ3967	–	–	4.1	4	–	–	–	–

	3C120 $A_V = 0.45$	
	Flux	EW
Hα	256.5	724
[OIII]$\lambda\lambda$4959, 5007	69.7	157
Hβ	44.8	98
Hγ + [OIII]λ4363	22.4	46
Hδ	7.3	13

Notes:
Fluxes (observer's frame) in units of 10^{-21} W cm^{-2}. Corrected for Galactic reddening.
Rest frame equivalent widths (EW) in Ångstroms.
†: Values for Hα in 1211+143 from Bechtold *et al.* (1987), corrected for Galactic reddening.

The Hα flux shown in Table 4 has been corrected for Galactic reddening in the same manner as for the rest of our sample. Bechtold *et al.* (1987) also give a flux measurement for Hβ, which when corrected for Galactic reddening yields 77.1×10^{-21} W cm^{-2}, in fair agreement with our own value of 62.6×10^{-21} W cm^{-2}. Thus it appears that we will not introduce a large error by adopting their Hα value, despite the fact that it is not contemporaneous with our optical and infrared work.

4.3 LINE RATIOS AND ERRORS

Table 5 presents details of the derived line ratios for each object. To derive a first order estimate of the errors on these ratios, we have assumed for the moment that the infrared lines have flux errors as tabulated in Table 3 (and thus exclude any error due to the flux calibration), and that the optical lines have flux errors of 20% (due to all possible effects). These error estimates are likely to be conservative ones, and are purely meant to be illustrative. Given that any internal estimate of the errors on our line fluxes is likely to be virtually meaningless in absolute terms, we feel that a better approach is to compare our present data with previous independent measurements. This will enable a more realistic estimate to be made of the measuring and calibration errors in our data. In Section 6 we will consider the effects of much larger errors on the ratios than those shown in Table 5, during the comparison of the observed ratios with the photoionization models.

5 Comparison of our spectrophotometry with previous work

Several of our objects have been studied on a number of previous occasions, both in the optical and the infrared. Before interpreting our derived line ratios, we propose to compare our present data with this earlier work so as to assess the reliability of our ratios. Given the notorious difficulty in obtaining good absolute spectrophotometry, it is worthwhile making a thorough and detailed

Table 5. Observed line ratios.

	Hα/Hβ	Paα/Hα	Brγ/Paα	Paα/Paβ
0736+017	3.57 (1.00)	0.133 (0.043)		
3C206	5.58 (1.56)	0.251 (0.119)		
0953+414	2.38 (0.67)	0.239 (0.068)		2.00 (1.26)
1001+054	3.25 (0.91)	0.211 (0.060)		
1151+117	3.39 (0.95)	0.248 (0.121)		
1211+143	2.44 (0.69)	0.301 (0.104)	0.196 (0.086)	
3C273	2.84 (0.80)	0.118 (0.026)		
1229+204	3.31 (0.93)	0.235 (0.121)		
3C120	5.73 (1.60)	0.296 (0.069)		

Note: Errors on ratios (calculated as described in the text) are shown in parentheses.

comparison for each object in turn. At this point we will solely concentrate on the line fluxes and ratios, and any evidence for variability in the lines and continuum of each object, a knowledge of which is necessary in order to make a fair comparison of our data with previous work. We will reserve a discussion of the far–infrared, polarization and other properties of each object until the interpretation in Section 7. In the following discussion we have corrected the fluxes obtained from the literature for Galactic extinction (where this has not been done by the authors themselves). All the equivalent widths discussed are rest–frame values, but the fluxes are presented in the observer's frame. Table 6 presents a comparison of our spectrophotometry with previous work. Details are given in the notes which follow.

0736+017. The emission line spectrum and variations of this quasar have been extensively discussed by Zheng & Burbidge (1986) who monitored the object's spectrum over the period 1978–1986. From 1978–1980 they noted that the Hβ flux dropped by some 40%, but over the period 1985–6 it increased again by $>$ 50%. The line variations generally occurred less than 1 year after the variations in the underlying continuum (leading them to conclude that the broad–line region in this object must be $<$ 1 light–year in size). Earlier, Netzer *et al.* (1979) had noted that the optical continuum varies by $\sim$ 1 mag. over a period of several months. This object is clearly highly variable, making a meaningful comparison of fluxes difficult. Zheng & Burbidge (1986) present line fluxes obtained in 1986, quoting an Hβ flux of 6.7×10^{-21} W cm^{-2} and a rest–frame equivalent width of 40Å. When this flux is calibrated against [OIII] λ5007, they obtain a value 7.4×10^{-21} W cm^{-2}. This flux is in moderate agreement with our value of 8.4×10^{-21} W cm^{-2}. Malkan & Moore (1986) obtained an Hβ flux of 8.6×10^{-21} W cm^{-2} in 1985 February, in excellent agreement with our value. There is no previous infrared spectroscopy of this quasar.

3C206. This quasar has no known history of emission–line variability, but the

Table 6. Summary of previous optical and infrared flux measurements.

	Line	This work	Previous measurements		
			Fluxes: 10^{-21} W cm^{-2}		
0736+017*	Hβ	8.4	7.4 (1)	8.6 (2)	
3C206	Hβ	5.0	3.2 (3)	7.5 (4)	
	Paα	7.0	4.9 (5)	3.3 (6)	
0953+414	Hβ	17.6	39.3 (7)		
	Hγ	10.0	11.4 (7)		
1001+054	Hα	23.7	22.8 (4)		
	Hβ	7.3	7.9 (4)		
1211+143	Hβ	62.6	72 (5)	77.1 (8)	
	[OIII]	21.3	25 (5)		
	Paα	46	22 (5)		
3C273	Hβ	182.0	175.5 (3)	222 (6)	174.5 (9)
	Paα	61	47 (10)	54 (11)	48 (6)
1229+204	Hα	81.0	85.6 (12)		
	Hβ	24.5	19.5 (12)		
3C120*	Hβ	44.8	66 (13)	53.5 (14)	
	Paα	76	27 (15)		

Key to references:

(1) Zheng & Burbidge (1986)
(2) Malkan & Moore (1986)
(3) Stockton & Mackenty (1987)
(4) Neugebauer *et al.* (1979)
(5) Soifer *et al.* (1981)
(6) Puetter *et al.* (1981)
(7) Green *et al.* (1980)
(8) Bechtold *et al.* (1987)
(9) Baldwin (1975)
(10) Ward *et al.* (1987)
(11) Sellgren *et al.* (1987)
(12) Wampler (1967)
(13) Rudy *et al.* (1987)
(14) Rafanelli (1985)
(15) Lacy *et al.* (1982)

Notes: All fluxes in observer's frame and corrected for Galactic reddening.
*: Emission line systems known to be highly variable.

continuum shows definite variations. Cutri *et al.* (1985) reported magnitude variations $\sim$ 1 mag. at V and $\sim$ 0.7 mag. at R. At K there seems to be little variation. Stockton & MacKenty (1987) studied this object as part of their survey of extended emission around quasars, obtaining a nuclear Hβ luminosity of $10^{42.42}\,\mathrm{erg\,s^{-1}}$, ($\mathrm{H_o} = 75\,\mathrm{km\,s^{-1}\,Mpc^{-1}}$, $q_o = 0$) which represents an observed flux of $3.2 \times 10^{-21}\,\mathrm{W\,cm^{-2}}$ rather lower than our value of $5.0 \times 10^{-21}\,\mathrm{W\,cm^{-2}}$. No date is given for their observation. Their equivalent width of 18Å is also much smaller than our value of 99Å. Neugebauer *et al.* (1979) obtained optical spectrophotometry in 1978 yielding a value for Hβ of $7.5 \times 10^{-21}\,\mathrm{W\,cm^{-2}}$, slightly higher than our value. They measured an equivalent width of 105Å. Soifer *et al.* (1981) obtained a Paα flux for this quasar of $(4.9 \pm 1.0) \times 10^{-21}\,\mathrm{W\,cm^{-2}}$, substantially lower than our observed value of $(7 \pm 3) \times 10^{-21}\,\mathrm{W\,cm^{-2}}$. Puetter *et al.* (1981) also observed Paα, obtaining a flux of $3.3 \times 10^{-21}\,\mathrm{W\,cm^{-2}}$, in fair agreement with Soifer *et al.* (1981) but again, lower than our value. On examination of these latter two groups' published infrared spectra of this object, it is apparent that the Soifer *et al.* (1981) spectrum is of very poor signal–to–noise, with the line barely detected, and that of Puetter *et al.* (1981), although of slightly better signal–to–noise, has virtually no continuum. We believe that these two groups have significantly underestimated the Paα flux, and thus their quoted ratios for Paα/Hα of 0.12($\pm$0.02) and 0.10 respectively are probably far too low. For comparison we obtain a value Paα/Hα=0.251

0953+414. Spectrophotometry has been obtained for this quasar on one previous occasion, Green *et al.* (1980) obtaining an Hβ flux of $39.3 \times 10^{-21}\,\mathrm{W\,cm^{-2}}$ (with an estimated error of 20%) and an equivalent width of 101Å. These are significantly larger than our values of $17.6 \times 10^{-21}\,\mathrm{W\,cm^{-2}}$ and 74Å. No date is given for their observations. Our Hγ values are in good agreement though, Green *et al.* (1980) obtaining $11.4 \times 10^{-21}\,\mathrm{W\,cm^{-2}}$ and 23Å as against our values of $10.0 \times 10^{-21}\,\mathrm{W\,cm^{-2}}$ and 34Å. There is no data for this object with respect to variability in either line or continuum emission, and no previous infrared

spectroscopy.

1001+054. The only previous spectrophotometry of this object is that obtained by Neugebauer *et al.* (1979) in 1978 May, who obtained an Hα flux of 22.8×10^{-21} W cm^{-2} and an equivalent width of 331Å. This flux is in excellent agreement with our value of 23.7×10^{-21} W cm^{-2} (EW=457Å). Their Hβ flux was 7.9×10^{-21} W cm^{-2} to be compared with our value of 7.3×10^{-21} W cm^{-2}. There is no data available regarding the variability of this object, and no previous infrared spectroscopy.

1151+117. This Palomar–Green quasar has no previous optical spectrophotometry, variability data, or infrared spectroscopy.

1211+143. As noted in Section 4.2, the Hβ flux obtained by Bechtold *et al.* (1987) for this quasar, 77.1×10^{-21} W cm^{-2} is in moderate agreement with our value of 62.6×10^{-21} W cm^{-2}. Soifer *et al.* (1981) obtained spectrophotometry of this object in 1979 May, yielding an Hβ flux 72×10^{-21} W cm^{-2}, in excellent agreement with our own value. They obtained a flux for [OIII] $\lambda\lambda$4959, 5007 of 25×10^{-21} W cm^{-2} to be compared with our value of 21.3×10^{-21} W cm^{-2}. The equivalent widths for Hβ obtained by Bechtold *et al.* (1987), Soifer *et al.* (1981) and ourselves are 74, 77 and 77 Å respectively. Barbieri & Romano (1984) discuss photographic photometry of this quasar obtained over a period of 15 years, and detected no variability ≥ 0.3 mag. during this time. The good agreement between the flux measurements noted above would tend to indicate that there is little variability in the emission–line spectrum either. Soifer *et al.* (1981) obtained a Paα flux in 1979 January of $(22 \pm 2) \times 10^{-21}$ W cm^{-2} to be compared with our value of $(46 \pm 13) \times 10^{-21}$ W cm^{-2}. Their spectrum is of better signal–to–noise than the one they obtained for 3C206, but they have very little continuum (two points on either side of a three point line) and we suspect that they are underestimating the Paα flux again. Our infrared spectrum is shown in Fig. 1(d).

3C273. There is little evidence for dramatic variability in 3C273, excepting the infrared to millimetre wavelength flare observed in 1983 by Robson *et al.* (1983). Optical monitoring by Courvoisier *et al.* (1987) revealed a V band variability $\sim 13\%$ over the period 1983 December to 1986 March, and similarly, Cutri *et al.* (1985) noted the lack of dramatic variability in the infrared, the maximum amplitude of any K band variation being 0.25 mag. Stockton & MacKenty (1987) obtained an Hβ flux (no date given) of 175.5×10^{-21} W cm^{-2}, in good agreement with our value of 182.0×10^{-21} W cm^{-2}. The Hβ flux obtained by Puetter *et al.* (1981) of 222×10^{-21} W cm^{-2} is larger than these two values. They also measure a larger equivalent width, 82Å than we do (58Å). Baldwin's (1975) estimate of the Hβ flux, expressed in the observer's frame is 174.5×10^{-21} W cm^{-2}, thus it would seem that the Puetter *et al.* (1981) value is somewhat large.

Ward *et al.* (1987) measured a Paα flux on 1984 January 28 of 47×10^{-21} W cm^{-2}, which is to be compared with our value of $(61 \pm 6) \times 10^{-21}$ W cm^{-2}, and those of Sellgren *et al.* (1983) of 54×10^{-21} W cm^{-2} and Puetter *et al.* (1981) of 48×10^{-21} W cm^{-2}. The range of values probably represents the measuring error, given the lack of observed variability in the infrared.

1229+204. This quasar has been studied on a number of occasions under the guise of a Seyfert 1 (Mrk771=Akn374=Ton1542). Peterson, Crenshaw & Meyers (1985) studied the emission–lines and continuum of this object, and observed a decrease in the continuum and Hβ flux in ~ 2 years of 14% and 13% respectively. Earlier, Peterson *et al.* (1982) had noted an increase in the strength of the emission lines over the period 1977–81, however, Osterbrock & Shuder (1982) could see no variation in the Balmer lines over this same period. These groups give no absolute spectrophotometry, but Wampler (1967) obtained Hα and Hβ fluxes of 85.6 and 19.5×10^{-21} W cm^{-2} respectively, to be compared with our values of 81.0 and 24.5×10^{-21} W cm^{-2}. The Hα values would be consistent with a lack variability over the period 1967–86. There has not been any previous

infrared spectroscopy of this object.

3C120. This broad–line radio galaxy, also frequently classed as a Seyfert 1, has a well studied history of emission–line and continuum variability. For example, Peterson *et al.* (1982) tabulate the Hβ luminosity over the period 1967–80 where it ranges from 25 to 8.7×10^{-48} W, although there did not seem to be a corresponding change in the continuum level. French & Miller (1981) and Oke, Readhead & Sargent (1981) had earlier noted that the emission–line strengths vary on timescales $\sim$ 1 year. Antonucci (1984b) studied the ratio Hβ/[OIII] λ5007 over a period of 4 years, during which it varied from 1.38–0.56, and assuming [OIII] λ5007 remains constant, indicates drastic variability. The optical spectrophotometry of Rudy *et al.* (1987) is most nearly contemporaneous with our own, and they obtained an Hβ flux of 66×10^{-21} W cm^{-2} on 1985 December 12, some twelve months before our own observation which yielded 44.8×10^{-21} W cm^{-2}. The Hα fluxes are in better agreement, their value of 231.0×10^{-21} W cm^{-2} to be compared with ours of 256.5×10^{-21} W cm^{-2}. Rafanelli (1985) observed 3C120 in 1982 October, obtaining a combined narrow– and broad–line component Hβ flux of 53.5×10^{-21} W cm^{-2}.

A Paα flux was obtained by Lacy *et al.* (1982) on 1979 December 16 of $(27 \pm 5) \times 10^{-21}$ W cm^{-2} which is very much lower than our value of $(76 \pm 9) \times 10^{-21}$ W cm^{-2}. Lacy *et al.* (1982) do not present their infrared spectrum so it is impossible to judge the quality of their data. Our spectrum is shown in Fig. 1(f).

In summary, it appears that our optical spectrophotometry is in good agreement with previous work and there are no apparent systematic errors: the mean value for the ratio of our observed fluxes to those obtained previously (and tabulated in Table 6) is 0.93 ± 0.24, and so is not significantly different from unity. However, our infrared spectrophotometry is in poor agreement with the previous

work of Soifer *et al.* (1981), Puetter *et al.* (1981) and Lacy *et al.* (1982), and our Paα fluxes are generally larger than those obtained by these groups. In as much as we can judge from their published spectra (or lack of them) we believe that this early work was either of insufficient signal–to–noise, or was lacking in a good continuum baseline (or indeed any baseline at all), making the accurate derivation of the Paα fluxes very difficult.

6 Comparison of the observed line ratios with photoionization models

In order to interpret the observed line ratios, we will take two initial assumptions as our starting point. Firstly, we will assume that the densities and optical depths of the line emitting regions in our objects are high enough so as to invalidate the case B approximation. An example of a recent density estimate for the broad–line region of an active galaxy is the work of Peterson *et al.* (1985) who studied the emission line variability of the Seyfert 1 Akn120. The observed variability timescales implied a line–emitting region region < 30 light–days in size, and coupled with the high observed luminosity, indicates either a very large ionization parameter, or $N_e > 5 \times 10^{10}\,\mathrm{cm}^{-3}$. A similar study of 5 low–redshift quasars by Zheng *et al.* (1987) led to a similar conclusion, namely that $N_e > 10^{11}\,\mathrm{cm}^{-3}$ or even higher, if a realistic value of the ionization parameter was required.

The recent high–density case B recombination calculations of Hummer & Storey (1987) confirm the long–held expectation that with $T_e \sim 10^4\,\mathrm{K}$, case B will not be appropriate at these high electron densities. Case B theory includes the assumption that the level populations for $n \geq 3$ are independent of those of levels 1 and 2. Hummer & Storey (1987) discuss conditions when $n = 1 \rightarrow 2$, $n = 1 \rightarrow 3$ and $n = 2 \rightarrow 3$ collisional transitions become important, thus invalidating this assumption. As a typical example, for electron temperatures $T_e = 5 \times 10^4\,\mathrm{K}$, the critical electron density for collisional $n = 2 \rightarrow 3$ excitation, such that it constitutes 10% of the total population of hydrogen, is only $2.6 \times 10^7\,\mathrm{cm}^{-3}$. At

higher temperatures, the critical density is even lower.

Our second initial assumption will be that some form of photoionization is responsible for the emitted line–spectrum, and so we propose to begin our analysis with a comparison of our observed ratios with three comprehensive photoionization models, those of Kwan (1984), Hubbard & Puetter (1985) and Collin–Souffrin *et al.* (1986).

6.1 Paα/Hα AND Hα/Hβ

Figure 3 plots the observed Paα/Hα line ratios against Hα/Hβ for our 8 quasars and one radio galaxy, along with a number of predicted ratios derived from the photoionization models. We will explore these models in some detail given that there seems to be little correspondence between the observed Paα/Hα ratios and those calculated by any of the models.

The models of Kwan (1984) are broadly based on the same code as used by Kwan & Krolick (1981); photoionization and heating in the line–emitting cloud is calculated under conditions of ionization, thermal and pressure equilibrium. Photoionization and collisional excitation from excited states of hydrogen are accounted for, and in determining thermal equilibrium, lines and continua of hydrogen, helium and the heavy elements commonly observed in quasars are included. The improved models of Kwan (1984) involve slabs of finite column densities (i.e. radiation is allowed to escape from both the illuminated and un–illuminated sides) rather than the semi–infinite slabs used in Kwan & Krolick (1981), and include a better modelling of OI and FeII. The models encompass particle densities (N_0) of $3 \times 10^8 - 3 \times 10^{10}\,\mathrm{cm}^{-3}$, ratios of incident ionizing photon densities to particle density (Γ) of 0.01-0.06, and column densities $\tau_L = 10^3 - 3 \times 10^6\,\mathrm{cm}^{-2}$, this latter quantity defined by the optical depth of the continuum at the Lyman edge.

Figure 3 plots the predicted Paα/Hα, Hα/Hβ ratios for Kwan's Models

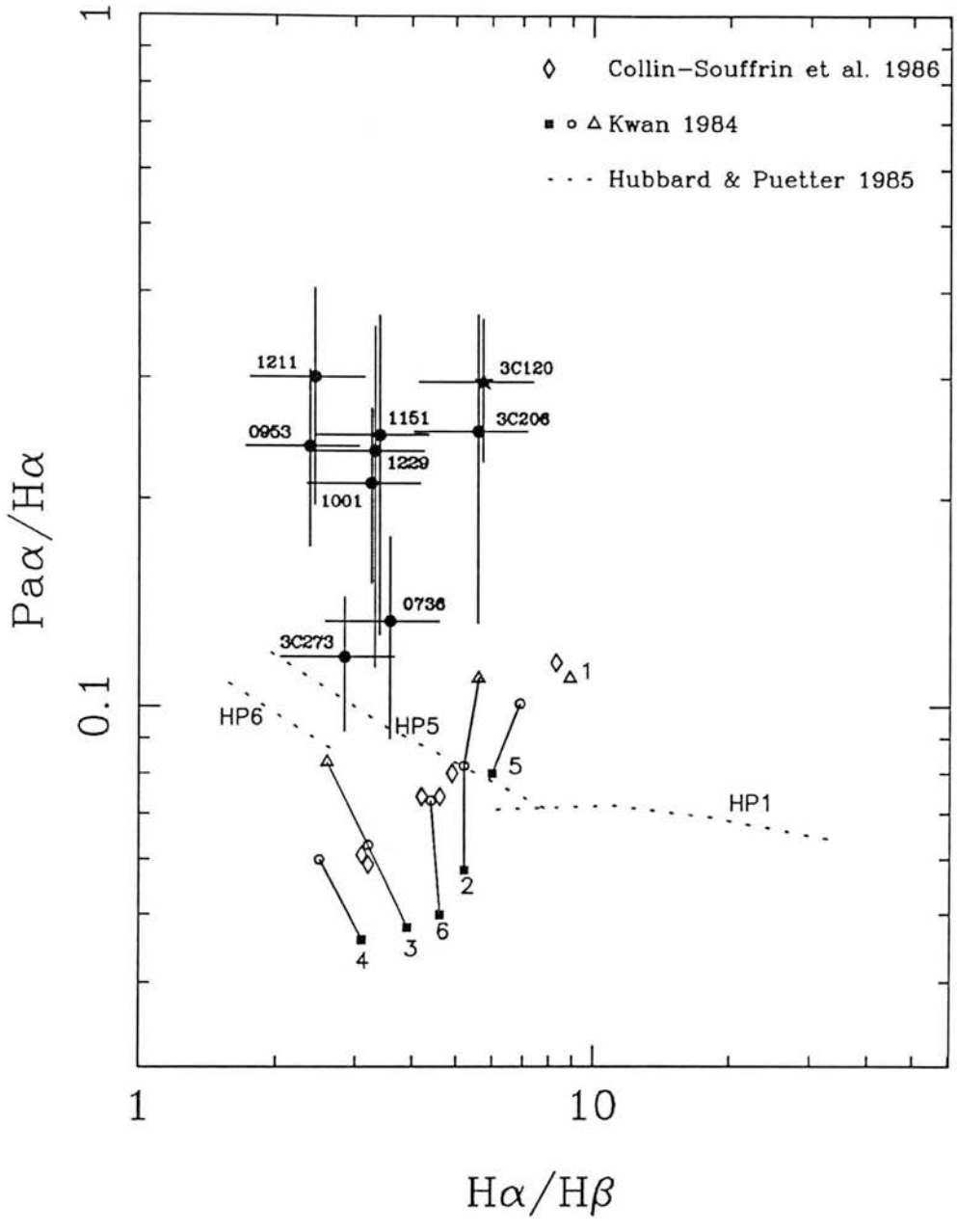

Figure 3. Line ratios for the eight quasars (filled circles) and one BLRG (star) observed in this present work. The error bars are calculated as discussed in the text. Predicted ratios from the photoionization models of Collin–Souffrin *et al.* (1986), Kwan (1984) and Hubbard & Puetter (1985) are shown. Open diamonds indicate the six models of Collin–Souffrin *et al.* (1986) (Models 0–5 in their nomenclature). The Kwan (1984) models are labelled 1–6 following the nomenclature used in that work – the ratios are taken directly from Kwan's Figure 1. The filled squares indicate optical depths $\tau_L = 3 \times 10^6$, the open circles 3×10^5 and the open triangles 3×10^4 respectively. Models 1, 5 and 6 from Hubbard & Puetter (1985) are shown as dotted lines, and are taken from their Figure 1(e).

1–6 (as shown in his Figure 1). In general, as one moves from large optical depths ($\tau_L = 3 \times 10^6\,\mathrm{cm}^{-2}$, the filled squares) to low optical depths ($\tau_L = 3\times10^4\,\mathrm{cm}^{-2}$, the open triangles) Pa$\alpha$/H$\alpha$ increases. These six models encompass particle densities $3 \times 10^8 - 3 \times 10^{10}\,\mathrm{cm}^{-3}$, and Pa$\alpha$/H$\alpha$ is fairly insensitive to this parameter. Model 4 has the highest particle density ($N_0 = 3 \times 10^{10}\,\mathrm{cm}^{-3}$) of the six models, and Model 1 the lowest ($3 \times 10^8\,\mathrm{cm}^{-3}$). In addition, Γ ranges over 0.01–0.06; Models 1–4 have Γ=0.03, Model 5 has Γ=0.01 and for Model 6, Γ=0.06. Although the models predict Hα/Hβ in good agreement with the observations, the predicted values of Paα/Hα are too small. To produce larger values for Paα/Hα in the context of these models one requires a smaller optical depth ($\tau_L < 3\times10^4\,\mathrm{cm}^{-2}$), and perhaps lower particle densities: Model 1 with the lowest value of N_0 produces the largest Paα/Hα ratio. In summary, none of the Kwan (1984) models can produce Paα/H$\alpha > 0.11$ for $N_0 = 3\times10^8$–$3\times10^{10}\,\mathrm{cm}^{-3}$, $\Gamma = 0.01 - 0.06$ and $\tau_L = 10^3 - 3 \times 10^6\,\mathrm{cm}^{-2}$.

Collin–Souffrin *et al.* (1986) present the latest version of their photoionization model which principally differs from that of Kwan (1984) in that a two component broad–line cloud model is assumed, and in the computational method used for solving the line transfer. They employ an exact numerical treatment rather than the local escape probability used by Kwan (1984). The calculations are for a finite slab and range over $N_0 = 3.6 \times 10^9 - 3.6 \times 10^{10}\,\mathrm{cm}^{-3}$, $\Gamma = 0.003 - 0.03$ and $\tau_L = 4.6 \times 10^5 - 2.6 \times 10^7\,\mathrm{cm}^{-2}$ (thus probing higher optical depths than Kwan 1984). A similar ionizing spectrum to Kwan (1984) is used, and temperatures are $T_e \sim 2 \times 10^4\,\mathrm{K}$. Their six 'representative' models are plotted as open diamonds on Fig. 3 and the ratios are calculated from the summed intensities (illuminated and un–illuminated sides) given in Table 2 of Collin–Souffrin *et al.* (1986). The agreement with the models of Kwan (1984) is good and the predicted Hα/Hβ ratios are again in good agreement with the observations. The largest predicted value for Paα/Hα is 0.116 (for their Model 1) which has $N_0 = 3.6 \times 10^9\,\mathrm{cm}^{-3}$, $\Gamma = 0.003$ and $\tau_L = 2.5 \times 10^7\,\mathrm{cm}^{-2}$. In

order to produce a larger Paα/Hα ratio in the context of these models, one requires $N_0 < 3.6 \times 10^9\,\mathrm{cm}^{-3}$, $\Gamma < 0.003$ or lower optical depths, ($\tau_L < 10^6\,\mathrm{cm}^{-2}$). These trends are in a similar sense to those implied by Kwan's (1984) models discussed above. However, our expectation (based on the above mentioned variability studies) is that the line–emitting regions will tend to have *greater* optical depths and particle densities ($N_0 > 10^{10}\,\mathrm{cm}^{-3}$) than those probed by the models. Thus it seems that there is a conflict between the physical parameters implied by the models in order to produce large values of Paα/Hα, and the physical conditions that we believe to be relevant for the line–emitting regions.

Finally, we consider the models of Hubbard & Puetter (1985). These offer a more exact calculation of the radiative transfer than was possible in Canfield & Puetter (1981), but at the expense of the exclusion of heavy elements and secondary ionizations from primary photoelectrons. Despite these caveats, they demonstrate that there is a good agreement between their models and the more exact treatment of Collin–Souffrin *et al.* (1982). They examine optical depths $\tau_L = 10^2 - 10^5\,\mathrm{cm}^{-2}$, ionizing fluxes ($F_0$) evaluated at 1 Rydberg of $10^{-7} - 10^{-9}\,\mathrm{erg\,s^{-1}\,cm^{-2}\,Hz^{-1}}$ and particle densities $N_0 = 5 \times 10^9 - 10^{12}\,\mathrm{cm}^{-3}$ at $T \sim 1.5 \times 10^4\,\mathrm{K}$. In Fig. 3 we show (as dotted lines) three of their six models, Models 1, 5 and 6 (labelled HP1, HP5 and HP6 respectively) and taken from Figure 1(e) of Hubbard & Puetter (1985). The other three models generally cover the same region of the Paα/Hα – Hα/Hβ plane. Again, there is broad agreement between these models and the observed Hα/Hβ ratios, and good agreement between these models and those of Kwan (1984) and Collin–Souffrin *et al.* (1986). Similarly, Paα/Hα never rises above 0.2. Model HP5 attains the largest value of Paα/Hα and is characterised by $F_0 = 10^{-8}\,\mathrm{erg\,s^{-1}\,cm^{-2}\,Hz^{-1}}$, $\tau_L = 2 \times 10^2\,\mathrm{cm}^{-2}$ and a particle density ranging between 5×10^9 and $10^{12}\,\mathrm{cm}^{-3}$, the large Pa$\alpha$/H$\alpha$ ratio being attained at the high particle density part of the track, although Hα/H$\beta \simeq 2$ at this point, and so is rather low.

To complete this comparison of the observations with photoionization theory we have considered a further two models, namely those of Mathews, Blumenthal & Grandi (1980) and Drake & Ulrich (1980) with the aim of establishing whether these models offer large Paα/Hα ratios. Mathews, Blumenthal & Grandi (1980) study the parameter space $N_0 = 10^8$–$10^{11}\,\mathrm{cm}^{-3}$, $T_e = 10^4$–$10^{10}\,\mathrm{K}$ and $\tau_L = 10^4$–$10^{10}\,\mathrm{cm}^{-2}$ and produce their largest Paα/Hα ratios of 0.119 with $N_0 = 10^9\,\mathrm{cm}^{-3}$, $T_e = 1.5 \times 10^4\,\mathrm{K}$ and $\Gamma = 0.01$ or 0.001. Hα/Hβ is in the range 4–5 for these two particular models. Drake & Ulrich (1980) probe the space $N_0 = 10^8 - 10^{15}\,\mathrm{cm}^{-3}$, $T_e = 5 \times 10^3 - 4 \times 10^4\,\mathrm{K}$ and $\tau_L = 10^4 - 10^6\,\mathrm{cm}^{-2}$ but do not include any allowance for non–hydrogenic atoms. Their largest value for Paα/Hα is $\simeq 0.20$, for $N_0 = 10^8 - 10^{10}\,\mathrm{cm}^{-3}$, $T_e = 5 \times 10^3\,\mathrm{K}$ and $\tau_L = 10^5\,\mathrm{cm}^{-2}$. Thus neither of these two models can wholly reconcile the data with pure photoionization theory.

Given that none of the above mentioned photoionization models can produce values of Paα/Hα > 0.2, at least for the areas of parameter space that they encompass, we will now reconsider the reliability of our data. Specifically, we will consider whether the adoption of much larger errors on our observed ratios can reconcile theory with observation. We will examine the three quasars with the largest observed Paα/Hα ratios, 3C206 (Paα/Hα=0.251), 0953+414 (Paα/Hα=0.239) and 1211+143 (Paα/Hα=0.301). If we pessimistically assume that the error on the absolute flux of Paα is 50% in each case, and that the optical lines have absolute flux errors of 40%, then the lowest values attainable for Paα/Hα are 0.090, 0.086 and 0.108 for each object respectively. These ratios would then be in good agreement with the photoionization models. If we now consider slightly smaller errors than this, for example, an error of 40% on the Paα fluxes and 30% on the optical fluxes, the respective lower limits for Paα/Hα are then 0.126, 0.120 and 151. These values would now be in disagreement with all the models of Kwan (1984), Collin–Souffrin *et al.* (1986), Mathews, Blumenthal & Grandi (1980), and all the Hubbard & Puetter (1985) models with the

possible exception of HP5. A reasonable agreement with the Drake & Ulrich (1980) models would be possible. However, as was evident from the comparison of our line fluxes with previous work, it seems very unlikely that our infrared lines have errors as large as 50% or that our optical lines are in error by as much as 40%. In addition, for these errors to conspire to produce Paα/Hα ratios as large as those observed, we would require errors in the sense that our measured optical line fluxes are 40% too *weak*, and our infrared fluxes 50% too *strong*. Thus we do not believe that the lack of agreement between the observed line ratios and the photoionization models can be adequately explained by inaccuracies in our data.

An option that may perhaps explain the comparatively high values of Paα/Hα observed in our objects is that the intrinsic line emission, whatever form that may take, is reddened by dust. In Fig. 4 we replot the observed Paα/Hα, Hα/Hβ ratios for our objects and examine the effect of reddening on two initial (i.e. zero–reddened) points in this plane. Two reddening vectors are shown (as dashed lines): the first assumes zero–reddened ratios of Hα/Hβ = 4.0 and Paα/Hα = 0.075, the approximate centroid of the region occupied by the photoionization models discussed above. The second vector assumes zero–reddened ratios equivalent to the observed line ratios in 3C273. Crosses indicate the expected line ratios modified by one and two magnitudes of reddening. In calculating the effects of reddening, we have assumed that the observed ionizing radiation is from a point source, modified by a slab of dust obeying the reddening law of Rieke & Lebofsky (1985). It is important to note that we have assumed that a Galactic reddening law is applicable for all our active galaxies. Nandy *et al.* (1981) show that the reddening curve in the Large Magellanic Cloud is quite dissimilar to the Galactic reddening law, and it is possible that our active galaxies also have a non–Galactic reddening law. However, in the absence of a precise knowledge of what form the reddening law should take, we can not do any better at present than to assume a Galactic model.

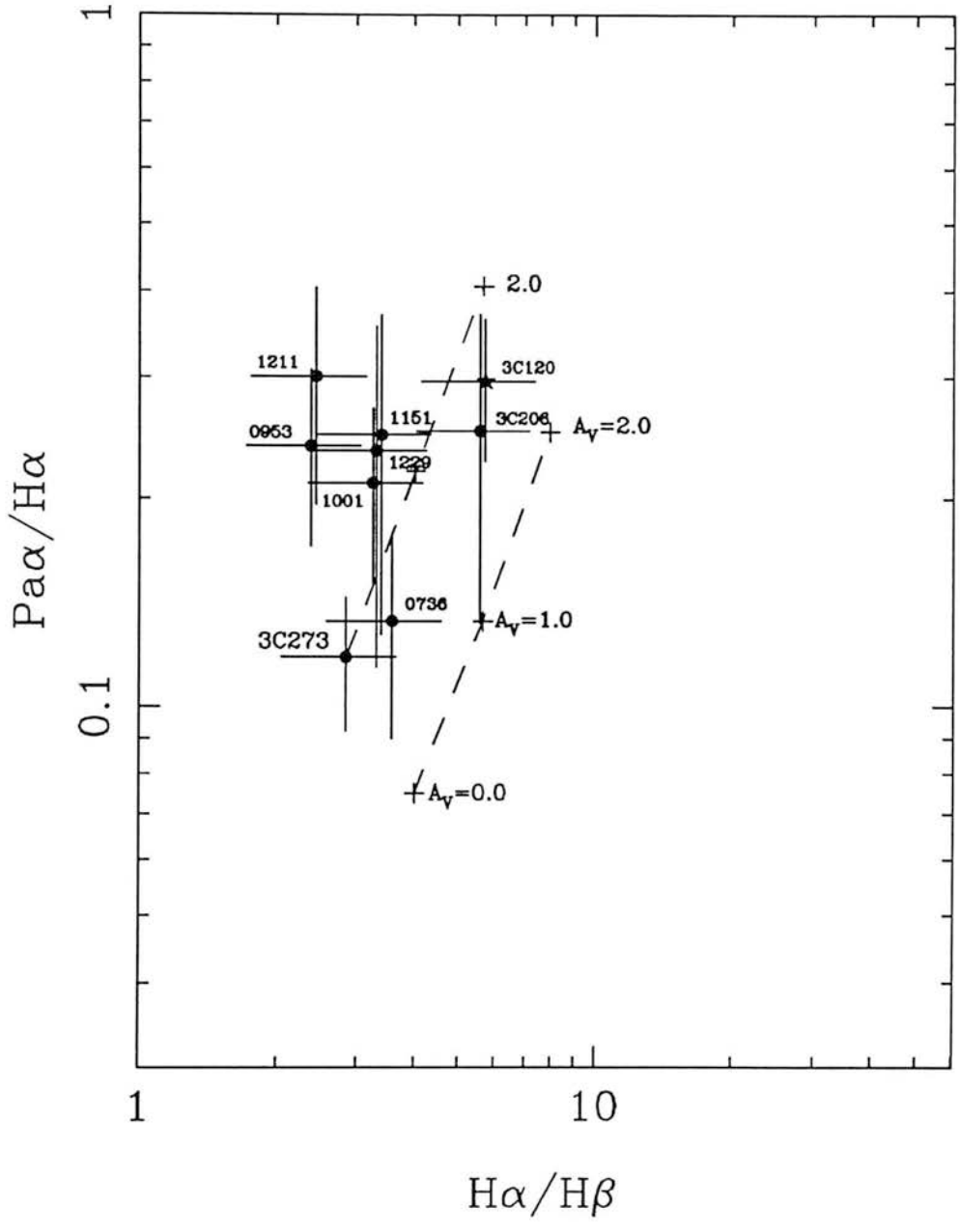

Figure 4. As for Fig. 3, but with the exclusion of the photoionization models. Reddening vectors assuming two different starting (i.e. zero–reddened) points are shown. One vector shows the effect of reddening the observed spectrum of 3C273, whilst the other takes as its starting point the approximate centroid of the models shown in Fig. 3.

It is clear that the reddened 'average' photoionization model plotted in Fig. 4 is not a good fit to the data, tending to produce larger values of Hα/Hβ than observed for any given value of Paα/Hα. It is apparent from the models plotted on Fig. 3 that for a reddened photoionization model to fit the data we must assume a zero-reddening point somewhere near to the upper ends of the Hubbard & Puetter (1985) models HP5 and HP6. Most of the other photoionization models will not produce a reddening vector that is in good agreement with the observations. However, the track which is equivalent to reddening 3C273 is in fair agreement with the data, except perhaps for the quasars 0953+414 and 1211+143 which tend to have rather low values of Hα/Hβ. Thus we may conclude from Fig. 4 that most of our objects have observed ratios that can be produced by reddening the observed line spectrum of 3C273 by between one and two magnitudes. If the intrinsic spectrum of 3C273 is itself modified by dust (thus producing the values we observe in this object) then the reddening inferred for the other quasars and 3C120 must be even greater than that indicated by the reddening vector plotted in Fig. 4.

6.2 OTHER LINE RATIOS

For two quasars we have obtained purely infrared (and thus reddening insensitive) line ratios, namely Paα/Paβ in 0953+414, and Brγ/Paα in 1211+143. In the few previous instances where the ratio Paα/Paβ has been observed (e.g. Ward *et al.* 1987) it has generally been used to measure the divergence from the the expected case B value. Our observed value of 2.00 ± 1.26 for 0953+414 is in fact quite close to the case B value of 2.1. The only photoionization models to study the Paβ line are those of Drake & Ulrich (1980), and they can readily produce values of Paα/Paβ very close to our observed value for a wide range of temperatures, electron densities and optical depths. This is in contrast to the situation discussed above for the Paα/Hα ratio where the Drake & Ulrich (1980) models can not produce values in excess of 0.2 for any combination of param-

eters, whilst the observed value for this quasar is 0.239 ± 0.068. The fact that the reddening *insensitive* ratio (Paα/Paβ) is in good agreement with the models, whilst the reddening *sensitive* ratio (Paα/Hα) is in poor agreement, would tend to lend support to the suggestion that the latter ratio is indeed affected by reddening, and argues strongly for the presence of dust in 0953+414. It should be noted, however, that the Drake & Ulrich (1980) models have been criticized on account of the hydrogen-line broadening formulation that they employed, although their line ratios are *not* strongly discrepant with those of Kwan (1984), Hubbard & Puetter (1985) and Collin-Souffrin *et al.* (1986). It would be very useful in this context to see calculations for Paβ (and Brγ) from these latter three models.

The models of Drake & Ulrich (1980) are again the only ones to consider the Brγ line. Several combinations of temperature, optical depth and density are capable of reproducing a ratio of Brγ/Paα close to our observed value in 1211+143 (0.196 ± 0.086). The successful models generally have high densities, $N_e = 10^{13-15}\,\mathrm{cm}^{-3}$. However, in all the successful cases, Paα/Hα is less than 0.1 (to be compared with our observed value of 0.301 ± 0.104) and Hα/Hβ is less than 2 (observed value 2.44 ± 0.69). As was the case for 0953+414, we have a situation where the observed reddening insensitive ratio (Brγ/Paα) can be well matched by the models, whereas the reddening sensitive ratio (Paα/Hα) is anomalously high, a result that can be understood by assuming that the quasar's intrinsic emission is subject to reddening.

6.3 OTHER REDDENING INDICATORS

It would appear from Fig. 4 that a possible explanation for the observed line ratios in the majority of our quasars and the BLRG 3C120 is that the intrinsic emission is modified by dust. It is important to reiterate that in reaching this conclusion, we need not assume that case B recombination is valid, neither do we need to assume that the intrinsic spectra are well described by *any* photoion-

ization model. We simply derive differential reddenings with respect to 3C273. We do not need to assume that 3C273 has zero–reddening either, although as we will show, this may in fact be the case. The major disadvantage of this differential technique is that 3C273 may be peculiar in some way, and may not be characteristic of the AGN population in general. Thus it may be a poor object with which to compare the rest of our sample.

In the light of the above interpretation for the ratios shown in Fig. 4, we propose to establish for each object whether there is any corroborating evidence for dust. Polarization measurements, mid– and far–infrared (*IRAS*) observations, and the overall spectral energy distributions, are just a few of the possible multi–wavelength dust indicators. We will begin with a discussion of 3C273 which has been extensively studied in the past and provides an opportunity to assess the merits of the numerous diagnostics that have been employed in order to infer the presence or absence of dust. In addition, we wish to establish whether our use of 3C273 as a fiducial 'intrinsic–spectrum' source is at all justified. The discussion of this object is thus relevant for the interpretation of the rest of our sample.

3C273. Polarization studies are potentially a useful diagnostic of the presence of dust, particularly if the wavelength dependence can be observed (Stockman, Moore & Angel 1984). However, reddening by dust is not the only process that can induce a significant polarization in an active galaxy, and the possible synchrotron contribution in the form of residual blazar emission (diluted by the normal quasar light) and polarization from electron scattering must be accounted for. Variability studies, in addition to wavelength dependent ones are also useful diagnostics, because variable polarization on short timescales ($\sim$1 month) indicates a synchrotron origin rather than dust. Smith *et al.* (1987) review recent polarization studies of 3C273 and note that no observation has yet resulted in a polarization $P > 3\%$. In their own work the polarization was always $<1\%$. Stockman, Moore & Angel (1984) measured $P = 0.20 - 0.39\%$

over a 2 year period. There are no wavelength dependent measurements, but Impey & Malkan (1988) reported a small polarization flare in 3C273, and this would seem to argue in favour of a synchrotron origin for the little polarization that is observed.

Observations in the mid– and far–infrared, such as those made by *IRAS* are another possible dust diagnostic. Neugebauer *et al.* (1986) have studied the $12 - 100\,\mu$m spectra of a large number of quasars with *IRAS* detections and can broadly classify them into two groups. Firstly, there are the flat–spectrum radio quasars where the *IRAS* spectra are just an interpolation between the non–thermal radio spectrum and the non–thermal optical spectrum, and so the $12 - 100\,\mu$m emission is likewise assumed to be non–thermal. Secondly, there are the steep–spectrum radio quasars (and those which are radio quiet) where it appears that the accompanying steep *IRAS* spectra are at least partly thermal in origin. The quasar 3C48, studied by Neugebauer, Soifer & Miley (1985) is the prototype of this class, where an examination of the continuum energy distribution led them to conclude that thermal re–radiation from dust ($T = 60 - 90\,$K) in the narrow–line region (or possibly in a larger dust–rich host galaxy) is responsible for the steep *IRAS* spectrum. Fig. 5 shows the spectral energy distribution (s.e.d.) of 3C273 from $12-100\,\mu$m. 3C273 is a flat–spectrum radio source, and because the *IRAS* spectrum is also very flat, this indicates that the emission in the $12 - 100\,\mu$m region is probably non–thermal.

There are several infrared features in the $2-4\,\mu$m and $8-13\,\mu$m regions that can be used as powerful dust diagnostics. Allen (1980) obtained a spectrum of 3C273 at the AAT in the $2-4\,\mu$m window (integrating for ~9000s) and detected the $3.3\,\mu$m feature, a common Galactic dust indicator. However, this observation was not confirmed by Lee *et al.* (1982) using the CVF at UKIRT after 5600s integration, thus the presence of the $3.3\,\mu$m feature in 3C273 is open to some doubt. Roche *et al.* (1984) observed 3C273 in the $8 - 13\,\mu$m region and found

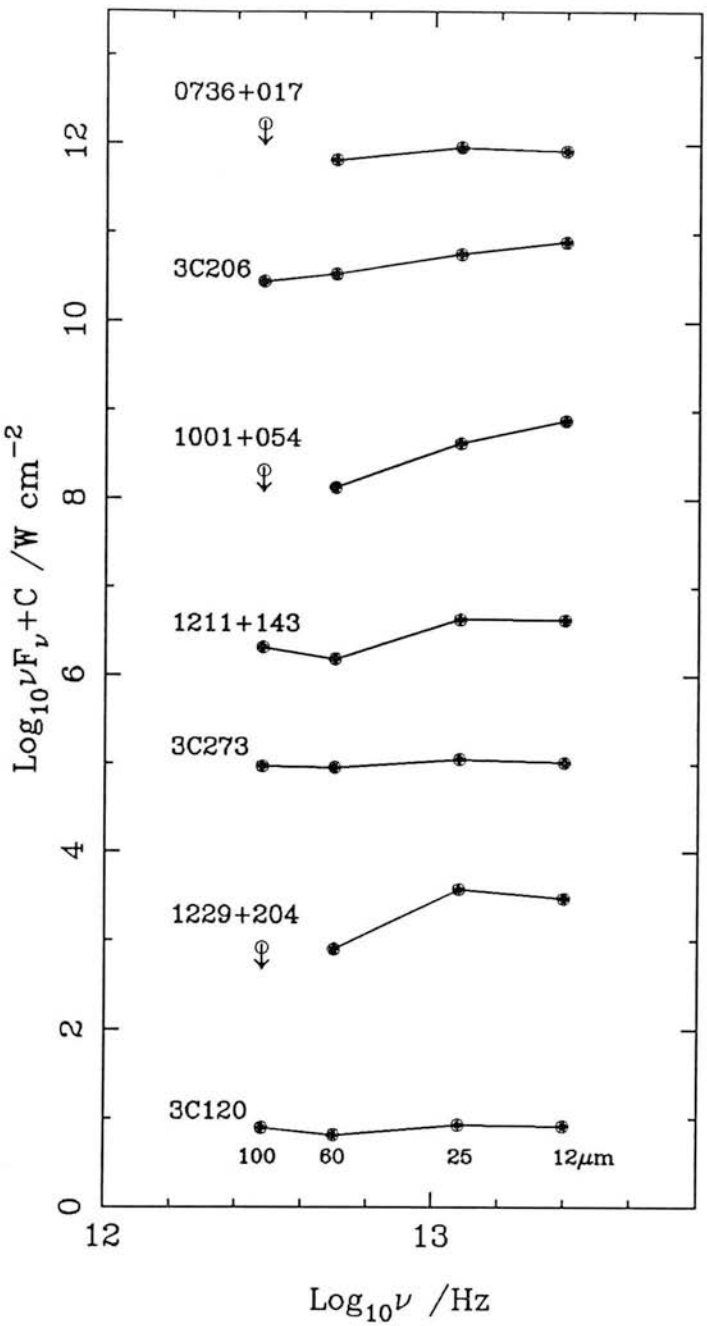

Figure 5. Spectral energy distributions from $12 - 100\,\mu$m for members of our sample that were observed by the *IRAS* satellite. In this representation, peaks correspond to maxima in the energy output, and flat spectra ($\alpha = 1$, $S_\nu \propto \nu^{-\alpha}$) are horizontal lines. Upper limits are shown by arrows. Data are from Neugebauer *et al.* (1986), Edelson (1986) and the *IRAS* Point Source Catalogue (version 2). 0953+414 was not detected in any of the four *IRAS* bands and so is omitted here.

no evidence for silicate features in the spectrum. If there is dust in 3C273, it would need to have 10 μm emission over a wide range of temperatures (so as to mimic a power–law). If there is any silicate dust present, it would have to be too cool to emit at 10 μm, or would need to be swamped by other dust components. As Aitken & Roche (1985) note, the small grains thought to be responsible for the narrow features are likely to be destroyed out to several 100 pc from the nucleus by the hard ultraviolet radiation field in active galaxies, so perhaps it is not surprising that no silicate features have been observed in this quasar.

The overall continuum of 3C273 has been subject to extensive modelling work (e.g. Barvainis 1987, Perry, Ward & Jones 1987, Edelson & Malkan 1986) and this too may provide constraints on internal extinction, particularly with respect to the so–called blue bump (generally shortward of 4000Å) and the 5 μm bump, two features commonly seen in active galaxy continua. Barvainis (1987) has modelled the 5 μm bump in 3C273 (first noted by Neugebauer *et al.* 1979, and extending from $2 - 10\,\mu$m) using grains which are heated to 1500 K at $\sim$1 pc from an ultraviolet source ($\sim 10^{39}$ W). Cooler grains farther away produce the emission longward of 2 μm. A mass of dust ~ 700 $M_\odot$ is required in 3C273 and the distribution can be clumpy or smooth. The luminosity of the bump is small compared with the optical–UV emission, thus only a small fraction of the nuclear continuum is being reprocessed: $\sim$17% of the UV needs to be absorbed to produce the bump. Edelson & Malkan (1986) estimate that the amount of internal reddening needed to obtain a good fit to the UV continuum is only $E(B-V) = 0.05$. Their 5 μm bump, however, needs a much larger dust mass than that modelled by Barvainis (1987). Although Puetter & Hubbard (1985) have argued that the 5 μm bump can be produced by free-free emission from a dense ($N_e = 10^{11-12}\,\mathrm{cm}^{-3}$) broad–line region, this model predicts that objects with strong bumps have depressed Paα/Hα, because high densities will make even the Paα optical depth large. Edelson & Malkan (1986) found no correlation between Paα/Hα and the strength of the 5 μm bump for a sample of 15 AGN,

which runs contrary to the Puetter & Hubbard (1985) hypothesis.

The usefulness of the 5 μm feature and the blue bump as dust diagnostics is probably rather limited, given the variety of interpretations that are possible. The fact that models that involve dust can successfully produce these features is not in itself evidence that dust is indeed present.

Finally, LeVan *et al.* (1984) have studied the line ratio HeI λ10830/HeI λ5876 with respect to Lyα/Hα in 3C273. This combination of ratios has the advantage that λ10830/λ5876 increases with increased reddening and decreases as the optical depth increases, whereas Lyα/Hα decreases both with increasing optical depth and reddening. They could not see any evidence from these ratios for reddening in 3C273.

In summary, there seems to be little evidence in 3C273 for anything larger than very minimal amounts of dust, and our choice of this object as a fiducial, 'intrinsic–spectrum' object on the Paα/Hα – Hα/Hβ plane is justified.

0736+017. This quasar is very close to 3C273 in Fig. 4, and is the least reddened member of our sample with respect to 3C273. It is classed as a highly polarized quasar (HPQ) by Stockman, Moore & Angel (1984), and generally has a polarization $P > 3\%$. These authors measured values of P in the range 0.5–5.6%. Malkan & Moore (1986) obtained $P = 5\%$ for this object and modelled the continuum as consisting of 75% BL Lac type emission. They ascribed the remaining 25% non–BL Lac component (essentially normal quasar light) to a power–law plus a weak blue bump, the latter being modelled as optically thick thermal emission perhaps from an accretion disk (Malkan & Sargent 1982). The emission is assumed to have a black–body temperature $T \sim 2 - 3 \times 10^4$ K. One polarization measurement, that of Moore & Stockman (1981) does show a wavelength dependence, values of $P = 4.97 \pm 0.27\%$ being observed in the blue, and $P = 6.12 \pm 0.20\%$ in the red. In addition, Holmes *et al.* (1984) obtained a K

band polarization of $7.3 \pm 4.3\%$ which is higher than these optical values. However, the trend of increasing polarization towards longer wavelengths is in the *reverse* sense expected from a contribution by dust, and it is probable that the blazar component in this object totally overwhelms any contribution from dust. In addition, it is worth noting that there is no strong wavelength dependence in the $BVRI$ polarimetry of Smith *et al.* (1987) so the situation is unclear. Smith *et al.* (1987) observed rapid daily variations in polarization: P (measured in the I band) changed from 6.9 ± 0.9 to $1.4 \pm 0.9\%$ during the course of two nights, which supports a synchrotron origin for the bulk of this object's polarization.

The source has a flat radio–spectrum, and the $12 - 100\,\mu$m s.e.d. (Fig. 5) is flat, indicating a non–thermal origin. Similarly, Malkan & Sargent (1982) had concluded from a study of the ultraviolet–optical–infrared continuum of this quasar, that much of the near–infrared emission is non–thermal. Gear *et al.* (1985) have studied the continuum energy distribution from $1\,\mu$m to 2 mm and find no evidence for excess emission caused by thermal radiation from either warm dust in the infrared, or cooler dust in the millimetre region.

Thus there is little evidence for substantial reddening in 0736+017, in good agreement with our observation of only a small differential reddening with respect to 3C273 on the $\mathrm{Pa}\alpha/\mathrm{H}\alpha$ – $\mathrm{H}\alpha/\mathrm{H}\beta$ plane.

3C206. This quasar is the most reddened of our sample with respect to 3C273, and the reddening vector implies $A_V \sim 1.5$. It has a steep radio–spectrum and the *IRAS* s.e.d. is also fairly steep (Fig. 5), the energy output at $12\,\mu$m being twice that at $100\,\mu$m, implying a thermal origin to the emission. Cutri *et al.* (1985) note that the near–infrared (K band) variability of 3C206 is negligible, whereas that at V has an amplitude $\sim$1 mag. and they suspect the near–infrared luminosity is produced by a component distinct form that which dominates the optical and the UV. The lack of correlation between the infrared and optical variability suggests a re–radiated spectrum. The polarization of 3C206 is low,

$P = 0.38 \pm 0.28\%$ (Stockman, Moore & Angel, 1984). In summary, there is good evidence that 3C206 does contain dust, in agreement with our observed line ratios in Fig. 4 being subject to some 1.5 mag. reddening with respect to 3C273.

0953+414. There have been few previous observations of this Palomar–Green quasar, and it was not detected in any of the four *IRAS* bands. Green *et al.* (1980) observed that it has a blue bump (peaking at 3600Å in the rest–frame) and noted that a single power–law was not a good fit to the spectrum, implying the need for a multicomponent model. This quasar lies a long way from the reddened 3C273 vector in Fig. 4, having a low Balmer decrement with respect to Paα/Hα. Although our Hβ flux is in poor agreement with that of Green *et al.* (1980) (in that it is lower), in order to obtain an erroneously small Hα/Hβ ratio we would require our Hα flux to have an even greater error with respect to that of Hβ.

1001+054. This radio–quiet quasar occupies a region of Fig. 4 indicative of $\sim$1 mag. of reddening with respect to 3C273. The *IRAS* $12 - 100\,\mu$m spectrum (Fig. 5) is very steep (there is no detection at $100\,\mu$m and the energy output at $12\,\mu$m is $\sim$6 times that at $60\,\mu$m). This suggests a thermal origin to the emission. The polarization ranges between $P = 0.77 \pm 0.22\%$ in 1978 February to $P = 0.25 \pm 0.34\%$ in 1979 April (Stockman, Moore & Angel, 1984) but there are no data regarding wavelength dependence or short–term variability.

1211+143. This quasar occupies a similar position on Fig. 4 to 0953+414, and is a long way from the reddened 3C273 vector. Bechtold *et al.* (1987) present an extensive discussion of this object, which has the highest X–ray to optical luminosity ratio of any Palomar–Green quasar. They estimate that the largest reddening allowed by the continuum is $E(B - V) = 0.10$. 1211+143 has a prominent blue bump which they model with an accretion disk (Malkan & Sargent 1982, Czerny & Elvis 1987). Abramowicz, Calvani & Madau (1987) draw

attention to the large excess of soft X–ray emission (< 1 keV) which is above the extrapolation of the > 2 keV power–law spectrum – if this is thermal then it is possibly connected with the blue bump and may be interpreted as the tail of a single very luminous thermal component, $T \sim 10^{5-6}$ K. The *IRAS* s.e.d. (Fig. 5) is moderately steep, showing a peak at $\sim$25 μm, and this observation, coupled with the quasar's lack of radio emission classifies it as a thermal spectrum. LeVan *et al.* (1984) observed HeI λ10830 in 1211+143 but were lacking the Lyα flux to enable it to be located on the reddening sensitive λ10830/λ5876 – Lyα/Hα plane. We have taken the Lyα flux from Bechtold *et al.* (1987) and derive ratios of log(Lyα/Hα)=0.39 and log(λ10830/λ5876)=0.71 using the optical and near–infrared line data given by LeVan *et al.* (1984). These values are indicative of little reddening on the λ10830/λ5876 – Lyα/Hα plane, lying very close to the Kwan & Krolick (1981) photoionization model prediction.

The above dust diagnostics are somewhat contradictory and it is clear that 1211+143 is peculiar, particularly with regard to its very high X-ray luminosity.

1229+204. This quasar occupies a region on Fig. 4 indicative of $\sim$1 mag. reddening with respect to 3C273. The *IRAS* s.e.d. is steep (Fig. 5), with no detection at 100 μm and a pronounced peak at 25 μm, analogous to that seen in the broad–line radio galaxy 3C390.3. Miley *et al.* (1984) interpreted this bump as being due to dust with $T \sim$ 180K. Thus there is strong evidence for a thermal origin to the *IRAS* spectrum. Sembay, Hanson & Coe (1987) have studied the short–term variability of this quasar in the $12 - 100\,\mu$m region over a period of 12 days using *IRAS* Additional Observations. No evidence for short–term variability was found, again supporting a re–radiated, thermal interpretation of the spectrum. The polarization is fairly small, ranging from $P = 0.40 - 0.61\%$ during a 2 year period (Stockman, Moore & Angel 1984), but no wavelength dependent studies have been done. Worrall *et al.* (1984) commented on the strong blue bump in this quasar.

3C120. This broad–line radio galaxy/Seyfert 1 lies about 1.5 mag. along the reddening vector from 3C273. It has a powerful UV continuum which shows the 2175Å dust absorption feature, from which Oke & Zimmerman (1979) estimated $E(B-V) = 0.38$ (equivalent to $A_V \simeq 1.14$). However, Edelson & Malkan (1986) inferred that $A_V = 0.18$ was necessary in order to obtain a good fit to the ultraviolet continuum, so there is obviously a problem with the interpretation of the ultraviolet spectrum in this object. Rudy *et al.* (1987) studied the ratios $\lambda 10830/\lambda 5876$ (both He I) and $\lambda 5876/\mathrm{H}\beta$, and although they argued that there was reddening in this object (the amount unspecified) they could not reconcile $\lambda 5876/\mathrm{H}\beta$ with reddening alone. They proposed that both HeI $\lambda 5876$ and $\mathrm{H}\beta$ are collisionally enhanced. Roche *et al.* (1984) obtained an $8-13\,\mu$m spectrum of 3C120 and, as was the case for 3C273, saw no evidence for silicate dust features. The radio spectrum of 3C120 is flat, as is the *IRAS* s.e.d. (Fig. 5), evidence for a a non–thermal spectrum. Antonucci (1984a) obtained polarimetry for 3C120 over a period of one month when P ranged from 0.86–1.12%. The polarization was independent of wavelength, again supporting a non–thermal synchrotron interpretation. Spectrophotometry has been obtained for the continuum in the $2-4\,\mu$m region by Rudy *et al.* (1982) who concluded that non–stellar radiation dominates the infrared flux. However, they comment that the infrared variability does not track with that seen in the optical (Penston *et al.* 1975) which is indicative of a re–radiated spectrum.

In summary, much of the evidence for and against reddening in this object seems contradictory, but the presence of $A_V \sim 1$ mag. of dust (as inferred from our line ratios) is by no means precluded, and the presence of the 2175Å absorption feature in this object is very encouraging.

7 Conclusions

1) None of the extant photoionization models (Hubbard & Puetter 1985, Collin–Souffrin *et al.* 1986, Kwan 1984, Drake & Ulrich 1980, Mathews, Blumenthal &

Grandi 1980, and references therein), for any of the regions of parameter space that they explore, predict values of Paα/Hα that are in good agreement with those observed in any of our quasars, or the BLRG 3C120, with the notable exception of 3C273. Generally, the predicted values of Paα/Hα are too low in comparison with our observed values. However, the observed values of the Balmer decrement Hα/Hβ are in good agreement with these models. In order for the Paα/Hα ratios in 3C206, 0953+414 and 1211+143 (our most extreme objects) to match *any* of the current photoionization models, we would require Paα fluxes that are 50% lower than those we measure *and* Balmer line fluxes that are 40% higher. However, a comparison of our spectrophotometry with a large body of previous work indicates that errors as large as these are rather unlikely.

2) The line ratios observed in the majority of our sample are not even well produced by reddened photoionization models, the reddened models tending to have larger values of Hα/Hβ for any given Paα/Hα ratio than observed. It is possible that the reddening law required for these active galaxies is different from the Galactic one. Whether the adoption of a non–Galactic reddening law could reconcile the data with the photoionization models is not clear.

3) The observed Paα/Hα and Hα/Hβ ratios in 3C273 can be matched (to within the observational errors) by a subset of the Hubbard & Puetter (1985) models. There is a large body of multiwavelength evidence to suggest that any reddening in 3C273 is minimal, and probably zero. This assertion, coupled with the fact that our observed line ratios in this object are the closest to the pure photoionization models, justifies the use of 3C273 in deriving differential reddenings for the rest of the sample. In interpreting the observed ratios in our other objects, we do not make any assumption about the physics of the line emission (photoionization or otherwise) other than to assume that 3C273 is a representative quasar.

4) The three quasars 3C206, 1001+054 and 1229+204 have between 1 and 2 mag. of reddening with respect to 3C273, and have other evidence to suggest that the reddenings derived from the Paα/Hα and Hα/Hβ ratios are justified. All three quasars have steep $12-100\,\mu$m *IRAS* spectra, with 1229+204 showing a pronounced $25\,\mu$m bump.

5) The quasar 0736+017 appears to be the least reddened of our objects with respect to 3C273, and this finding, coupled with the general lack of firm corroborating evidence in support of the presence of dust indicates that any reddening in this object is minimal, and may be very close to zero.

6) The situation for 3C120 is less clear, but a significant reddening ($A_V \sim 1-2$ mag.) as inferred from our line ratios is not ruled out, and there is some strong evidence (such as the presence of the 2175Å absorption feature) that supports the presence of dust.

7) The quasars 0953+414 and 1211+143 occupy a region of the Paα/Hα – Hα/Hβ plane some distance from the reddened 3C273 vector, in the sense of having depressed Hα emission with respect to Hβ. They can not be adequately described by a reddened 3C273 spectrum. However, the good agreement of the observed reddening *insensitive* infrared line ratios (Paα/Paβ in 0953+414 and Brγ/Paα in 1211+143) with the photoionization models, but the poor agreement seen in the reddening *sensitive* Paα/Hα ratios with the models suggests that these two quasars are also subject to reddening. The departure from the 3C273 reddening vector implies that the intrinsic spectrum in these objects is not well described by that of 3C273. 1211+143 is known to have some peculiar properties, particularly with regard to its excessive X–ray emission.

Perhaps the most puzzling aspect of this present investigation is the singular lack of success shown by the majority of the photoionization models (reddened *or* unreddened) to predict the observed Paα/Hα ratios for most of the objects

studied here. This is despite the fact that the latest models allow for the high densities that we expect to be characteristic of the line–emitting regions of active galaxies, and thus encompass what appear to be the relevant regions of parameter space. The lack of agreement with the observations suggests that there is some fundamental parameter which is not being accounted for in these models. Thus these present observations present a challenge to the modellers, and any future work should not omit the inclusion of calculations for the Paβ and Brγ lines.

Acknowledgments

We are grateful to Tom Geballe and Rudy LePoole for support at UKIRT and the INT respectively, and to Anne Fraser for on–line literature searches. Reddened line–ratios were calculated by Phil Puxley. This data was reduced on STARLINK at the Royal Observatory, Edinburgh. MGY was supported by a research studentship from the Science and Engineering Research Council during this work.

References

Abramowicz, M.A., Calvani, M. & Madau, P., 1987. *Comments Astrophys.*, **12**, 67.

Aitken, D.K. & Roche, P.F., 1985. *Mon. Not. R. astr. Soc.*, **213**, 777.

Allen, D.A., 1980. *Nature*, **284**, 323.

Antonucci, R.R.J., 1984a. *Astrophys. J.*, **278**, 499.

Antonucci, R.R.J., 1984b. *Astrophys. J.*, **281**, 112.

Baldwin, J.A., 1975. *Astrophys. J.*, **201**, 26.

Barbieri, C. & Romano, G., 1984. *Acta Astron.*, **34**, 117.

Barvainis, R., 1987. *Astrophys. J.*, **320**, 537.

Bechtold, J., Czerny, B., Elvis, M., Fabbiano, G. & Green, R.F., 1987. *Astrophys. J.*, **314**, 699.

Burstein, D. & Heiles, C., 1982. *Astr. J.*, **87**, 1165.

Canfield, R.C. & Puetter, R.C., 1981. *Astrophys. J.*, **243**, 390.

Collin–Souffrin, S., Dumont, S., Joly, M. & Péquignot, D., 1986. *Astr. Astrophys.*, **166**, 27.

Collin–Souffrin, S., Dumont, S. & Tully, J., 1982. *Astr. Astrophys.*, **106**, 362.

Courvoisier, T.J.-L., Turner, M.J.L., Robson, E.I., Gear, W.K., Staubert, R., Blecha, A., Bouchet, P., Falomo, R., Valtonen, M., & Teräsranta, H., 1987. *Astr. Astrophys.*, **176**, 197.

Cutri, R.M., Wiśniewski, W.Z., Rieke, G.H. & Lebofsky, M.J., 1985. *Astrophys. J.*, **296**, 423.

Czerny, B. & Elvis, M., 1987. *Astrophys. J.*, **321**, 305.

Drake, S.A. & Ulrich, R.K., 1980. *Astrophys. J. Suppl.*, **42**, 351.

Edelson, R.A., 1986. *Astrophys. J.*, **309**, L69.

Edelson, R.A. & Malkan, M.A., 1986. *Astrophys. J.*, **308**, 59.

French, H.B. & Miller, J.S., 1981. *Publ. astr. Soc. Pacific*, **92**, 753.

Gear, W.K., Robson, E.I., Ade, P.A.R., Griffin, M.J., Brown, L.M.J., Smith, M.G., Nolt, I.G., Radostitz, J.V., Veeder, G. & Lebofsky, L., 1985. *Astrophys. J.*, **291**, 511.

Grandi, S.A., 1983. *Astrophys. J.*, **268**, 591.

Green, R.F., Pier, J.R., Schmidt, M., Estabrook, F.B., Lane, A.L. &Wahlquist, H.D., 1980. *Astrophys. J.*, **239**, 483.

Hewitt, A. & Burbidge, G., 1987. *Astrophys. J. Suppl.*, **63**, 1.

Holmes, P.A., Brand, P.W.J.L., Impey, C.D. & Williams, P.M., 1984. *Mon. Not. R. astr. Soc.*, **210**, 961.

Hubbard, E.N. & Puetter, R.C., 1985. *Astrophys. J.*, **290**, 394.

Hummer, D.G. & Storey, P.J., 1987. *Mon. Not. R. astr. Soc.*, **224**, 801.

Impey, C.D. & Malkan, M.A., 1988. In preparation.

Krolick, J.H. & McKee, C.F., 1978. *Astrophys. J. Suppl.*, **37**, 459.

Kwan, J., 1984. *Astrophys. J.*, **283**, 70.

Kwan, J. & Krolick, J.H., 1979. *Astrophys. J.*, **233**, L91.

Kwan, J. & Krolick, J.H., 1981. *Astrophys. J.*, **250**, 478.

Lacy, J.H., Soifer, B.T., Neugebauer, G., Matthews, K., Malkan, M., Becklin, E.E., Wu, C.-C., Boggess, A. & Gull, T.R., 1982. *Astrophys. J.*, **256**, 75.

Lee, T.J., Beattie, D.H., Gatley, I., Brand, P.W.J.L., Jones, T. & Hyland, A.R., 1982. *Nature*, **295**, 214.

LeVan, P.D., Puetter, R.C., Smith, H.E. & Rudy, R.J., 1984. *Astrophys. J.*, **284**, 23.

Malkan, M.A. & Moore, R.L., 1986. *Astrophys. J.*, **300**, 216.

Malkan, M.A. & Sargent, W.L.W., 1982. *Astrophys. J.*, **254**, 22.

Mathews, W.G., Blumenthal, G.R. & Grandi, S.A., 1980. *Astrophys. J.*, **235**, 971.

McAlary, C.W., Rieke, G.H., Lebofsky, M.J. & Stocke, J.T., 1986. *Astrophys. J.*, **301**, 105.

Miley, G., Neugebauer, G., Clegg, P.E., Harris, S., Rowan–Robinson, M., Soifer, B.T., Young, E., 1984. *Astrophys. J.*, **278**, L79.

Moore, R.L. & Stockman, H.S., 1981. *Astrophys. J.*, **243**, 60.

Nandy, K., Morgan, D.H., Willis, A.J., Wilson, R., Gondhalekar, P.M. & Houziaux, L., 1981. *Mon. Not. R. astr. Soc.*, **196**, 955.

Netzer, H., Wills, B.J., Uotomo, A.K., Rybski, P.M., & Tull, R.G., 1979. *Astrophys. J.*, **232**, L155.

Neugebauer, G., Miley, G.K., Soifer, B.T. & Clegg, P.E., 1986. *Astrophys. J.*, **308**, 815.

Neugebauer, G., Oke, J.B., Becklin, E.E. & Mathews, K., 1979. *Astrophys. J.*, **230**, 79.

Neugebauer, G., Soifer, B.T. & Miley, G., 1985. *Astrophys. J.*, **295**, L27.

Oke, J.B., 1974. *Astrophys. J. Suppl.*, **27**, 21.

Oke, J.B. & Zimmerman, B., 1979. *Astrophys. J.*, **231**, L13.

Oke, J.B., Readhead, A.C.S. & Sargent, W.L.W., 1981. *Publ. astr. Soc. Pacific*, **92**, 758.

Osterbrock, D.E. & Shuder, J.M., 1982. *Astrophys. J.*, **49**, 149.

Penston, M.V., Penston, M.J., Selmes, R.A., Becklin, E.E. & Neugebauer, G., 1975. *Mon. Not. R. astr. Soc.*, **169**, 357.

Perry, J.J., Ward, M.J. & Jones, M., 1987. *Mon. Not. R. astr. Soc.*, **228**, 623.

Peterson, B.M., 1987. *Astrophys. J.*, **312**, 79.

Peterson, B.M., Crenshaw, D.M. & Meyers, K.A., 1985. *Astrophys. J.*, **298**, 283.

Peterson, B.M., Foltz, C.B., Byard, P.L. & Wagner, R.M., 1982. *Astrophys. J. Suppl.*, **49**, 469.

Peterson, B.M., Meyers, K.A., Capriotti, E.R., Foltz, C.B., Wilkes, B.J. & Miller, H.R., 1985. *Astrophys. J.*, **292**, 164.

Puetter, R.C. & Hubbard, E.N., 1985. *Astrophys. J.*, **295**, 394.

Puetter, R.C., Smith, H.E., Willner, S.P. & Pipher, J.L., 1981. *Astrophys. J.*, **243**, 345.

Rafanelli, P., 1985. *Astr. Astrophys.*, **146**, 17.

Rieke, G.H. & Lebofsky, M.J., 1985. *Astrophys. J.*, **288**, 618.

Robson, E.I., Gear, W.K., Clegg, P.E., Ade, P.A.R., Smith, M.G., Griffin, M.J., Nolt, I.G., Radostitz, J.V. & Howard, R.J., 1983. *Nature*, **305**, 194.

Roche, P.F., Aitken, D.K., Phillips, M.M. & Whitmore, B., 1984. *Mon. Not. R. astr. Soc.*, **207**, 35.

Rudy, R.J., Jones, B., LeVan, P.D., Puetter, R.C., Smith, H.E., Willner, S.P., Tokunaga, A.T., 1982. *Astrophys. J.*, **257**, 570.

Rudy, R.J., Rossano, G.S., Puetter, R.C. & Cohen, R.D., 1987. *Astr. J.*, **93**, 284.

Sellgren, K., Soifer, B.T., Neugebauer, G., Matthews, K., 1983. *Publ. astr. Soc. Pacific*, **95**, 289.

Sembay, S., Hanson, C.G. & Coe, M.J., 1987. *Mon. Not. R. astr. Soc.*, **226**, 137.

Smith, P.S., Balonek, T.J., Elston, R. & Heckert, P.A., 1987. *Astrophys. J. Suppl.*, **64**, 459.

Soifer, B.T., Neugebauer, G., Oke, J.B. & Matthews, K., 1981. *Astrophys. J.*, **243**, 369.

Stockman, H.S., Moore, R.L. & Angel, J.R.P., 1984. *Astrophys. J.*, **279**, 485.

Stockton, A. & MacKenty, J.W., 1987. *Astrophys. J.*, **316**, 584.

Wampler, E.J., 1967. *Publ. astr. Soc. Pacific*, **79**, 210.

Ward, M.J., Geballe, T., Smith, M., Wade, R. & Williams, P., 1987. *Astrophys. J.*, **316**, 138.

Worrall, D.M., Puschell, J.J., Bruhweiler, F.C., Miller, H.R., Aller, M.F., & Aller, H.D., 1984. *Publ. astr. Soc. Pacific*, **96**, 699.

Zheng, W. & Burbidge, E.M., 1986. *Astrophys. J.*, **306**, L67.

Zheng, W., Burbidge, E.M., Smith, H.E., Cohen, R.D. & Bradley, S.E., 1987. *Astrophys. J.*, **322**, 164.

Postscript at February 1988.

We're still puzzling over this one. Can it really be the case that the large amount of effort that has gone into numerically modelling the photoionization processes has largely been in vain? It was particularly striking in our work that neither the reddened or unreddened models could adequately model our observed line ratios. The reason why the models are failing is not at all obvious, particularly in as much as they now attempt to model realistic particle densities, which was not the case 5-10 years ago. As was apparent from the discussion in this paper, the numerous proposed dust diagnostics are often in contradiction with each other, or at least open to a variety of interpretations. In order to make any progress it is probable that we need to concentrate on signatures that are unique to dust, such as the 2175Å feature in the ultraviolet: polarization, line and continuum measurements are all subject to a number of interpretations, and can only be used as corroborating evidence for dust. On their own, they are of little use as dust diagnostics.

ACKNOWLEDGEMENTS

In addition to the people mentioned in the acknowledgements to each paper I would like to thank my collaborators, particularly John Peacock and Lance Miller, for putting up with me and spotting the deliberate mistakes.

I am grateful for the superb facilities of the Royal Observatory, Edinburgh, and in particular to the staffs of the Library, Plate Library and Computing Section.

Finally, no acknowledgements list would be complete without an unbridled outburst of namedropping full of appalling in–jokes and I am genuinely grateful to Hans Zinnecker for dissuading me from looking at the problem of metallicity, Peter Brand for asking embarassing questions, James Dunlop for snorting like a peeg, Andrew Mead for confirming my suspicions about socialists, James More for making me feel under–dressed, John Rayner for making me feel young, Mark McCaughrean for ensuring I never developed an inferiority complex, Mark Bird for not snorting at all, Brian Boyle for beer in Beijing, Alan Heavens for being sceptical, Klaus Meisenheimer for being German, Neil Heydon-Dumbleton for dispelling any desire to get a real job, Chris Collins for dispelling my belief in primeval galaxies, Phil Puxley for dispelling my belief in infrared astronomy, Toby Moore for doing likewise for millimetre astronomy, Stuart Lumsden for extolling the virtues of hard work, Paul Mitchell for introducing me to really bad music, Crispin Keable for attempting to be cool, Ron Garden for attempting to be an astronomer, Mike Burton for succeeding in being a Philistine, Dolores Walther for cookies, Thor Wold for failing to appreciate my sense of humour, Joel Aycock for operating UKIRT, Ann Savage for lending me her shower, Liz Gibson for running the Department, Maureen McLean for not noticing where her stationery was going, Janice Murray for not noticing, Sue Tritton for always being so helpful in the Plate Library, Prof Stibbs for improving my lecturing technique, Mr Pan for showing me the sights and smells of Shanghai, Dr Kalafi for going back to Iran, Charlie for pathetic attempts at taxi driving, Frau Berliner for only a marginally better attempt at accordian playing, Philippe Véron for an even better attempt at a death–defying stunt at La Silla, the Chileno night–assistant who thought Dec$=-35°$ was north of $-34°$, and finally Malcolm Longair for being both my supervisor and the Astronomer Royal for Scotland, thus leaving me completely to my own devices.